行 政 院 國 家 科 學 委 員 會 委 託 計 畫 成 果 報 告

具有智慧型天線寬頻的 CDMA 基地站收發機之研製-W-CDMA 智慧型天線（子計畫二）

Smart Antennas for W-CDMA Systems

計 劃 編 號 ： NSC89-2219-E-002-035

執 行 期 間 ：87 年 5 月 1 日至 90 年 7 月 31 日

計 畫 主 持 人 ：李學智　教授

執 行 單 位 ： 國立台灣大學電信工程學研究所

日　　　　期： 中 華 民 國 90 年 7 月

摘要

在本中，我們首先簡單描述時變射頻通道衰落的特性和寬展頻通訊系統的實體層規格，然後，針對基地台使用陣列天線的第三代寬展頻通訊系統，我們提出通道參數估測方法及無線電波束形成方法。

以便在多重接收干擾信號(MAI)中，能夠準確估測欲接收信號者的通道參數，這些參數含有訊號到達時間，訊號波的來向和訊號的強度，我們首先提出增加接收信號與干擾雜訊比的方法，這個方法是藉由連續同調相加不同指標位元(pilot bits)的匹配濾波器輸出和非同調相加所有天線陣列位元的匹配濾波器輸出結果，經由這兩種訊號處理過程，欲接收者的信號強度可以大幅的提升。然後，將得到的通道估測數據應用到資料接收通道，運用二維耙型(2D-RAKE))信號組合技巧，我們可以發現欲接收資料的信號干擾雜訊比值極接近理論計算值。

我們也比較不同無線電波束集成方法的信號上傳及下傳資料的信號干擾雜訊比值。在資料上傳部分，我們發現波束來向(DOA)方法和共軛複數(complex conjugate)方法有非常相近的信號干擾雜訊比值，然而共軛複數方法只需要較少的運算處理時間;直接矩陣逆轉(DMI)方法與波束來向方法比較，我們發現當只有少數人同時在上傳資料時，直接矩陣轉方法有較佳的信號干擾雜訊比值，但是這種優勢隨著人數的增加而降低，最後會接近波束來向方法的結果。直接矩陣逆轉方法的缺點是需要較長的運算處理時間。

在資料下傳部分，針對直接短陣逆轉方法，我們得到一個信號干擾雜訊比值的解析解表示式，由電腦模擬的數據結果發現與解析解值非常相近。除此之外，我們也比較單一波束(single-beam)集成方法與複合波束(multiple-beam)集成方法，在資料上傳及下傳時遭遇到不同的通道衰落時，其接收到的信號干擾雜訊比值結果，當信號干擾比值在很低的範圍時，我們發現複合波束會有較佳的信號干擾雜訊比值結果，這是因為單一波束受到信號極度衰落的結果，反之，當信號干擾雜訊比值較大時，單一波束會有較佳的接收信號干擾雜訊比值結果，這是因為單一波束集成方法在波的傳遞方向有較大的天線增益，較小的波束涵蓋範疇，以及可以維持調變碼的正交特性。

最後，我們使用最新採購的向量通道量測儀模擬寬展頻通訊系統，以實際量

測到的通道參數數據，評估及比較不同波束集成方法的上傳及下傳資料傳輸品質，在資料下傳時，信號干擾雜訊比值結果與行動器(mobile)所在的位置有很高的聯動性，同時，實驗的模擬結果也顯示波束來向方法所得到的信號干擾雜訊比值結果會比直接矩陣逆轉方法好，其理由及結果均會在內文中一一詳細說明。

Abstract

In this thesis we briefly review the time-varying radio fading channel characteristics and the specification of the physical layer of the W-CDMA communication system. We propose channel parameters estimation algorithms and beamforming algorithms for the 3G W-CDMA basestation transceiver employing antenna array.

To accurately estimate the channel parameters, including the Time of arrival (TOA), Direction of arrival (DOA), and complex amplitude of the desired user's signal in the presence of multiple-access interference (MAI), we propose a method to increase the SINR of the resultant delay profile, which is obtained by coherently integrating the matched filter output over different pilot bits and incoherently integrating all matched filter outputs of antenna array elements. With these two stages of integration, the desired signals are greatly enhanced. We exploit the estimated channel parameters to the data-branch for 2D-RAKE combining and find that the SINR performance after RAKE receiver can approach the theoretical values.

We compare the uplink and downlink SINR performance obtained by different beamforming methods. In the uplink, we found that the DOA method and the complex conjugate method almost have the same SINR performance. However, the complex conjugate method doesn't need any computational loading. The DMI (Direct Matrix Inversion) method can have much better performance than the DOA method when few users are present in the channel. When the number of users is much greater than the number of antenna element, however, we found that these two methods almost have the same performance. Nevertheless, the DMI method requires much higher computation loading. We have derived an analytical form of the SINR after 2D-RAKE receiver for the DMI method and the simulation results are very close to the analytic value.

In the downlink, we compare the sing-beam and multiple-beam beamforming techniques considering the independent fading of the uplink and downlink. We found

that the multiple-beam method has a better SINR performance in the low SINR region because the single-beam method is more likely to suffer from deep fading. While in the moderate of high SINR region, the single-beam method has a much better SINR performance because it has a higher antenna gain in the main path direction, a smaller angular coverage of the mainlobe and the orthogonality between different code sequences.

We employ the channel data measured by a newly purchased vector channel sounder to estimate the W-CDMA system and compare the uplink and downlink SINR performance using different beamforming techniques. In the uplink we found that the SINR performance obtained by measurement data has the same trend as that obtained by the simulation data. However, the SINR performance is very location dependent in the downlink. The SINR performance obtained by the DMI method is worse than that obtained by the DOA method. Explanations of the reasons are given in the context.

Contents

List of Tables

List of Figures

Chapter 1 Introduction

Future wireless communication systems will provide multiple services to their customers that are not supported by presently deployed or introduced systems. Most of the second generation digital cellular and personal communication service (PCS) systems operating in these days are designed to provide relatively low rate voice-oriented services. Therefore, in these systems there are difficulties in accommodating emerging wireless communication services that require higher data rates, enhanced quality of service, and various traffic types such as voice, wireless packet data, and wireless multimedia. Standardization process for the third generation (3G) mobile radio service, namely International Mobile Telecommunications 2000 (IMT-2000), is on its almost final stage under International Telecommunication Union Radio Communication (ITU-R). The IMT-2000 radio interface is a wideband spread spectrum radio interface that uses Wideband Code Division Multiple Access (W-CDMA) technology to meet the needs of the 3G wireless communication systems [1]. Because W-CDMA uses variable rate techniques in digital processing, it can easily achieve multirate transmissions. It has major advantages for high-speed connections to the Internet and it allows the construction of mobile multimedia networks that can cover from low to high speeds.

1.1 Concepts of Spatial and Time Diversity

In CDMA communication systems, multiple users share the same frequency band. Unique channel is created by having each user directly modulate their information by a unique, high bit rate code sequence that is essentially uncorrelated with those assigned to other users. The uncorrelated property (sometimes called the mutual orthogonality) of the code sequences allows simultaneous transmissions in the same channel. This property allows spread spectrum to be as a multiple access method. Since the codes are not exactly orthogonal and exhibit correlation sidelobes, the multiple access interference (MAI) from other transmitters becomes a major adverse impact on the CDMA systems [2]. The more simultaneous users there are, the poorer any one user's signal is received. In addition, multipath components also cause interference. The net interference, MAI and multipath interferences, severely limits the multi-access capacity of the CDMA system. Since CDMA capacity is usually interference limited (unlike Frequency Division Multiple Access (FDMA) and Time Division Multiple Access (TDMA), capacities are primarily bandwidth limited) [3], any reduction in interference will directly increase the capacity.

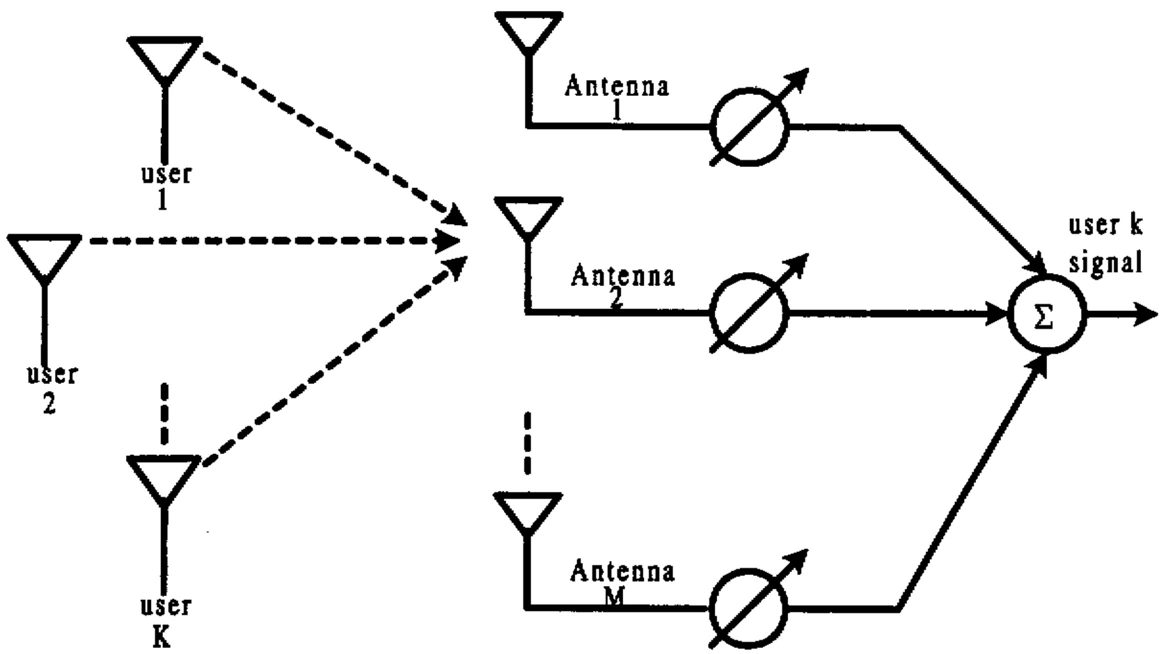

Fig. 1.1 Wireless communication system employing antenna array with M elements at basestation receiver signals from Kusers

One approach to increase the system capacity is the use of spatial processing with basestation array antenna [4,5,6]. Fig. 1.1 shows a digital wireless communication system employing antenna array with M antenna elements at the basestation to receive signals from K users. These K users operate at the same frequency and various multipath signals arrive at the basestation simultaneously. These multipath signals interfere with the desired signals. Using spatial processing at the cell site can improve system capacity. The increase in system capacity by using antenna arrays in

CDMA comes from reducing co-channel interference from users within own cell and neighboring cells. This reduced interference leads to an increase in capacity. Furthermore, an antenna array has the ability to significantly reduces signal variations (i.e., peak-to-peak fading) [7,8]. Since the reliability and quality of a wireless communication system strongly depend on the depth and rate of fading, this reduction of the signal variation greatly enhances system performance, and thus significantly increases the capacity of the system.

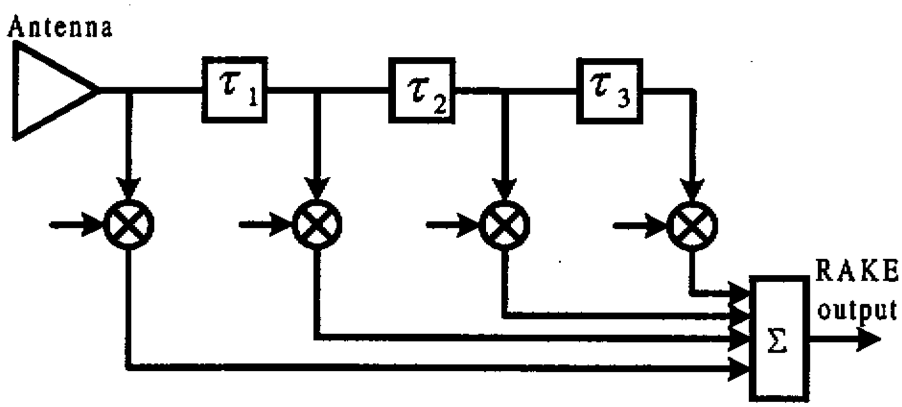

Fig. 1.2 1D-RAKE receiver

Another approach to increase the system performance is the use of time diversity with a RAKE receiver [9,10]. The structure of the RAKE receiver is shown in Fig. 1.2. The signal present at each tap of the RAKE receiver is simply a delayed version of the incident signal. Despite the multipath is a troublesome effect in many communication channels, however, the multipath signals are not interference but carry information. If we suppress the multipath signals, we do not utilize signal energy efficiently. In CDMA systems, users transmit signals that are nearly orthogonal through the use of specially designed codes. The semi-orthogonality of the codes makes it possible for the receiver to estimate the multipath response of each user separately. After estimating the multipath response of the channel, the received signals are fed into a RAKE combiner that coherently sums the multipath components. By properly combining multipath components the system performance can be greatly improved. We refer to this as a 1-D or temporal RAKE receiver since only temporal structure is exploited.

1.2 Motivation

In recent years, a two-dimensional RAKE (2D-RAKE) receiver has been proposed for the CDMA systems [11,12,13,14], where multiple antenna elements and sophisticated signal processors, including beamformers, matched filters, and RAKE combiners are employed to enhance the signal in spatial and temporal domains and suppress the interference. The signal-to-interference-and-noise-ratio (SINR) can therefore be much improved and the system capacity can be greatly increased. With this structure the channel parameters, such as the time of arrival (TOA), direction of arrival (DOA), and complex amplitude of the multipaths can be estimated, and then these information can be utilized for later coherent RAKE combining and downlink beamforming.

In this thesis, we propose a space-time adaptive RAKE receiver for W-CDMA mobile radio systems that provides optimum combination of space-time samples for maximizing the SINR by suppressing MAI and mitigating the fading effects and optimally combining the multipath signals. We evaluate the SINR performance both in uplink and downlink. We model effects of path loss, fading, shadowing, multiple access interference, and the thermal noise; and show that by using an antenna array at the basestation, both in receive and transmit, the system capacity can be increased several-fold.

1.3 Thesis Overview

In this introductory chapter, we have attempted to lay the background for the subject material of this thesis. In chapter 2 we describe a statistical vector channel model based on the physical propagation environment and its statistical properties. The vector channel model will be used in the later chapters of the thesis. In chapter 3, we overview the physical channel and multiplexing structure for dedicated channel with ETSI (European Telecommunications Standards Institute) W-CDMA

(UTRA-FDD) [15]. In chapter 4, we introduce our space-time approach incorporation in the structure of W-CDMA system for estimating the channel parameters and for optimum beamforming, and construct a space-time receiver model to exploit both the spatial and temporal structure of the received multipath signals to maximize performance. We then evaluate the SINR performance of the uplink as a function of the number of users, number of antenna elements, and data transmission rates in chapter 5. The issue of transmitting downlink multiple signals in antenna array system is addressed in chapter 6. In this work we will focus on the FDD case. We study the transmission schemes so that both system capacity and SINR performance for communication over multipath fading channel can be improved.

There are many different adaptive array algorithms that have been proposed. These proposed adaptive array algorithms can be easily combined with our proposed channel estimation algorithm for 2D-RAKE receiver adaptation. In chapter 7 a comparison of different adaptive array techniques is presented. In chapter 8, we briefly summarize the principle and functions of the newly purchased vector channel sounder. We use this vector channel sounder to measure the real channel characteristics on the campus. The measurement data are then employed to simulate the W-CDMA signals and to evaluate the effectiveness of the algorithms we proposed in the previous chapters. Finally, chapter 9 contains concluding remarks and a summary of the thesis.

1.4 Thesis Contributions

Contributions of this thesis are described as follows:

- We have proposed channel parameters estimation algorithms and beamforming algorithms for the 3G W-CDMA basesatation transceiver employing antenna array, which is based on the understanding of the channel characteristics, the correlation properties of the code sequence, the data structure of the physical channel, and the architecture of the basestation;
- We have proposed an effective method to suppress the MAI and increase the SINR of the resultant delay profile, which is obtained by coherently integrating the

matched filter output over different pilot bits and incoherent integrating all matched filter outputs of antenna array element,

- We have compared the uplink and downlink SINR performance obtained by different beamforming methods, including the DOA method, the Complex conjugate method, the DMI method, and the Code Filtering method. We have found that the DOA method and the Complex Conjugate method almost have the same SINR performance;
- We found that the DMI method has the best performance among the different beamforming methods in the uplink, but it has poor performance in the downlink.
- We have proved that the uplink SINR performance after RAKE receiver can approach the theoretical value;
- We have derived an analytical form of the SINR after 2D-RAKE receiver for the DMI method and the simulation results are very close to the analytic values;
- We have compared the single-beam and multiple-beam beamforming techniques considering the independent fading of the uplink and downlink. In the downlink, We found that the multiple-beam method has a better SINR performance in the low SINR region and the single-beam method has a much better SINR performance in the moderate or high SINR region; and
- We have exploited the real channel data measured by a newly purchased vector channel sounder system to simulate the W-CDMA system and compare the uplink and downlink SINR performance using different beamforming techniques.

Chapter 2 Channel Characteristics and Modeling for Wireless Communications

The wireless channel in mobile radio poses a great challenge as a medium for reliable high-speed communication. When a radio signal is transmitted in a wireless channel, the wave propagates and interacts with physical objects and structures therein, such as buildings, hills, streets, pedestrians, lamp poles, trees, and moving vehicles. The effect can cause fluctuations in the received signal's amplitude, phase, and angle of arrival, referred to as multipath fading. The fading effects of mobile communication can be characterized into two types: small-scale (short-term) fading and large-scale (long-term) fading. Small-scale fading is also called fast fading because multipath components interfere each other and the received fields have great fluctuation over a small area [16]. Large-scale fading represents the average signal power attenuation or path loss due to motion over large area [17]. The effects of short-term fading on communications performance are usually described by the error-rate performance of specific modulation schemes. The large-scale fading variations determine the cell coverage. In order to analyze the performance of the wireless communication systems, it is necessary to define statistical models that reasonably approximate the propagation environment. Many statistical models for scalar (single antenna) and vector (multiple antennas) channels have been reported [18,19,20,21]. In order to analyze performance of our proposed adaptive antenna array techniques, it is also necessary to understand statistical vector channel models.

In this chapter, we will first describe the wireless propagation environment. Then, the model and theoretic analysis of scalar wireless channels with fading correlation is evaluated. Based on the scalar wireless channel model and following the Rayleigh's and GWSSUS (Gaussian Wide Sense Stationary Uncorrelated Scattering) vector channel models [22,23], we will derive a statistical and time-variant wireless vector channel model.

2.1 Fundamentals of Radio Propagation

Basically, if propagating characteristics of radio channels are not specified, one usually infers that the signal attenuation versus distance behaves as if propagation takes place over ideal free space. In this idealized free space model, the attenuation of RF (radio frequency) energy between the transmitter and receiver föllows an inverse-square law. The receiver power expressed in terms of transmitted power is attenuated by a factor, where this factor is called path loss or frees space loss. The path loss for the free space model when antenna gains are included is given by

$$PL\ (dB) = 10\ \log \frac{P_t}{P_r} = -10\ \log\left[\frac{G_t G_r \lambda^2}{(4\pi)^2 R^2}\right] \qquad (2\text{-}1)$$

where P_t is the transmitted power, P_r is the received power, G_t is the transmitter antenna gain, G_r is the receiver antenna gain, R is the transmitter and receiver separation distance in meters, and λ is the wavelength in meters.

In a mobile radio channel, a single direct path between the base station and a mobile is seldom the only ideal case for propagation, and hence the free space propagation model of equation (2-1) is in most case inaccurate. For example, a typical mobile radio channel in an urban, the signals travel between the base station and mobile that may be obstructed by several large buildings. Usually, the dense structures have large dimensions compared to the signal wavelength, which cause the waves diffraction. Diffraction is a phenomenon that accounts for RF energy traveling from transmitter to receiver without a line-of-sight (LOS) path between the two. It is often called shadowing effect. This type of fading varies with distances that are proportional to the size of obstructions, and is also referred to as slow fading. The statistics of slow fading provides a way of computing an estimation of path loss as a function of distance. This is described in terms of a mean-path loss (nth-power law) and a Log-normally distributed variation about the mean distance-dependent value [17]. The value of n depends on the specific propagation environment. For example, in free space, n is equal to 2, and when obstructions are present, n will have a larger value. Table 2.1 lists typical path loss exponents obtained in various mobile radio environments [24].

Table 2.1 Path loss Exponents for different environments

Environment	Path Loss Exponent, n
Free space	2
Urban area cellular	2.7 to 3.5
Shadowed urban cellular radio	3 to 5
In building line-of-sight	1.6 to 1.8
Obstructed in building	4 to 6
Obstructed in factories	2 to 3

In addition to the slowing fading, the signals obstructed by the dense structures also yield spreads both in time and angle. An illustration of such an environment is shown in Fig. 2.1.

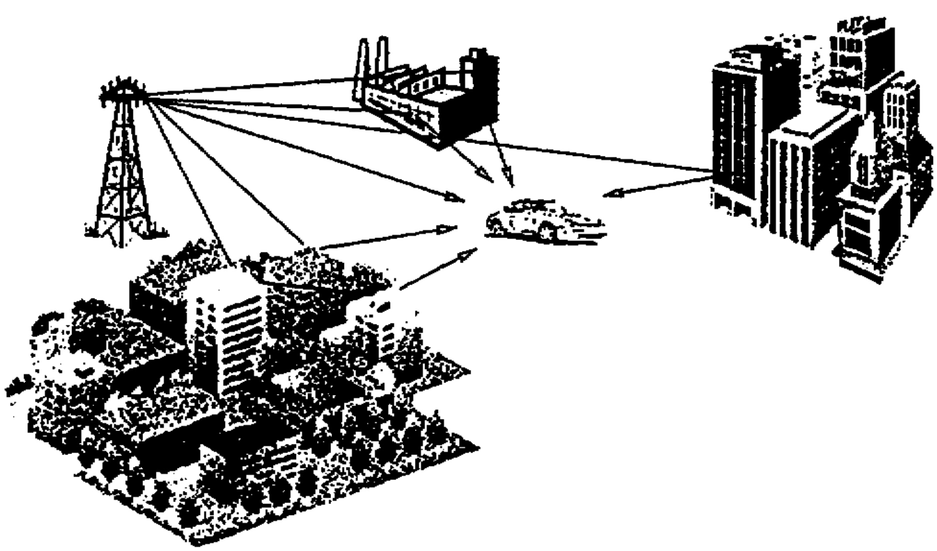

Fig. 2.1 Multiple reception of a signal from reflected and diffracted paths leads to the multipath-fading phenomenon

Besides the time and angle spreading, the amplitude of received signal has a variation due to the phase difference of each path signal, which causes destructive and constructive interference. The resulting variations in the signal amplitude, called multipath fading, vary over distance proportional to the signal wavelength; thus, this type of signal fading is referred to as fast fading.

A mobile radio roaming over a large area usually experiences both types of fading: fast fading superimposed on slow fading and these multipath fadings are the major sources of digital radio communication impairment. Therefore, throughout the rest of this chapter, the statistical model of fast fading channel will be described in detail, and the vector channel model will be built upon the understanding of multipath fading by incorporating additional concepts, such as time delay spread, angle spread, and adaptive array antenna.

2.2 Fast Fading

The statistical model for the fast fading is based on a physical propagation environment consisting of a large number of isolated scatterers with unknown locations and reflection properties.

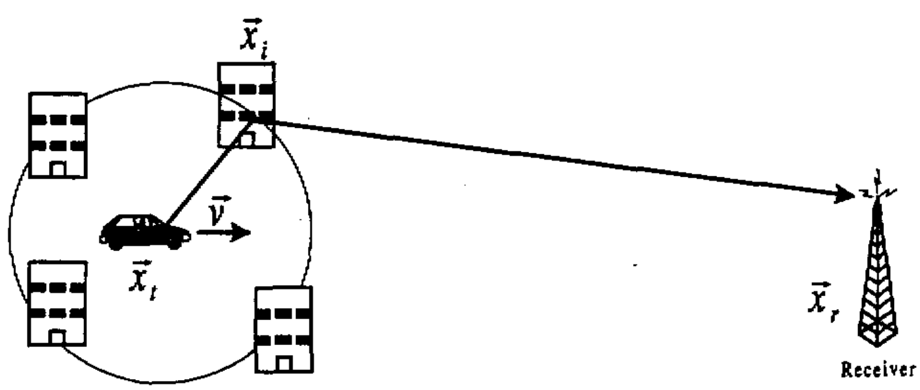

Fig. 2.2 An illustration of the scalar channel

Fig. 2.2 illustrates the scalar mobile radio channel, where the mobile is moving with a velocity vector $\vec{v} = v\hat{v}$. The path delay from the scatterer to the receiver is $\tau_i = c^{-1}(|\ \vec{x}_t - \vec{x}_i\ | + |\ \vec{x}_i - \vec{x}_r\ |)$, where c is the velocity of light, $\vec{x}_t, \vec{x}_i$, and $\vec{x}_r$ are positions of the transmitter, scatterer, and receiver, respectively. Here, only single reflection is considered. Assume that all scatterers are discrete and the geometrical optics approximation is valid, such a scattering configuration leads to δ -peaks impulse response, giving

$$h(\tau) = A\sum_{i}^{L} a_i\delta(\tau - \tau_i) \qquad (2\text{-}2)$$

where A is a real-value number characterizing the long-term propagation loss and L is the total number of multipaths. Here we assumed that the propagation distance spread $\Delta r = \max_i(r_i) - \min_i(r_i)$ is much less than the propagation distance r_i for all i and, therefore, that the attenuation with distance is the same for each component and can be assumed A=1. This is true in general if all reflectors are within the vicinity of the mobile. For the i-th multipath component, a_i^2 is the fraction power of the i-th path. Let the transmitted signal be

$$x(t) = s(t)\cdot e^{j(2\pi ft+\phi_0)} \qquad (2\text{-}3)$$

where $s(t)$ is the complex baseband signal with bandwidth B, f is the carrier frequency, and ϕ_0 is an arbitrary initial phase. Based on the physical electromagnetic wave propagation mechanism [25], we can model the received signal $y(t)$ as the superposition of all multipath components and an additive white Gaussian noise (AWGN) $n(t)$; the corresponding received signal can be written as

$$y(t) = \sum_{i=1}^{L} a_i s(t-\tau_i)e^{(j2\pi f(t-\tau_i)+j(\vec{k}_i\cdot\vec{v})t+\phi_0)} + n(t) \qquad (2\text{-}4)$$

where $\vec{k}_i = k\hat{k}_i$ is the vector wave number.

Let ς_i denote the angle between $\vec{k}_i$ and $\vec{v}$ around the mobile, the term $\vec{k}_i \cdot \vec{v}$ can be written as

$$\begin{aligned} \vec{k}_i \cdot \vec{v} &= (kv)\cos\varsigma_i \\ &= (2\pi v/\lambda)\cos\varsigma_i \\ &= w_d \cos\varsigma_i \qquad (2\text{-}5) \end{aligned}$$

where $w_d = 2\pi v/\lambda$ is the maximum Doppler frequency and λ is the wavelength of the carrier. By (2-4) and (2-5), we can rewrite (2-4) as

$$y(t) = \sum_{i=1}^{L} a_i s(t-\tau_i) e^{(j2\pi f(t-\tau_i)+jw_d\cos\varsigma_i+\phi_0)} + n(t) \qquad (2\text{-}6)$$

If we define the multipath delay spread by

$$T_d = \max_i(\tau_i) - \min_i(\tau_i) \qquad (2\text{-}7)$$

is much less than the inverse bandwidth of the signal ($T_d \ll B^{-1}$), i.e. the observed impulse response is the contributions within a time interval $[\min_i x(\tau_i), \max_i x(\tau_i)]$ from multipaths with the same resolution bin τ_0. This kind of channel is termed flat fading channel. Under this assumption, (2-6) can be rewritten as

$$y(t) \approx s(t-\tau_0)(\sum_{i=1}^{L} a_i e^{j\phi_i(t)}) \cdot e^{j2\pi ft} + n(t)$$

$$= s(t-\tau_0)\beta(t)e^{j2\pi ft} + n(t) \qquad (2\text{-}8)$$

where $\phi_i(t) = w_d \cos \varsigma_i t + \phi_0 - 2\pi f \tau_i$

and

$$\beta(t) = \sum_{i=1}^{L} a_i e^{j\phi_i(t)} = \alpha(t)e^{j\phi(t)} \quad . \qquad (2\text{-}9)$$

The phase $\phi_i(t)$ modulo 2π can be modeled as independent and identically-distributed (i.i.d.) random variables uniformly distributed over $[0, 2\pi]$ and $\alpha(t)$ is the random short-term fading factor. According to the central limit theorem, $\beta(t)$ will approach a zero-mean complex Gaussian random variable as the number of multipaths is large and no correlation between them. In this case $|\alpha(t)|$ has a Rayleigh distribution

$$p(\alpha) = \frac{\alpha}{\sigma} e^{-\alpha^2/2\sigma^2} \qquad (2\text{-}10)$$

where $\sigma^2 = E[\alpha^2]$. The fading phenomenon is primarily a result of the time variations in the phases $\{\phi_i(t)\}$. That is, the randomly time-variant phases $\{\phi_i(t)\}$ associated with the vector $\{a_i e^{j\phi_i(t)}\}$ at times result in the vectors adding destructively or constructively. Fig. 2.3 shows the magnitude for a simulated multipath Rayleigh fading channel as a function of time. The mobile is assumed to be moving with w_d =494(rad). The figure shows that the distance traveled by the mobile in the time interval between adjacent nulls is on the order of a half-wavelength (λ /2). The result is consistent with [24].

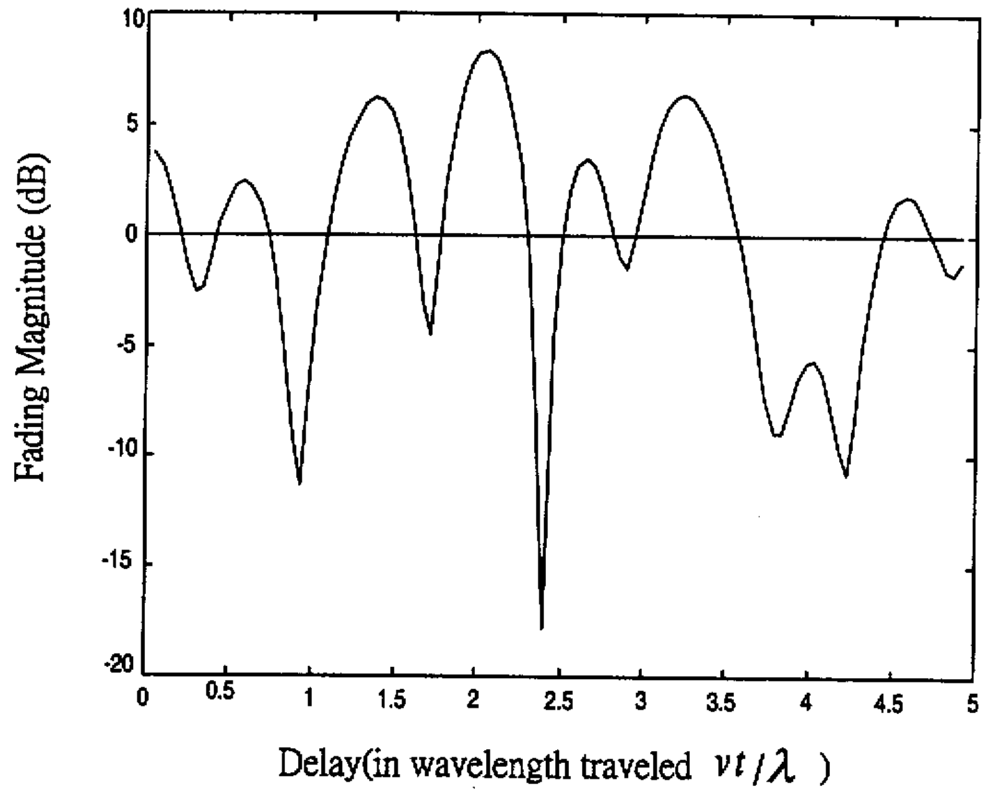

Fig. 2.3 Magnitude of a Rayleigh fading channel: $f_d = 80\ Hz$

Another important function in quantifying the time-varying behavior of the impulse response is the correlation function, giving information about the time development of the fading structure. The auto-correlation function of the fading factor $\beta(t)$ is given by

$$R(\Delta t) = \left\langle \beta(t)\beta^*(t+\Delta t) \right\rangle \qquad (2\text{-}11)$$

where the angular parenthesis denotes averaging over the statistical quantity enclosed.

Neglecting the time dependence of the multipath amplitudes and assuming statistical independence of amplitudes a_i, time delay τ_i and angles ς_i, substituting (2-9) into (2-11), the correlation function $R(\Delta t)$ can be shown that [19]

$$R(\Delta t) = \sum_i \left\langle a^2(\varsigma_i) \right\rangle \left\langle e^{jw_d \cos\varsigma_i \Delta t} \right\rangle$$
$$= \int_0^{2\pi} d\varsigma P(\varsigma) e^{jw_d \cos\varsigma \Delta t} \qquad \text{(2-12)}$$

where we have introduced the angle distribution of the incident power $P(\varsigma)$. Assuming that $P(\varsigma)$ is a uniform distribution with $P(\varsigma) = 1/2\pi$, which corresponds to waves incident uniformly from all directions, it is the traditional model widely used in the mobile radio channel simulations [18,25]. Substituting $P(\varsigma) = 1/2\pi$ into (2-12), we obtain the popular normalized correlation function [25]

$$R(\Delta t) = J_0(w_d \Delta t) \qquad \text{(2-13)}$$

where $J_0(\cdot)$ is the Bessel function of the first kind with order zero. Taking the Fourier transform on both sides of (2-13), we obtain the following U-shape power spectrum density [24,26]

$$s(w) = \frac{2}{w_d}(1 - (\frac{w}{w_d})^2)^{-1/2}, \qquad | w | < w_d \ . \qquad \text{(2-14)}$$

Fig. 2.4 compare the simulated auto-correlation function with the theoretic one for w_d =494(rad). We observe that the magnitude of the simulated auto-correlation function closely resembles the theoretic one. The level of correlation will determine the performance of spatial diversity. In general, larger spacing results in lower correlation, which provides an increased diversity gain for physical antenna element spacing.

Fig. 2.5 shows the simulated U-shape power spectrum density, in which for the value w close to $\pm w_d$ =494(rad) the Doppler component rises to two high peaks at the edges of the spectrum. This should not be surprising, since any dynamic change in the channel (especially, any phase modulation) can be interpreted as due to path length changes, hence, as having Doppler shift. This can be used by a basestation to determine the vehicular speed of a mobile user.

In broadband system, it means that the bandwidth of transmitted signal is not much less than inverse of the multipath delay spread, then the narrowband assumption $s(t-\tau_i) \approx s(t-\tau_0)$ is no longer valid. In this case, the resolution is far better, detailed structures in the impulse response are detectable, leading to frequency-selective fading. The multipath components in a frequency-selective fading channel could be associated into a few groups where the delay spread of each group is much less than the inverse of the signal bandwidth. If we assume a finite number of resolvable paths, (2-8) can be rewritten as

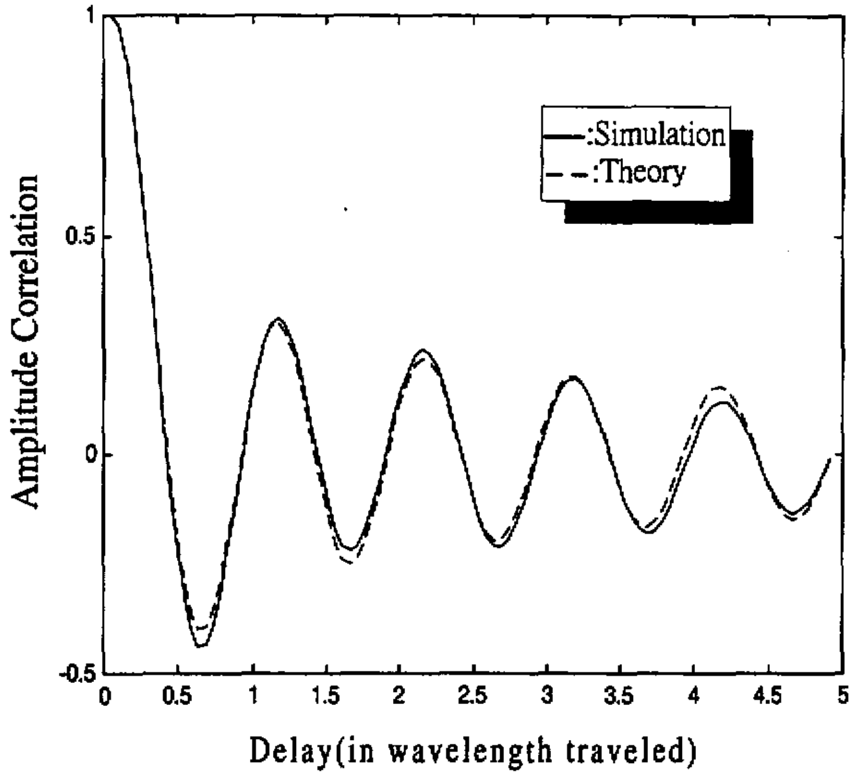

function vs. delay (in wavelength traveled vt/λ)

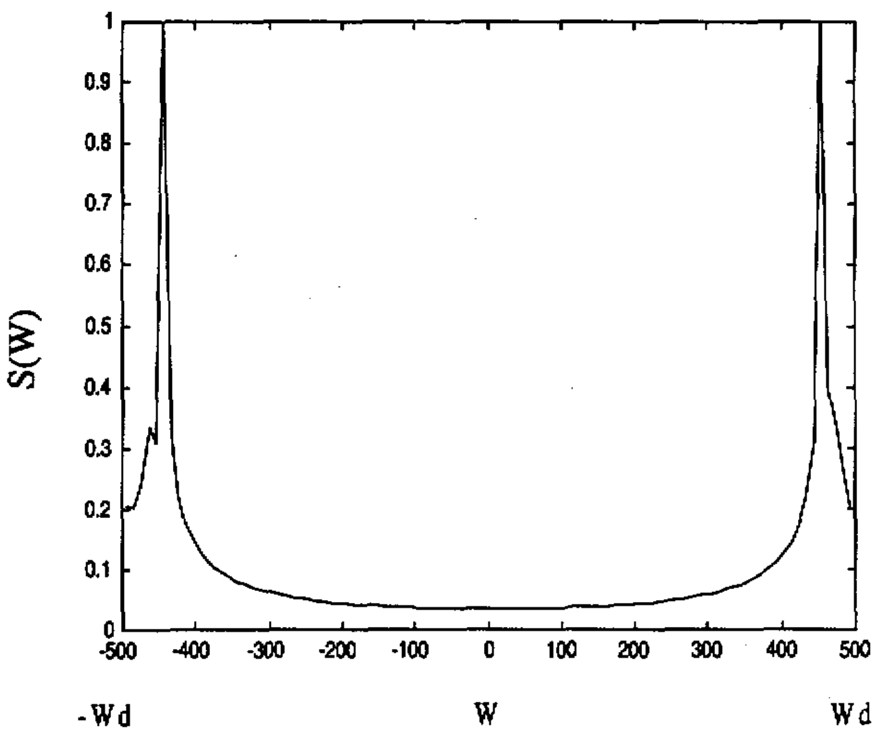

$$y(t) = \sum_{l=1}^{L} A_l x(t - \tau_l) \beta_l(t) + n(t) \qquad (2\text{-}15)$$

where L in this case represents the number of resolvable paths or subpath clusters and A_l is the long-term propagation loss of each resolvable path. The complex gains $\beta_l(t) = \alpha_l(t) e^{j\phi_l(t)}$ are independent complex Gaussian processes. The impulse response of frequency-selective fading channel can be represented by

$$h(t) = \sum_{l=1}^{L} A_l \delta(t - \tau_l) \alpha_l(t) e^{j\phi_l(t)} . \qquad (2\text{-}16)$$

The time correlation property for the complex gain $\beta_l(t)$ is also described by the correlation function in (2-13).

2-3 Vector Mobile Radio Channel

In recent years, array antennas have been proposed as a technique to suppress interfering signals, therefore increasing both the performance and capacity of cellular systems. For example, in W-CDMA systems employing adaptive antennas, the angular (or spatial) distribution of the multipath components is important in determining the performance of the radio link. To properly analyze and implement smart antennas and to exploit spatial processing in emerging wireless systems, accurate radio channel models that incorporate spatial characteristics are necessary. In the vector channel model developed below, we assume that the mobile is in the far field and that the mobile and the antenna array are in the same plane. Under the assumptions, only azimuth angles are considered in the following propagation environment.

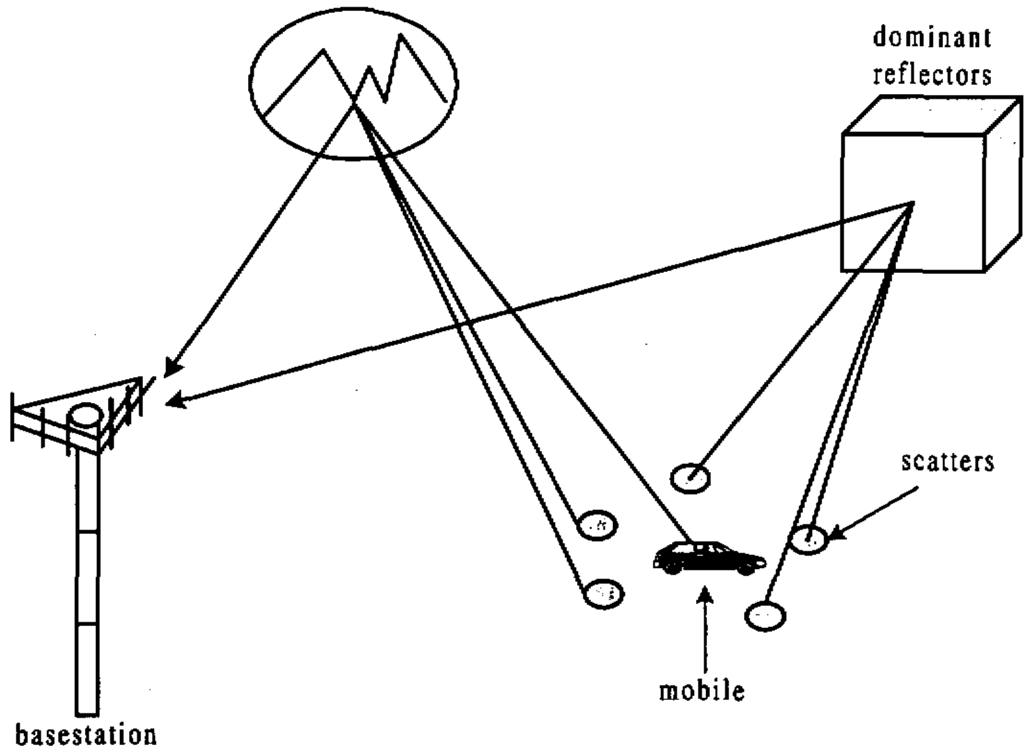

Fig. 2.6 Illustration of Rayleigh's and GWSSUS vector channel model signal environment

The signal fading described in the previous section assumed that receiving antenna is a single antenna. At the mobile station, the signal arrives at the receive antenna coming from all directions due to the radio waves bouncing from the surrounding scatterers. Thus, the angle of arrival being uniformly distributed over [0, 2π] is a valid assumption. However, the distribution of angle of arrival (AOA) at the basestation is quite different. The multipath components at the basestation are restricted to an angular region, Δ, and the distribution of the AOA is no longer uniform over [0, 2π]. A number of realistic spatial channel models have been proposed [20,21,22,23]. Some of models provide information about only one single channel characteristic, such as angle spread to predict the correlation between the signals received by two elements as a function of element spacing at the basestation or mobile. The other models attempt to capture all the properties of the wireless channel, such as Rayleigh's and GWSSUS vector channel models. Fig. 2.6 illustrates the vector mobile radio channel.

The antenna array of the basestation is assumed to be a uniform linear array (ULA).

The individual elements of the array are ideal sectorized antennas with a sector of 120° degrees. The propagation environment considered is densely populated with large dominant reflectors such as large buildings and other structure. The model assumes that the antenna array is mounted relatively high and there is no signal scattering from scatterers near the base station. It is assumed that at particular instant of time, the channel is characterized by L resolvable multipath. Some multipaths are built up by a large number of local scaterers around the mobile, while others are reflected from large dominant reflectors. The amplitude of each multipath component is modeled as a Rayleigh superimposed on Log-Normal distributed random variable while the phase shift is uniformly distributed. The direction of arrival (DOA) for each path is determined by the physical location of the corresponding dominant reflector.

Assuming that the antenna array is a narrowband array, i.e. the time taken for the wavefront to pass through the array is much smaller than the symbol duration. For a ULA with spacing d between elements, taking the first element as the reference point, the array response vector can be written as [27,28]

$$\mathbf{a}(\theta)=[1, e^{j2\pi f \sin\theta\, d/c}, \cdots, e^{j2\pi f \sin\theta (M-1) d/c}]^T \tag{2-19}$$

where f, c, and T denote the carrier frequency, speed of light, and transpose operator, respectively. By including resolvable multipath and array response vector, the channel impulse response in (2-16) can be modified to yield the vector channel impulse response as

$$\begin{aligned}\mathbf{h}(t) &= \sum_{l=1}^{L} A_l \delta(t-\tau_l)\alpha_l(t) e^{j\phi_l(t)}\, \mathbf{a}(\theta_l) \\ &= \sum_{l=1}^{L} \delta(t-\tau_l)\, \mathbf{v}(t)\end{aligned} \tag{2-20}$$

where $\mathbf{v}(t)$ is defined as the complex channel vector. For frequency-selective fading vector channels, the corresponding received signal at the basestation (2-8) can be rewritten as

$$\mathbf{y}(t)=\sum_{l=1}^{L} A_l x(t-\tau_l)\mathbf{v}(t)+\mathbf{n}(t) \qquad (2\text{-}21)$$

It is noted that each propagation path arriving at the basestation has its own time delay and DOA, which causes delay spread and angle spread in the received signal.

The vector channel model can be simulated in the following manner. For a given user, L dominant reflectors are generated. By changing the number of dominant reflector paths, the density of the simulation environment can be varied from a sparse rural model to a dense urban model. For each path, $\beta_l(t)=\alpha_l(t)e^{j\phi_l(t)}$ is generated by using Eq. (2-9) with a complex Gaussian distribution. The path delay values are generated from a uniform distribution over [0, $\tau_{\max}$]. The DOA for each path is taken from uniformly distributed over [-$\pi/3$, $\pi/3$].

The antenna array at the basestation can be beamformed in the uplink and downlink to increase SINR, where a set of weights is employed to reduce received (transmitted) co-channel interference in the uplink (downlink). The parameters determine the uplink (downlink) weight vectors for performing on the received (transmitted) signals that is based on spatial signature [29], array responses, or direction information (DOAs) [30,31]. This weight vectors are usually estimated from the uplink signals. As the mobile position varies, the DOA of each path will change. The DOAs are varied according to relative positions among the basestation, the reflectors and the mobile station. Thus, if changes in the spatial channel are small over the time from start of the uplink slot to the end of the downlink slot, will the downlink and uplink channel be approximately the same. Only then can the estimated spatial signatures or DOAs from uplink be used directly in the downlink.

Now we show a simulation example with the channel model to present the variation of channel during 3ms. There is one desired user and one interfering mobile all traveling at speed of 50km/hr. Each mobile has 12 random dominant reflectors. Six reflectors are restricted to an angular interval of 10^0 centered at a mean angle θ.

The other dominant reflectors are uniformly distributed over [$-\pi/3, \pi/3$]. An example of simulation results is shown in Fig. 2.7. Fig. 2.7 (a) shows a polar plot of the amplitudes and DOAs of each multipath. Obviously, the amplitude and DOA have little variation during a short time interval. It is also noted that each multipath has an independent Rayleigh fading. The DOA and relative TOA of the multipaths of the desired user are shown in Fig. 2.7 (b). This yields an environment with a realistic spread of the signal both in time and angle.

2.4 summary

In this chapter, we overview the radio channel models and describe some propagation characteristics associated with a wireless radio channel. Based on the Rayleigh's and GWSSUS models we derive a dynamic vector channel model. Such a model is important in order to understand the antenna array channels and evaluate performance of the proposed 2D-RAKE receiver.

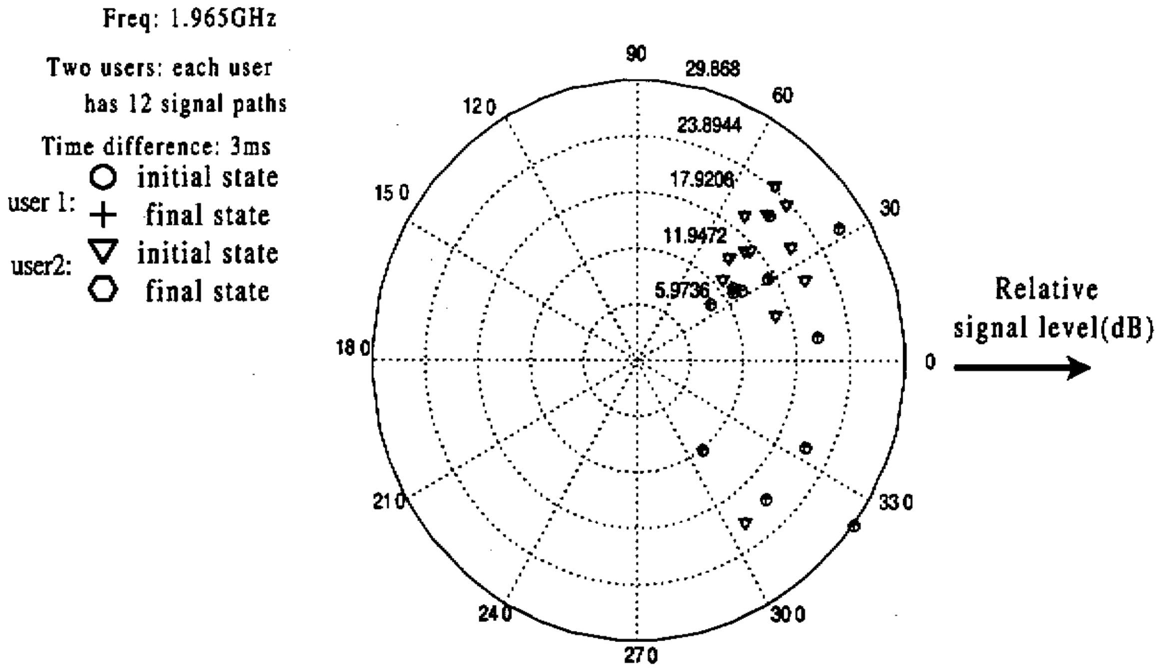

(a)

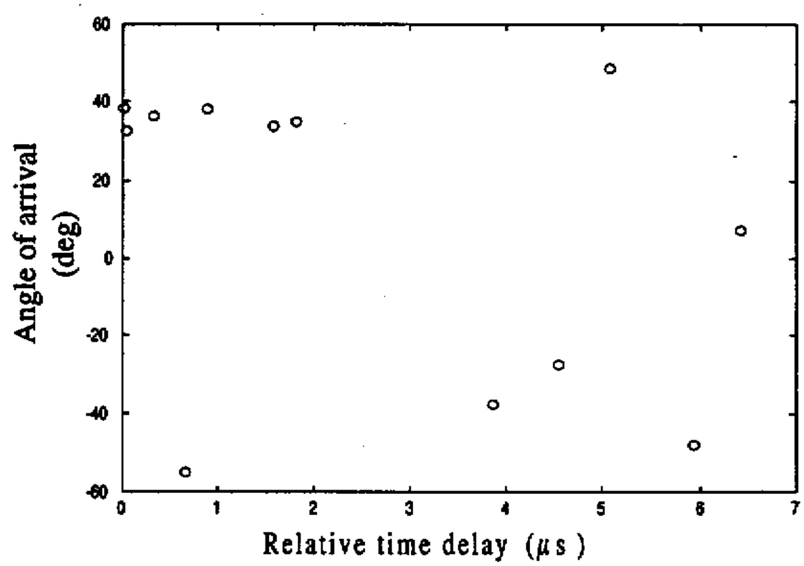

(b)

Fig. 2.7 A 2D-channel impulse response for urban macrocell: (a)path loss with respect to reference distance (1m) vs. DOA, (b) 2D-channel impulse response (DOA vs. time delay)

Chapter 3 Overview of the Wideband CDMA Wireless Communication System

In CDMA communication systems, all mobile users share the same carrier frequency and multiple access can be achieved by assigning each user a specific spreading code. Under the ideal case, orthogonality among the spreading codes can be assumed. The orthogonality of the spreading codes with a time correlation operation makes CDMA communication system possible for simultaneous transmissions in the same frequency band. The desired user with a successfully detected spreading code can get the access and the other users get the noise due to decorrelation. Each user operates independently with no knowledge of other users. This is the reason why CDMA system can have multiple access ability, just as TDMA and FDMA system can.

Another advantage for CDMA is its fully utilization of the time dispersive effects of multipath channels. Multipath is a troublesome effect in many communications, especially for narrowband communication systems. Besides the direct path signal, many other reflected paths arrived at the receiver with different delays and attenuation resulting in fading as described in last chapter. In CDMA systems, the use of a signal with bandwidth much higher than the channel coherent bandwidth can resolve the multipath components, which will mitigate the multipath fading effects and provide path diversities to improve the link performance. The diversity is exploited by the use of a RAKE receiver, which use several fingers to combine the dominant multipath signals. The currently IS-95 CDMA standard already incorporates a RAKE receiver with four fingers in uplink and three fingers in downlink [32]. Thus, CDMA has advantages over TDMA and FDMA and improve performance in terms of capacity or coverage.

Despite the existing IS-95 technology shows its effectiveness in capacity, it has some weak points as compared to conventional wireline services. For example, high qualities of voice communication, use of widespread voice band data service and high-speed data communication are impossible. Wideband CDMA is a strong candidate for the radio access of the third generation mobile communication system, and many researches have been down in this area [33,34,35]. W-CDMA is defined as a direct sequence spread spectrum multiple access scheme where the information is spread over a bandwidth of approximately 5 MHz or more. W-CDMA can provide broadband data to support video, internet access, and other high-speed data services. Future wideband systems may have some new features compared to the existing IS-95 systems, such as pilot-symbol-assisted channel estimation, coherent multi-code DS-CDMA, diversity handover and so on. In the rest of this chapter, we will briefly describe the different signal processing function used for uplink and downlink physical channels of the W-CDMA concept selected by ETSI for the FDD component of UTRA. The information presented is based on a chip rate of 4.096Mcps/s. The chip rate can be extended for higher chip rates of 8.192Mcps/s and 16.384Mcps/s.

3.1 Uplink Physical Channel

Figure 3.1 illustrates the spreading and modulation for the case of a signal uplink physical channel. There are two types of uplink physical channels, physical data channel and control channel. The data and control channels are separated and modulated by separate BPSK on the I- and Q-channel respectively. The I- and Q-branches are then spread to the chip rate with two different channelization codes c_D/c_C (real spreading) and subsequently complex scrambled by a mobile user equipment specific complex scrambling code c_{scramb} (complex scrambling). The I-Q/code results to a signal with envelope properties identical to normal QPSK although the data and control channels have large power difference. The control channel has a fixed bit rate channel with 16Kbits/sec and has a spreading ratio of 256. The data channel uses spreading ratios from 256 down to 4, which respect to the data rates from

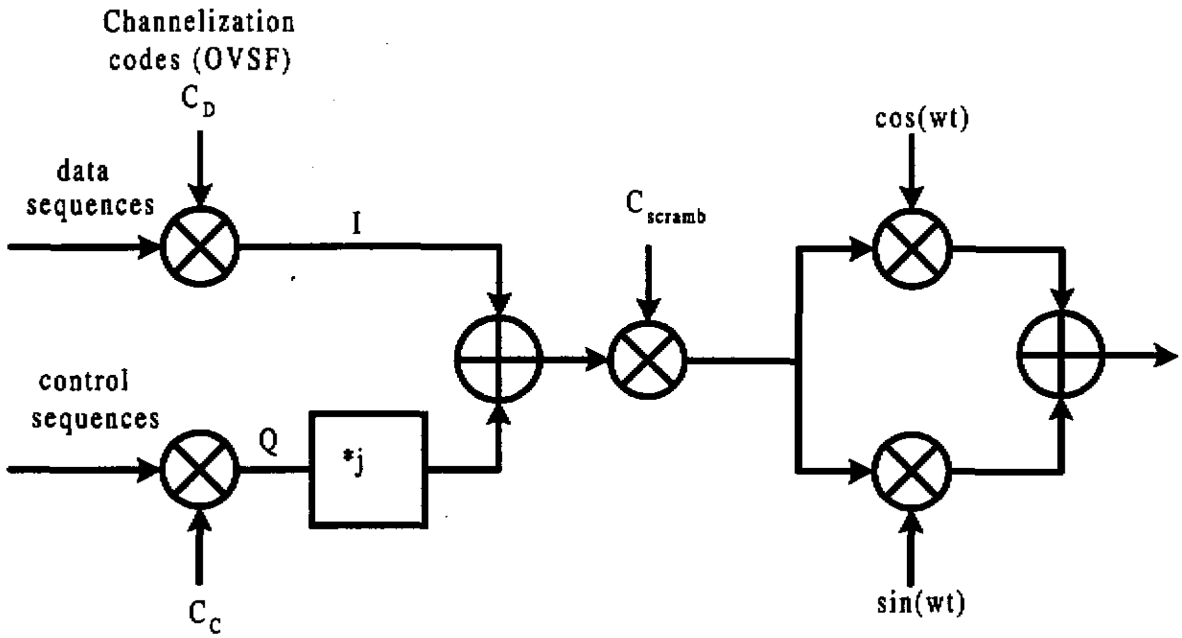

Figure 3.1 Spreading/modulation for uplink dedicated physical channel

16Kbits/sec up to 1024Kbits/sec. The channelization codes of figure 3.1 are Orthogonal Variable Spreading Factor (OVSF) codes that preserve the orthogonality between different users' physical channels. The OVSF codes can be described by using the code tree of figure 3.2, where SF represents the spreading factor and c_{ij} is the OVSF code. All codes within the code tree cannot be used simultaneously by one mobile user. The number of available channelization codes is not fixed but depends on the data rate and spreading factor of each physical channel. This means that the data rate is allowed to vary frame-by-frame. This is referred to as a variable spreading factor (VSF) technique [15]. Either short or long scrambling codes should be used on the uplink. In order to minimize the cell search time, the short code with an orthogonal short Gold code of length 256 chips spanning one symbol is used. However, in certain cases, the use of short codes may lead to bad cross-correlation properties, especially with very small spreading factor.

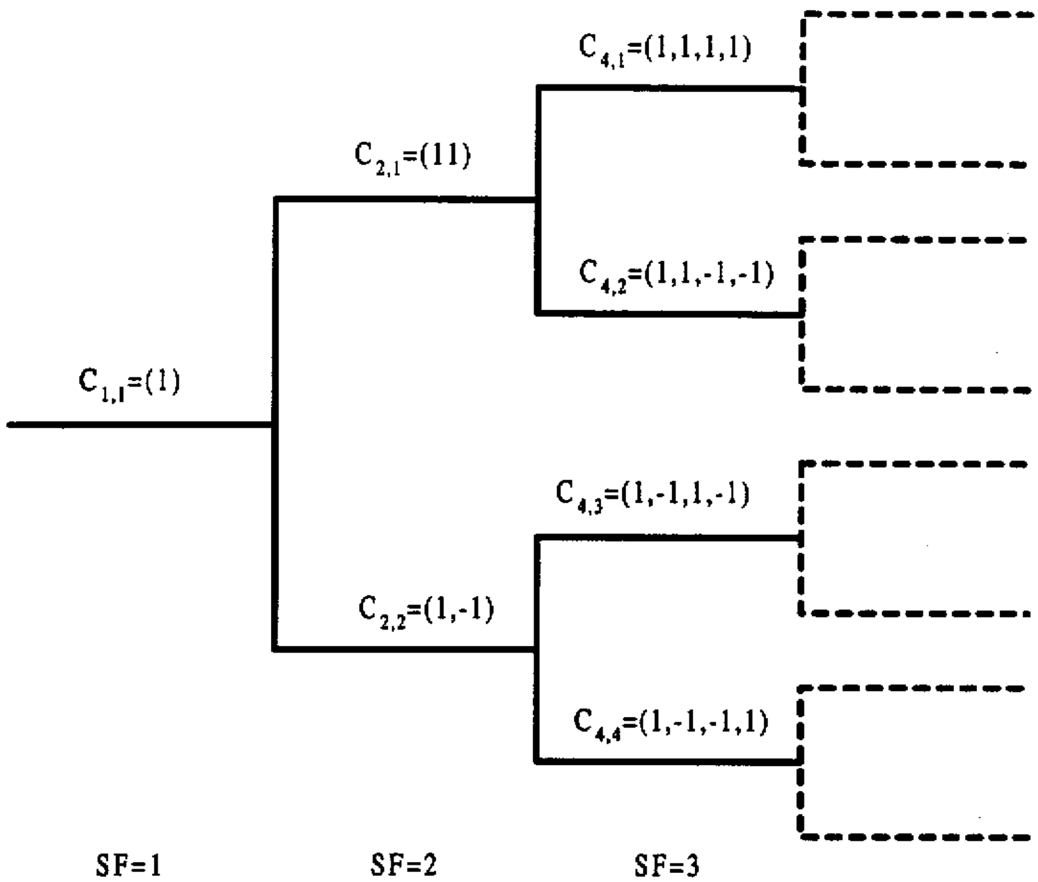

Figure 3.2 Code-tree for generation of Orthogonal Variable Spreading Factor (OVSF) codes

In cells, where there is no gain in implementation using the short code, the long code is used instead due to its better interference averaging properties. A long code is defined to be a sequence with a period that exceeds the duration of a data symbol. The long code (40960 chips) proposed by W-CDMA systems uses a long Gold sequences with repetition period of 2^{41}-1 chips.

The control information consists of known pilot bits to support channel estimation for coherent detection, transmit power-control (TPC) commands, and an optional transport-format indicator (TFI). The TFI informs the receiver about the instantaneous parameters of the different transport channels multiplexed on the uplink physical control channel. Figure 3.3 shows the frame structure of the uplink physical channel. Each frame of length 10ms is split into 16 slots, each of which 0.625ms long.

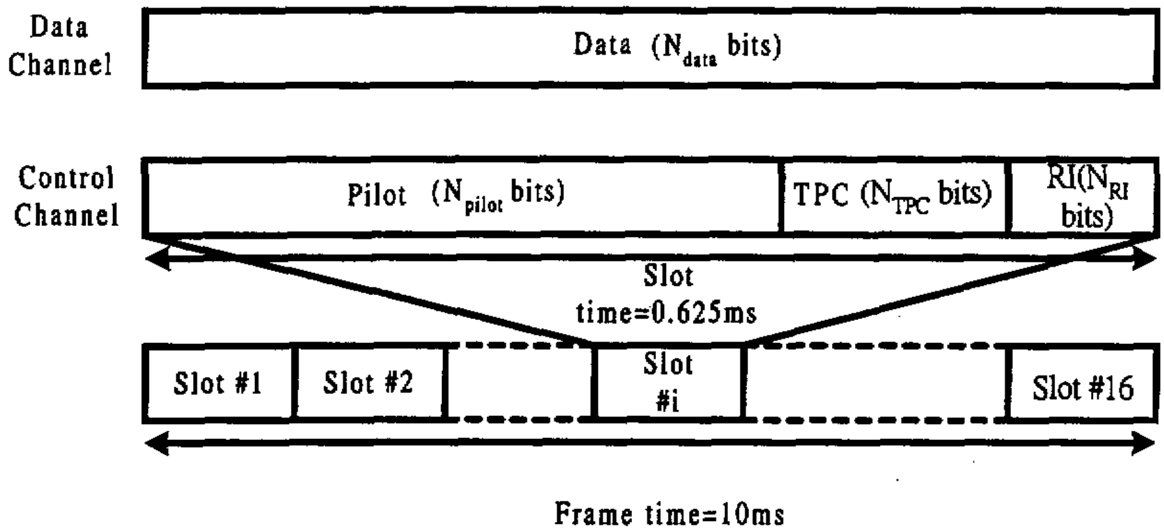

Figure 3.3 Frame structure for Uplink

3.2 Downlink Physical Channel

The downlink physical channel has structure different from the uplink physical channel. In the downlink the control and data channels use time multiplexing where they are jointly sharing a QPSK modulated channel and share the symbols inside 0.625ms time slot so that control information is always in the beginning of the slot. The known pilot symbols are used for channel estimation at the mobile unit. Figure 3.4 shows the frame structure of the downlink physical channel. Each frame of length 10ms is split into 16 time slots, each of which 0.625ms long. The reasons for the different design between the uplink and the downlink channel structures come from the different requirements. In the uplink it is important to have such a solution which leads to efficient modulation from the amplifier power utilization point of view and avoids multicode usage as long as possible. This is because the power level in the I- and Q-branches is unbalanced due to their possibly different bit-rates. Hence the I- and Q-branches with a complex scrambling code can improve the power level by reducing the peak-to-average power fluctuation and release the linearity requirement of power amplifier [32]. Also using continuous pilot in the uplink makes demodulation of uplink channels at the base station easier, and therefore the hardware complexity of the base station modem can be reduced [36].

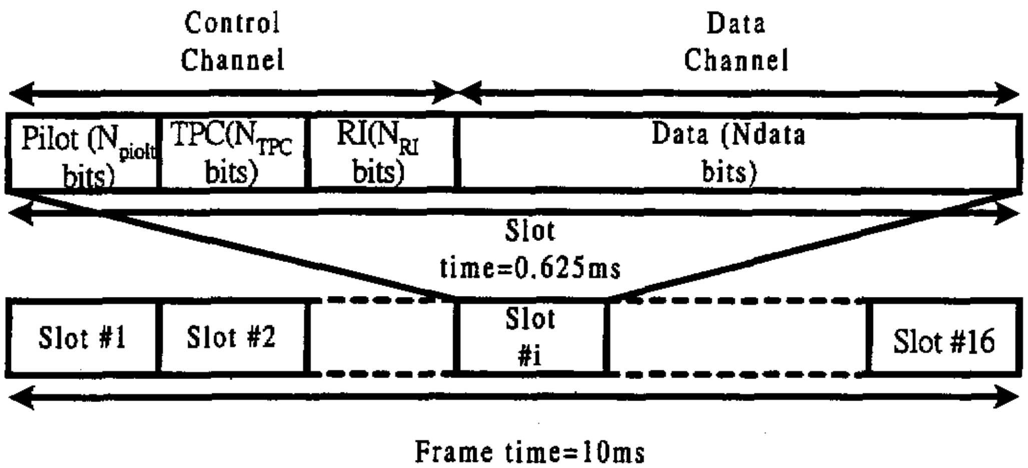

Figure 3.4 Frame structure for Downlink

In the downlink channelization codes and scrambling codes are also employed. The channelization codes are the same as used in the uplink, which preserve the orthogonality between downlink channels of different rates and spreading factors. The scrambling code (40960 chips) uses a short or long Gold code sequence with repetition period of 2^{18}-1 or 2^{41}-1 chips, respectively. The purpose of using a short Gold code in the downlink is to fascinate a fast cell search. Different physical channels use different channelization codes, while the scrambling codes used for all physical channels in one cell are all the same. Figure 3.5 illustrates the spreading and modulation for the case of a single downlink physical channel. Data modulation is QPSK where each pair of two bits is serial-to-parallel converted and mapped to the I- and Q-branches. They are then spread to the chip rate with the same channelization code c_{ch} (real spreading) and subsequently scrambled by the same cell specific scrambling code (real scrambling).

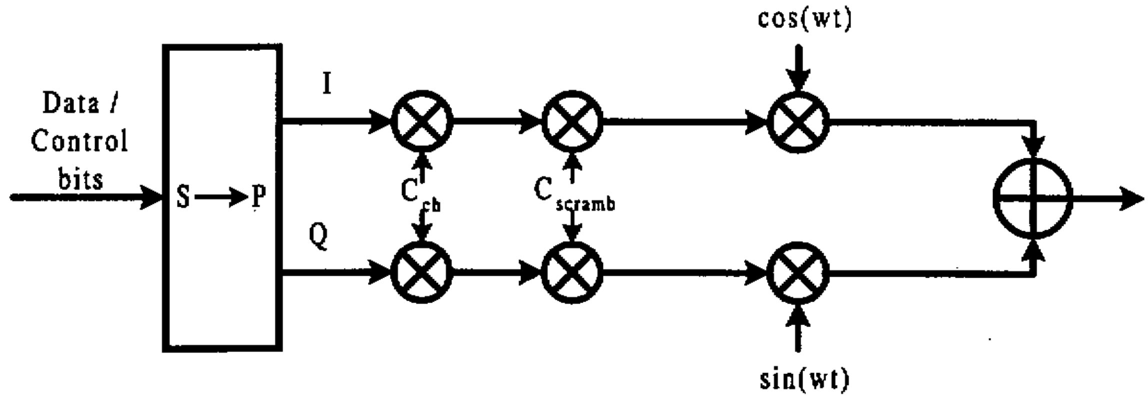

Figure 3.5 Spreadong/modulation for downlink dedicated physical channel

3.3 Summary

In this chapter, we briefly described the signal processing functions separately applied in the uplink and downlink physical channel. The physical data channel and control channel is I/Q code multiplexed in the uplink and time multiplexed in the downlink. In the following chapters, we will exploit an advanced array signal processing technique, which is based on the signal processing functions used in physical channel. And the result will put W-CDMA wireless communication systems into practice from theoretical argument.

Chapter 4 Channel Estimation Algorithm of 2D-RAKE Receiver for the W-CDMA System

The number of cellular subscribers continues to grow at a rapid pace, service providers are forced to find new methods to increase capacity of their networks. As the number of users per cell increases, the level of interference seen by any user also increases. To accommodate more users in a cell, cell splitting is usually employed, where bigger cells are split into smaller ones. Smaller cell size results in increased interference from neighboring cells. Co-channel interference becomes a performance-limiting factor, especially after cell splitting when the available channels are reused in smaller sized cells over the same service area and the same total bandwidth. In a CDMA system, system performance is very much dependent on MAI which is caused by the cross-correlation between the desired user's signal and other users' signals from the own cell and neighboring cells. An adaptive antenna array at the basestation can significantly reduce co-channel interference and, hence, increase the capacity of the cell. In addition to the spatial processing with basestation antenna arrays, the receiver can exploit the time diversity (RAKE combiner) to provide a more efficient combining of multipath signals. The SINR can therefore be much improved and the system capacity can be greatly increased. With this structure the channel parameters, such as the direction of arrival (DOA), time of arrival (TOA), and complex amplitude of the multipaths have to be estimated and these information can be utilized for later spatial processing, coherent RAKE combining and downlink beamforming. This requires the transmission of a pilot signal to obtain good channel parameter estimates. Such a 2D-RAKE receiver can be easily incorporated into the proposed W-CDMA standards.

In the W-CDMA system proposed by ETSI, pilot symbols-aided channel estimation is used in both the uplink and downlink. In the uplink, the data and pilot are separately BPSK modulated on the I- and Q-branch separately. Every user uses different long or short scrambling codes. At the receiving end, after passing through the matched filter the desired signal can be enhanced by a factor of the processing gain and the interference can be suppressed. The time domain output of the matched filter gives the TOA of the multipaths. Conventionally the TOAs are estimated by the matched filter output integrated over 1 pilot bit interval. Due to the nonzero cross-correlation between the chip sequences of the desired user and the interferers, at the matched filter output we may not be able to differentiate the desired signal from the interference when the number of undesired users increases to a certain amount. The chosen paths for later RAKE combining may be the wrong paths and this will degrade the SINR performance after RAKE combining. In this chapter we will propose algorithms that the TOA of the desired paths can be accurately obtained.

Many adaptive-array processing algorithms have been proposed to optimize the SINR [27,37]. The basic concept is to synthesize a beam pattern so that the interfering signals can be nulled. However, the number of interfering signals that can be nulled is only M-1 if M antenna elements are used. In fact, in the W-CDMA systems the number of interfering signals is usually much greater than the number of antenna elements. Therefore, the conventional adaptive array processing algorithms are not effective in reducing the interference. In this chapter we propose algorithms to determine the DOA of the desired signals and propose simple beamforming methods to point the main beam to the desired user.

4.1. Space-Time Signal Model

A broadband system means that the bandwidth of the transmitted signal is comparable to or greater than the inverse of the multipath delay spread. In the broadband system, detailed structures of the impulse response can be obtained. The multipath components in a broadband system can be associated into a few groups and each group has a delay spread much less than the inverse of the signal bandwidth. Each group can also have different fading effects. If we assume that there are a finite number of resolvable paths, the impulse response of the *k-th* user can be written as

$$h_k(t) = \sum_{l=1}^{L_k} \alpha_{k,l} e^{j\phi_{k,l}} \delta(t - \tau_{k,l}) \qquad (4.1)$$

where $\alpha_{k,l}$, $\phi_{k,l}$, and $\tau_{k,l}$ are the amplitude, phase shift, and time delay of the *l-th* multipath component, and L_k is the number of paths. In mobile communication systems, the time delay for the wavefront passing through the antenna array is much smaller than the chip interval T_c and therefore, the antenna array can be considered as a narrowband array. For a ULA with spacing d between elements, taking the 1st element as the reference point, the $\mathrm{M} \times 1$ array response vector $\mathbf{a}_k$ for the *k-th* user can be written as

$$\mathbf{a}(\theta_{k,l}) = [1,\ e^{j2\pi d \sin\theta_{k,l}/\lambda}, \ldots,\ e^{j2\pi (M-1) d \sin\theta_{k,l}/\lambda}]^{\mathrm{T}} \qquad (4.2)$$

where $\theta_{k,l}$ is the DOA of the *l-th* path of the *k-th* user and the superscript T represents the transpose operator. The set of array response vector for all angles of arrival is referred to as the array manifold [26]. Assuming there are K users, the received baseband signal vector $\boldsymbol{x}(\mathrm{t})$ can be written as

$$\mathbf{x}(t) = \sum_{k=1}^{K} \sum_{l=1}^{L_k} \sqrt{p_k} \alpha_{k,l} e^{j\phi_{k,l}} \sum_{n=-\infty}^{n=\infty} b_k(n) c_k(t - nT_b - \tau_{k,l}) \mathbf{a}(\theta_{k,l}) + \boldsymbol{n}(t) \qquad (4.3)$$

where p_k is the average power from the *k-th* user, $b_k(n)$ is the *n-th* bit value, $c_k(t)$ is the spreading waveform assigned to the *k-th* user and T_b is the bit period. The thermal noise $\boldsymbol{n}(t)$ is assumed to be white in both time and space and has a variance σ^2, i.e.,

$$E(\mathbf{n}_i(t_1)\mathbf{n}_j^H(t_2)) = \sigma^2 \mathbf{I} \delta(t_1 - t_2) \delta(i - j) \qquad (4.4)$$

where $\boldsymbol{n}_m(\mathrm{t})$ is the thermal noise of the *m-th* antenna element, $(\cdot)^{\mathrm{H}}$ denotes the Hermitian transpose, and $\mathbf{I}$ is the MxM identity matrix.

In the next section, we will propose an algorithm to estimate the channel parameters $\alpha_{k,l}$, $\tau_{k,l}$, $\phi_{k,l}$ and $\theta_{k,l}$, which respectively denote the gain, delay, phase and the DOA of the paths received by the desired user in eq.(4.3).

4.2 New Algorithm for Channel Estimation

In the W-CDMA system proposed by ETSI, the known pilot bits can be used as the reference signals for channel parameter estimation. In the reverse link, the data and pilot are separately BPSK modulated on the I- and Q-branch respectively. The binary data and pilot bits are spread using different OVSF (Orthogonal Variable Spreading Factor) codes to preserve orthogonality between the data and pilot channels. Every user's pilot channel uses the same OVSF code for spreading, but each user's data channel uses different OVSF codes for spreading. The purpose is to keep the orthogonality between different users' data channel that can be preserved or transmitted on either I- or Q-branch. Following, we will firstly consider the mathematical model for the RF channel observed at an antenna array and introduce how to separate the I- and Q-branch data sequence. The Q-branch pilot sequence could be exploited to estimate the channel amplitudes, phases, and array response vectors.

4.2.1 I- and Q-branches Demodulation

Referring back to Fig. 3.1 the baseband representation of the In-phase and Quadrature components of the signal to be transmitted is

$$v_b = \sum_{n=0}^{N-1}(b_d + jb_p)u_1(t - nT_b) \tag{4.5}$$

where $\{b_d\}$ and $\{b_p\} \in (\pm 1)$ represent In-phase data sequence with equal probability and Quadrature known pilot sequence, respectively, and

$$u_1(t) = \begin{cases} 1 & 0 \le t \le T_b \\ 0 & otherwise \end{cases} \tag{4.6}$$

Assuming that data and pilot sequence have the same transmitted rates for convenience. Each information component is multiplied by the following OVSF codes:

$$c_d = \sum_{i=0}^{I-1} c_n^{(I)} u_2(t - iT_c) \tag{4.7}$$

and

$$c_c = \sum_{i=0}^{I-1} c_n^{(Q)} u_2(t - iT_c) \tag{4.8}$$

where $c_n^{(I)}$ and $c_n^{(Q)} \in \{\pm 1\}$ are associated into different OVSF codes in I- and Q-branch, respectively, T_c is the chip duration, I is the number of chips in OVSF code (or chips / bit) and

$$u_2(t) = \begin{cases} 1 & 0 \le t \le T_c \\ 0 & otherwise \end{cases} \tag{4.9}$$

A further complex scrambling code is multiplied so that the basestation can differentiate the different mobile signals. The W-CDMA systems use the complex Gold code as complex scrambling code. The Q-branch Gold code is a shifted version of the I-branch Gold code, where a shift of 1024 chips was recommended. Let $c_s^{(I)}$ and $c_s^{(Q)}$ be the I- and Q-branch scrambling codes, respectively. The output of Fig. 3.1 becomes:

$$\begin{aligned} v_t(t) = \sum_{n=0}^{N-1} \sum_{i=0}^{I-1} [& (b_d c_n^{(I)} c_s^{(I)} - b_p c_n^{(Q)} c_s^{(Q)}) \cos w_c t \\ & - (b_d c_n^{(I)} c_s^{(Q)} + b_p c_n^{(Q)} c_s^{(I)}) \sin(w_c t)] u(t - iT_c - nT_b) \end{aligned} \tag{4.10}$$

With equation (4.1) and if only one user is assumed and the thermal noise is negligible, it is a straightforward matter to see that the received signal at one of antenna elements is

$$x_R(t) = \sum_{n=0}^{N-1}\sum_{i=0}^{I-1}\sum_{l=1}^{L}\alpha_l e^{j\phi_l}[(b_d c_n^{(I)} c_s^{(I)} - b_p c_n^{(Q)} c_s^{(Q)})\cos w_c t$$
$$-(b_d c_n^{(I)} c_s^{(Q)} + b_p c_n^{(Q)} c_s^{(I)})\sin(w_c t)]u(t - iT_c - nT_b - \tau_l) \quad (4.11)$$

where w_c is the carrier frequency. Assuming that initial carrier recovery can be achieved during random access duration or following information sequences. One method of separating out the I- and Q-branch data at basestation is shown in Fig. 4.1.

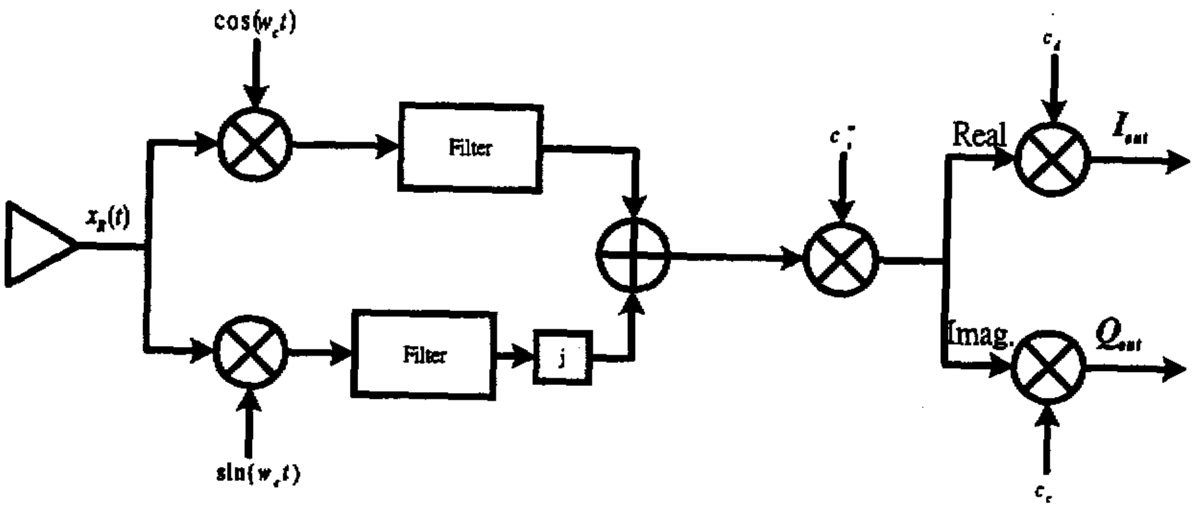

Fig. 4.1 The structure of basestation receiver for each array element

The received signal $x_R(t)$ is mixed down to baseband, multiplied by the conjugate complex scrambling code c_s^*, taking real and imaginary part multiplied by C_d and C_c respectively, and integrated over one bit period. Assuming as negligible the contribution of the auto-correlation of C_s, C_d, and C_c, when $\tau_i \neq \tau_j$, the demodulation output of I_{out} and Q_{out} are given by

$$I_{out}(t)=T_b\sum_{n=0}^{N-1}\sum_{l=1}^{L}b_d\alpha_l e^{j\phi}\delta(t-nT_b-\tau_l) \tag{4.12}$$

and

$$Q_{out}(t)=T_b\sum_{n=0}^{N-1}\sum_{l=1}^{L}b_p\alpha_l e^{j\phi}\delta(t-nT_b-\tau_l) \tag{4.13}$$

Obviously, the data and pilot sequences can be separated with the known OVSF and scrambling codes. If the Q_{out} outputs of all antenna elements are considered, equation (4.13) can be rewritten as

$$\mathbf{Q}_{out}(t)=T_b\sum_{n=0}^{N-1}\sum_{l=1}^{L}b_p\alpha_l e^{j\phi}\delta(t-nT_b-\tau_l)\mathbf{a}(\theta_l) \tag{4.14}$$

In equation (4.14), channel amplitudes, phases, and array vectors can be estimated by multiplying Q_{out} with the known bit sequence b_p.

4.2.2 Algorithm for Channel Estimation

In a multipath scenario, different paths will arrives at the receiver with different delays, the orthogonality of codes by oneself and among different users tends to diminish because of increasing inter-path interference. After having completed acquisitions of the spreading sequence of each user k, the Q branch is coherently demodulated and the received signal is despreaded. The matched filter is used to distinguish the desired user's signals from the co-channel interference. The time-domain output of the matched filter is referred to as the delay profile, and its time resolution is about the chip interval T_c.

Without loss of generality, assume that the 1st user is the desired user and code synchronization has been obtained with respect to the first user's signal. The output of the matched filter for the *n-th* pilot bit can be written as

$$Q_{out}(\tau)=T_b b_{1,p}(n)\sum_{l=1}^{L}\alpha_{1,l}e^{j\phi_{1,l}}\delta(\tau-\tau_{1,l})\mathbf{a}_1(\theta_{1,l})$$

$$+\mathbf{s}_1(\tau)+\mathbf{m}_1(\tau)+\eta_1(\tau) \quad , \; 0 \le \tau \le T_b \qquad (4.15)$$

where s_1 is the self-interference signal vector due to other multipath components of the first user, m_1 is the MAI vector, and η_1 is due to the thermal noise.

In (4.15), the noise term η_1 can be written as

$$\eta_1(\tau)=\int_{(n-1)T_b+\tau}^{nT_b+\tau} n(t)\tilde{c}_1(t-\tau)dt \qquad (4.16)$$

where $\tilde{c}_k = c_{k,s}^* \cdot c_d$ is the inner product of complex conjugate scrambling and OVSF of pilot code. We can show that η_1 is a Gaussian random vector with a mean of zero and a variance of $\sigma^2\mathbf{I}$.

The self-interference due to other multipath components is given by

$$\mathbf{s}_1(\tau)=\sum_{l=1}^{L_1}\alpha_{1,l}e^{j\phi_{1,l}}\mathbf{a}_1(\theta_{1,l})(b_{1,p}^{n}r^{1,1}(\tau_{1,l},\tau)+b_{1,p}^{n-1}\hat{r}^{1,1}(\tau_{1,l},\tau))\Big|_{\tau\neq\tau_{1,l}}$$
$$+\sum_{\substack{l=1\\ l\neq j}}^{L_1}\alpha_{1,l}e^{j\phi_{1,l}}\mathbf{a}_1(\theta_{1,l})(b_{1,p}^{n}r^{1,1}(\tau_{1,l},\tau_{1,j})+b_{1,p}^{n-1}\hat{r}^{1,1}(\tau_{1,l},\tau_{1,j}))\Big|_{\tau=\tau_{1,l}}$$

(4.17)

With equation (4.17), it may be shown that the first term gives the non-zero correlation sidelobe due to non-perfect orthogonality of codes. The second term accounts for interference due to multipath interference of the desired user. Also, we can write the MAI due to other user's signal as

$$\mathbf{m}_1(\tau)=\sum_{k=2}^{K}\sum_{l=1}^{L_k}\alpha_{k,l}e^{j\phi_{k,l}}\mathbf{a}_k(\theta_{k,l})(b_{k,p}^{n}r^{1,k}(\tau_{k,l},\tau)+b_{k,p}^{n-1}\hat{r}^{1,k}(\tau_{k,l},\tau)) \qquad (4.18)$$

where $b_{k,p}^{n}$ and $b_{k,p}^{n-1}$ represent the *n-th* and (*n*-1)-*th* pilot bits of the *k-th* user that are received at time t due to multipath delays, and the correlation terms are defined as

$$r^{m,n}(\tau_1,\tau_2)=\int_{nT_b+\tau_1}^{nT_b+\tau_2}\widetilde{c}_i(t-\tau_1)\widetilde{c}_j(t-\tau_2)dt \tag{4.19}$$

$$\hat{r}^{m,n}(\tau_1,\tau_2)=\int_{(n-1)T_b+\tau_2}^{nT_b+\tau_1}\widetilde{c}_i(t-\tau_1)\widetilde{c}_j(t-\tau_2)dt \tag{4.20}$$

Due to the non-zero cross-correlation $m_l(\tau)$, the SINR of the matched filter output decreases as the number of undesired users increases. If the number of undesired users is small, one can easily distinguish the desired signal from the interference because the desired signal can be enhanced by a factor of the processing gain T_b/T_c. However, as the number of undesired users increases to a certain amount, the most significant path components in the delay profile may come from the undesired users. If the wrong components were used for RAKE combining, the system performance will be greatly degraded. In order to correctly extract the paths of the desired user and suppress the undesired peaks, we propose a method to increase the SINR at the output of the matched filter.

In the Q channel, each pilot bit has a fixed spreading factor of 256. Either short or long scrambling codes can be used on the reverse link. In order to effectively reduce the MAI, we adopt the long scrambling codes in the following analysis. The long scrambling code is modulo of sum 40960 chip segments of two binary m-sequences generated by means of two generator polynomials of degree 41. The scrambling code has a period of one radio frame of 10ms. Thus, each pilot bit has a different spreading chip sequence and each can be considered as an independent and random. If $\sum_{k=1}^{K} L_k$ were large enough, the MAI for each pilot bit can be modeled as independent Gaussian noise [38,39]. Following [40], it can be shown that s_1+m_1 has a zero mean and is an uncorrelated random noise. Assume that a time slot (with 0.625ms duration) contains N pilot bits. The time delays of multipaths of the desired user are conventionally estimated by the matched filter output for 1 pilot bit (eq.(4.15)). Here we propose a method, the coherent integration method. In the proposed method, the delay profiles for each N pilot bits (1 slot time) are first consecutively obtained and then coherently integrated and averaged to obtain the mean delay profile. It is noted that during a slot time period, the total phase change of the desired signal due to Doppler shift is small (for example, a mobile speed of 100km/hr will cause a maximum phase change of 41^0 at a carrier frequency of 2GHz). Therefore the desired signal can be enhanced about N times after coherent integration. With this approach, the mean delay profile $\bar{z}_1^m(\tau)$ at the m^{th} element is evaluated by

$$\bar{z}_1^m(\tau) = \frac{1}{N}\sum_{n=1}^{N} Q_{out}{}_{1,n}^{m}(\tau) \tag{4.21}$$

where $Q_{out}{}_{1,n}^{m}$ represents the matched filter output of the *n-th* pilot bit for the *m-th* antenna element. It is noted that in the mean delay profile, for those time bins corresponding to the delay times of the desired user's multipaths, their magnitudes will be increased N times after coherent integration. While for all other bins, their magnitudes will be reduced because bit values of different users are independently and identically distributed. Therefore, the *SINR* of the desired bins can be greatly improved and these bin locations can be more unambiguously identified.

However, each resolvable delay group also contains many multipaths, which will cause fading across the antenna arrays. Therefore, there is possibility that $|\bar{z}_1^m(\tau_{1l})|$ is small for some element m and its value may be smaller than that of other bins. In that case we may choose the wrong bins for the RAKE combining, which will degrade the detection performance. To mitigate this fading effect and ensure that the desired time bins can be correctly identified, we propose a simple algorithm. We incoherently integrate the absolute value of the mean delay profile over the M elements as follows:

$$\bar{\bar{z}}_1(\tau) = \frac{1}{M}\sum_{m=1}^{M} \left| \bar{z}_1^m(\tau) \right| \qquad (4.22)$$

After incoherent integration, the fading effect across the array can be greatly eliminated.

Next we have to determine the required TOA and DOA of the dominant paths of the desired user for the RAKE receiver. Assume that there are P fingers in the RAKE receiver. In the following we propose an algorithm to estimate the TOA and DOA of the dominant multipaths of the desired user. The proposed algorithm is as follows:

1. Find the P largest values among the absolute mean delay profile after incoherent integration and the corresponding time bins.
2. Set a threshold that is x dB below the greatest value. Retain only those time bins whose values are greater than the threshold. Denote these time bins as $\tilde{\tau}_{1,p}$. $\{\tilde{\tau}_{1,p}\}$ is a smaller set of $\{\tau_{1,l}\}$.
3. For each of the retained time bin $\tilde{\tau}_{1,p}$, use the sampled values $\bar{z}_1^m(\tilde{\tau}_{1,p})$ of all antenna elements to estimate the DOA of the paths arriving within this time bin interval. Information of the DOAs can be used for determining the weightings of the uplink and downlink beamformers. Many algorithms have been proposed [4,30,41]. However, these approaches need heavy computation time. Here we use the conventional Fourier transform method to estimate the DOA. It is noted that by using the array manifold and applying the Fourier transform to $\bar{z}_1^m(\tilde{\tau}_{1,p})$ with respect to the array element m, positions of the peaks give the estimation of the DOA and amplitudes of the peak values give the estimation of the path gains and phases of multipaths. Denote the above estimated parameters as $\tilde{\theta}_{1,p}$, $\tilde{\alpha}_{1,p}$, and [illegible]. In order to have a better estimation of the channel parameters, zeros

padding can be applied to $\bar{z}_1^m(\tilde{\tau}_{1,p})$ before taking the Fourier transform.

4.3 Simulation Results

In this section we will demonstrate numerical results to evaluate the performance and merit of our proposed channel estimation algorithm.

In the following simulations, we assume that in the control channel a slot time (0.625ms) contains 6 pilot bits (3 symbols) and these 6 pilot bits are used to estimate the channel parameters. Consider a uniformly spaced linear array with 7 antenna elements and $\lambda/2$ spacing. The major radio link parameters of the simulations are listed in Table 4.1.

Assume that the noise power for each antenna elements is 10 dB below the individual user's power. The parameters about the desired user are shown in Table 4.2. There are three paths and the DOA are -40^0, 0^0, 40^0 respectively; the relative time delays are at 0, $4T_c$, and $8T_c$ respectively, where T_c is the chip duration; the relative path amplitudes are 1, 0.65, and 0.8 respectively; and the phases are π, $\pi/2$, and $3/2\,\pi$ respectively. Assume that there are K active co-channel users and each user also has 3 multipaths. Further assume that the distributions of the parameters $\alpha_{k,l}$, $\phi_{k,l}$, and $\tau_{k,l}$ for the undesired users are Rayleigh, uniform over $[0, 2\pi]$, and uniform over $[0, \tau_{max}]$ respectively, where τ_{max} is the maximum delay spread of the channel. Also assume that the DOA $\theta_{k,l}$ of the undesired users are uniformly distributed over $[-\pi/3, \pi/3]$.

Table 4.1 Radio link parameters of the simulations

Chip rate (Bandwidth)	4.096 Mcps (5MHz)
Carrier frequency (Uplink/Downlink)	1.965 GHz
Pilot bits/slot (Uplink/Downlink)	6 bits/4 bits

Bit rates	16 Kbps
Processing gain	256
Spreading code	Truncated-Gold sequence (40960×2^{41})
Modulation	BPSK
Slot time	0.625ms

Table 4.2 Channel parameters and the estimated results

PATH#	1	2	3
$\theta_{1,1}$	-40^o	0^o	40^o
$\tau_{1,1}$	0	$4T_C$	$8T_C$
$\alpha_{1,1}$	1	0.65	0.8
$\phi_{1,1}$ (rad)	3.1416	1.5708	4.7124
$\hat{\theta}$	$-38.86^o \pm 0.74^o$	$-0.06^o \pm 1^o$	$39.49^o \pm 1.57^o$
$\hat{\alpha}$	1	0.649 ± 0.06	0.76 ± 0.116
$\hat{\phi}$ (rad)	3.298 ± 0.12	1.554 ± 0.18	4.678 ± 0.237

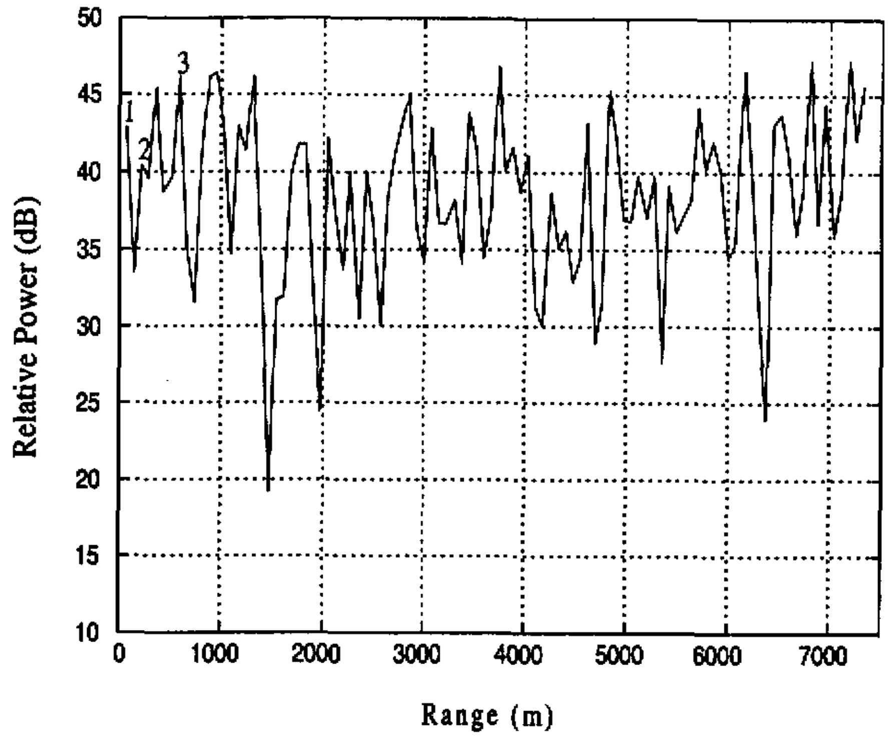

Shown in Fig. 4.2 is an example of the output of the matched filter, or the delay profile, of an antenna element, which is obtained by passing the received fields through the matched filter and integrated over one pilot bit period. It is seen that there are many peaks and we cannot distinguish the desired signal peaks from the interfering signal peaks. If we coherently integrate the matched filter outputs over 6 pilot bits, the results for element 1 to element 7 are shown from Fig. 4.3(a) to Fig.4.3(g) respectively. By comparing Fig. 4.2 and Fig. 4.3, one can easily find that the values of the desired paths (noted by 1, 2, 3 in the figures) for all antenna elements have been greatly enhanced. However, for the same signal path different antenna elements have different magnitudes due to the multipath fading. This fading effect may cause the peak of the desired signal lower than that of the interference as indicated in Figs. 4.3(c), 4.3(d), and 4.3(e). In that case we may choose the wrong TOA for the RAKE combining. If we further incoherently integrate the mean delays over 7 antenna elements as expressed by eq. (4.22), the result is shown in Fig. 4.3(h).

It is noted that the undesired signal peaks have been reduced and the desired paths can be correctly identified. We then set a threshold, 7 dB below the greatest value [42], in Fig 4.3(h) to determine the TOAs, which are the positions of the three largest peaks. Denote these TOAs as $\tilde{\tau}_{1,p}$.

Next, for each $\tilde{\tau}_{1,p}$, we use the array manifold and take the Fourier transform of $\bar{z}_1^m(\tilde{\tau}_{1,p})$, as expressed by eq. (4.21), with respect to m to estimate the DOA of the desired path. An interpolation realized by zero padding to 32 has been applied in the FFT so that the DOA can be more finely sampled. The results after FFT for the three paths are shown in Figs. 4.4(a) to 4.4(c). The peak position corresponds to the DOA and its amplitude corresponds to the path attenuation. We have conducted 500 simulations, using independent random parameter sets of the undesired users, to estimate the channel parameters. The mean value and standard deviation of each parameter are also shown in Table 4.2. From the simulation results, it is seen that our proposed algorithm can effectively reduce the MAI and accurately extract the channel parameters. The estimated multipath delay profile is shown in Fig. 4.5. As we can see, the peak values of the estimated profile occur at the delays of $\tilde{\tau}_{1,p}$ that correspond to the actual delays. We have also used many different parameter sets of the desired user and their channel parameters can also be accurately estimated.

In order to further evaluate the merit and reliability of our proposed algorithm, we have also conducted simulations to statistically count the total number of TOA positions that are not correctly selected. For each different number of active users, we conducted 1000 simulations using independent random sets of parameters of the undesired users. For each simulation, the channel parameters of the desired user are kept the same. In each delay profile we choose the three positions with the three largest values to represent the TOA of the three multipaths of the desired user.

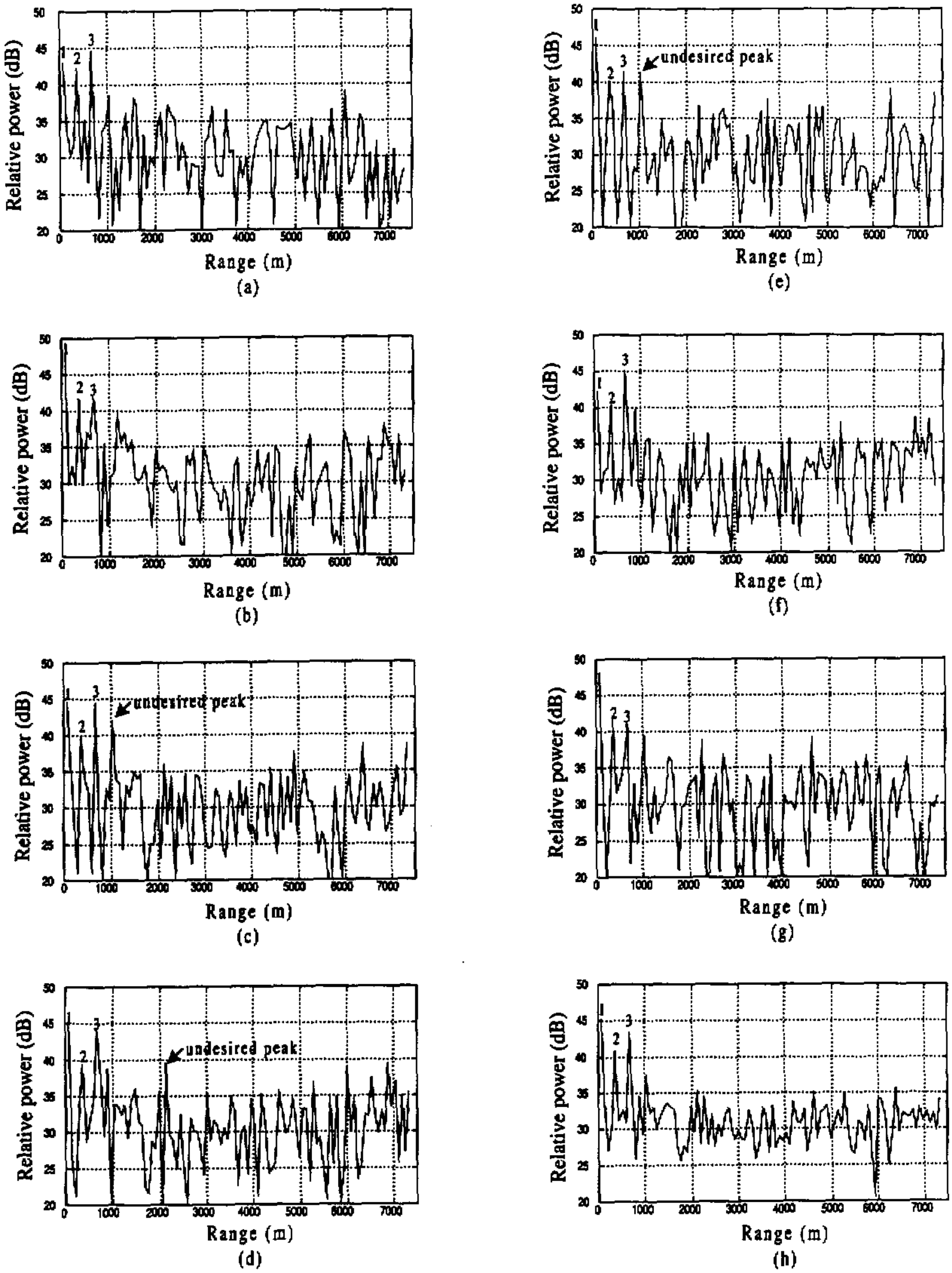

Fig. 4.3 Matched filter output (power delay profile) of all antenna elements from m=1 to m=7: (a) ~ (g). with coherent integration over 6 pilot bits, (h). power delay profile with coherent integration over 6 pilot bits and incoherent integration over 7 antenna elements.

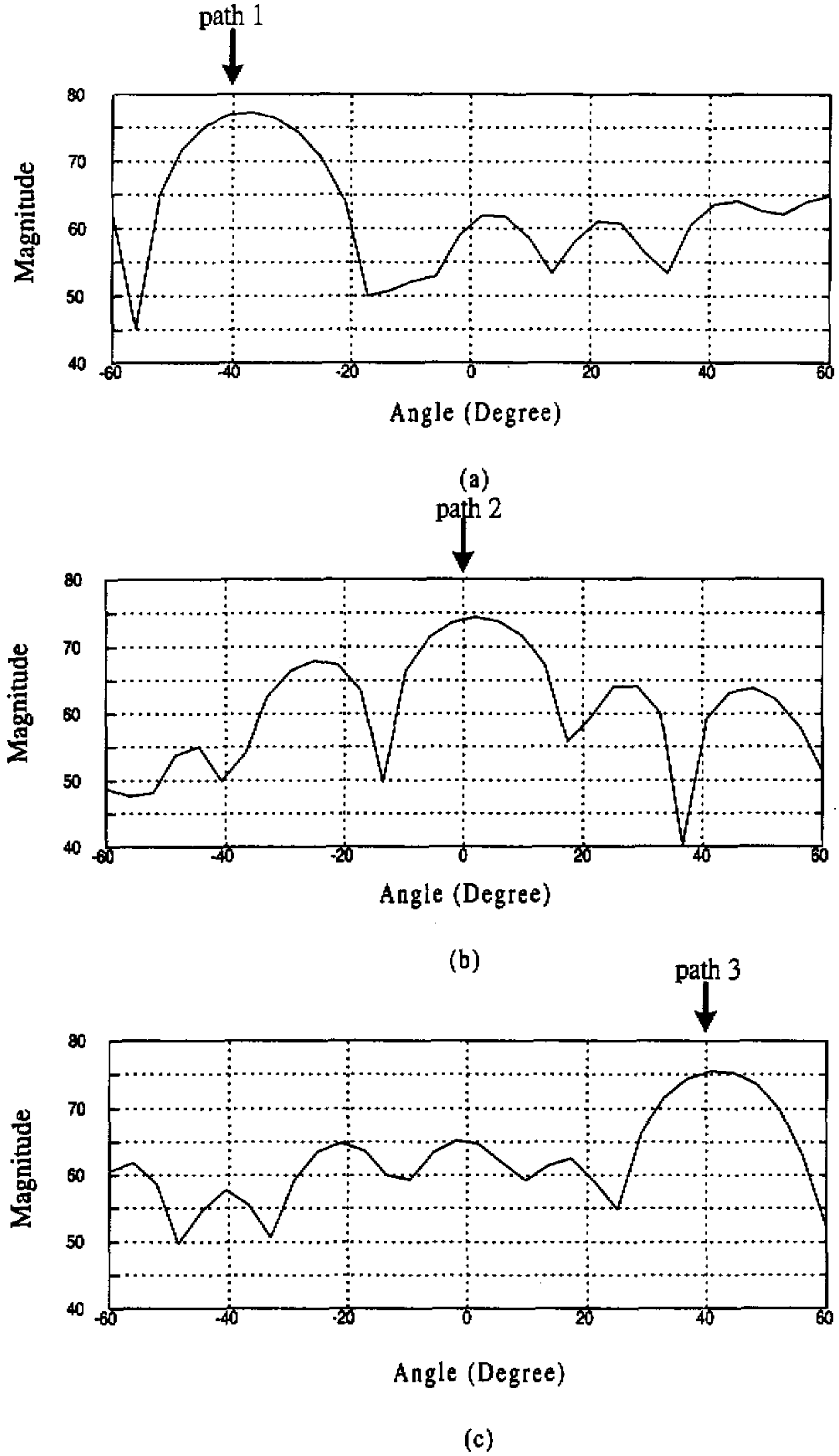

Fig. 4.4 Estimated DOA of desired signal paths: (a). path 1 (-40^0), (b). path2 (0^0), (c). path 3 (40^0)

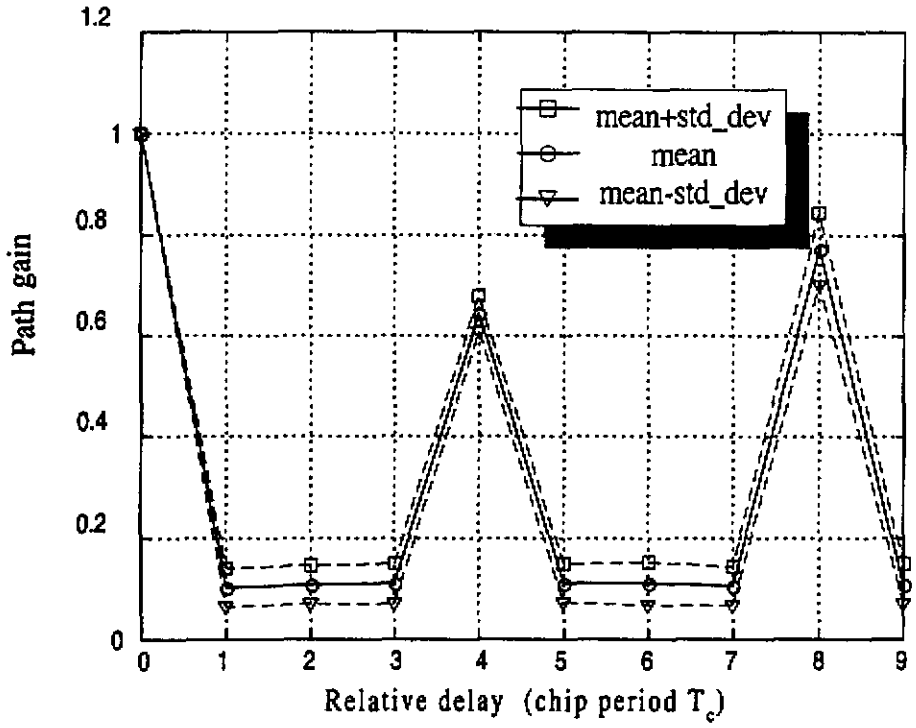

antenna elements in a 3 path scenario

Among the 3000 positions (corresponding to 1000 simulations) chosen, we count the number of positions that are not correctly positioned. Four methods are used to obtain the delay profile. First, one single pilot bit and one antenna element are used. Second, one antenna element and six pilot bits (with coherent integration) are used. Third, one pilot bit and seven antenna elements (with incoherent integration) are used. Fourth, 6 pilot bits (with coherent integration) and seven antenna elements (with incoherent integration) are used. The number of wrong positions for various methods and various numbers of active users is shown in Table 4.3. It is seen that with coherent integration the number of wrong positions can be reduced about N times (N is the number of pilot bits) and with incoherent integration the number of wrong positions can be further reduced about 1.5 ~ 2 times.

Table 4.3 Number of wrong TOA positions as a function of number of active users for various detection methods.

Users / Methods	1	3	5	7	9	11	13	15	20	30	40	50	60
Method 1	0	5	51	239	456	695	895	1098	1557	2006	2322	2450	2459
Method 2	0	0	0	0	0	1	7	8	35	108	304	515	713
Method 3	0	0	2	12	78	206	317	579	966	1471	1850	2190	2479
Method 4	0	0	0	0	0	0	0	0	0	0	8	38	125

4.4 Summary

In this chapter, we have proposed an algorithm to suppress the MAI and estimate the channel parameters of the desired user for the W-CDMA system. We first propose a method to increase the SINR at the output of the matched filter. The improvement in SINR of the matched filter output is observed, which is proportional to the number of available pilot bits. Additional improvement is obtained by incoherently integrating all matched filter output of antenna arrays. We then employ the array manifold and apply the FFT scheme to estimate the channel parameters, including the amplitudes, phases, and DOAs of dominant paths. After the multipath parameters of the channel have been estimated, the received signal is passed into a 2D-RAKE correlator that is matched to the channel's response of the transmission waveform. In chapter 5, we will apply these estimated channel parameters to 2D-RAKE receiver to implement the beamforming approach and coherent RAKE combining.

Chapter 5 Performance of 2D-RAKE Receiver for W-CDMA System

As presented in chapter 2, multipath signals are present in digital radio communication systems. The algorithms considered in previous chapter were used to estimate the channel parameters of dominant path signals. These parameters include TOA, DOA, path phase, and path amplitude have been determined following the channel estimation algorithm. In this section, the use of adaptive antenna arrays in conjunction with the use of RAKE receiver will be presented.

The capacity of a cellular communication system is usually defined as the number of active users in a cell which has an acceptable level of transmission quality. As a cellular communication system becomes more densely populated, the system performance is no longer background noise limited, but rather than co-channel interference limited. The SINR performance refers to the ability of the algorithm to increase the array output SINR by either spatially processing the desired signal, coherently combining multipath components, or both. The SINR performance is a good measurement of how well the algorithm being able to receive the desired signal and reject interference. Many adaptive array processing algorithms have been proposed to optimize the SINR [27,37]. The basic concept is to synthesize a beam pattern so that the interfering signals can be nulled. However, the number of interfering signals that can be nulled is only M-1 if M antenna elements are used. In fact, in the W-CDMA systems the number of interfering signals is usually much greater than the number of antenna elements. Therefore, the conventional adaptive array processing algorithms are not effective in reducing the interference. In this chapter we will utilize the estimated DOA of the desired signals and proposed simple beamforming method to point the main beam to the desired user and suppress the multi-user interference.

The performance of 2D-RAKE receiver have been studied and evaluated [13,14]. It was found that the SINR performance is abruptly degraded when the number of interferer exceeds a certain amount. The main reason of degradation is that MAI may exceed the signal and the paths selected for RAKE combining are not accurately determined as the number of the interferers is increased. We will compare the SINR performance obtained by the conventional method and by our proposed algorithm.

5.1 Reception of 2D-RAKE receiver

The typical technique used for multipath reception with a single antenna element is the use of a RAKE receiver, which is called 1D-RAKE receiver. The structure of the 1D-RAKE receiver was shown in Fig. 1.1. For CDMA systems the time delay, Δ, between adjacent taps is equal to the chip duration T_c. The signal present at each tap of the RAKE receiver is simply a delayed version of the incident signal. Since the most of the signal power puts in several dominant path components, matching with these dominant components provides sufficient performance. Therefore, the RAKE receiver can be simplified by implementing only a small number of tapes in the chip-rate matched filter. Each of the dominant signals is then delayed and multiplied by an appropriate complex weight, and then summed together to give the RAKE receiver output. Depending on the multipath structure of the signal environment, properly combining multipath components can dramatically increase system performance. The use of an adaptive antenna array in conjunction with a RAKE receiver can produce even further performance enhancements.

The structure of the 2D-RAKE receiver is shown in Fig. 5.1. The signals received by each array element are first passed through P correlators determined by the estimated TOAs. Each correlator is matched to the desired user's code $\tilde{C}$ with a time shift of $\tilde{\tau}_{1,p}$, the estimated time delay of the desired signal path. The SINR of

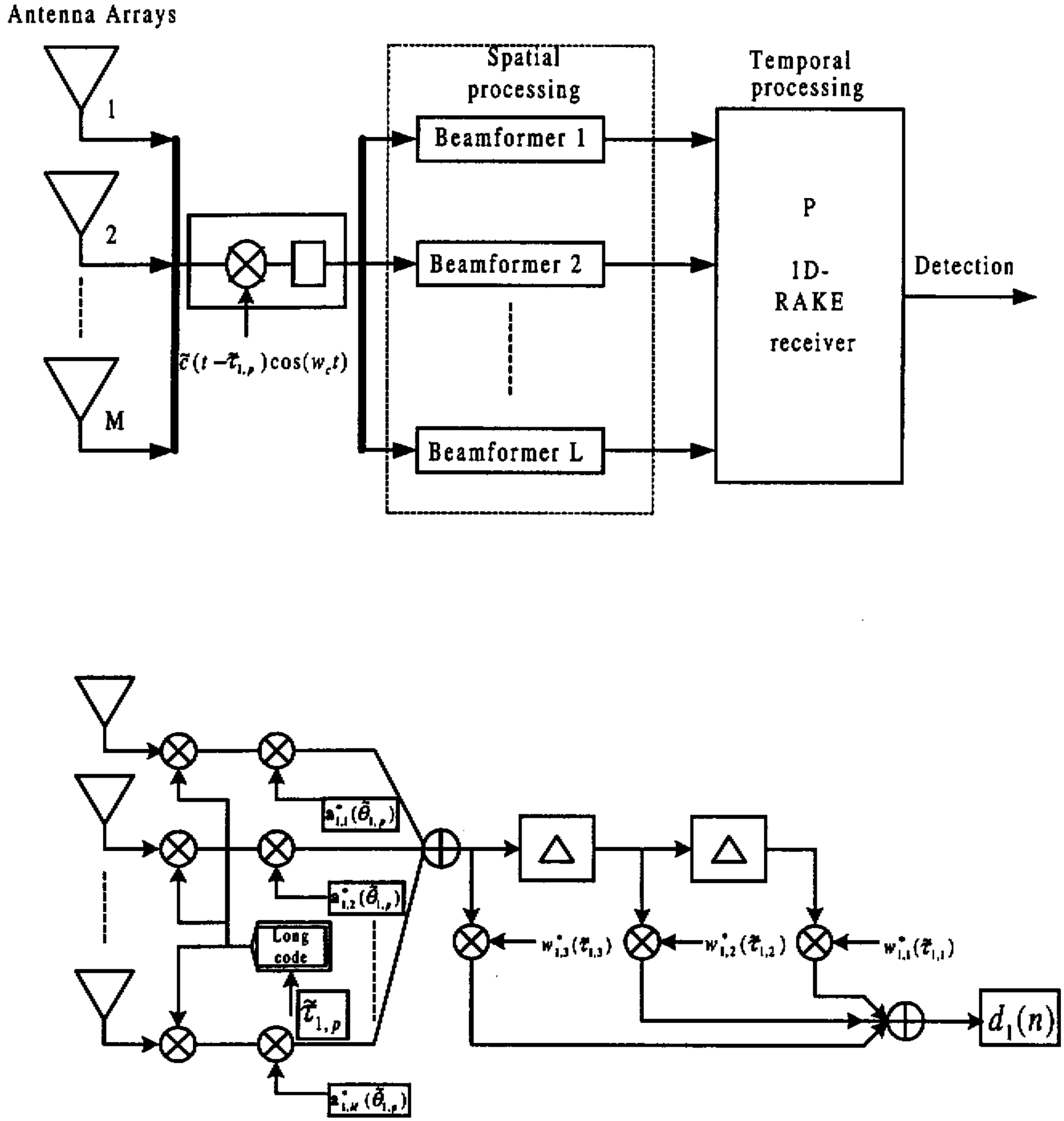

Fig. 5.1 Block diagram of 2D-RAKE receiver

correlator can be improved by a spreading gain $G=T_b/T_c$. Each correlator output contains the desired signal and MAI. These correlator outputs of each antenna element are then passed through a beamformer to further enhance the desired signal. The beamformer is beamformed to the DOA of the desired signal which arrived within the time bin of $\tilde{\tau}_{1,p}$. This is implemented by multiplying the correlator output vector with the beamforming vector $\mathbf{a}_1^*(\tilde{\theta}_{1,p})$ depending on the estimated DOAs ($\tilde{\theta}_{1,p}$). The spatial combiner is intended to output the strongest among the M received branches with the same arrival delays. It should be noted that the beamforming vectors are used to coherently recombine the received signals in spatial domain, and thus an optimal direction reception can be achieved. After the P beamformers have completed the beamforming process, their outputs are fed into a 1D-RAKE combiner to coherently integrate the desired multipath signals. The beamformers and the 1D-RAKE combiner constitute the 2D-RAKE receiver. In the RAKE combiner we adopt the maximum ratio algorithm [45]. By the coherent combination of multipath signals received with different time delay, a temporal diversity reception can be achieved, further improving the receiving SINR at the RAKE output. With eq. (4.3) and the estimated channel parameters, the output of the 2D-RAKE receiver can be expressed by

$$
\begin{aligned}
d_1(n) &= \frac{1}{T_c}\sum_{p=1}^{P} w_{1,p}^* \mathbf{a}_{1,p}^* \int_{(n-1)T_b+\tilde{\tau}_{1,p}}^{nT_b+\tilde{\tau}_{1,p}} \tilde{c}(t-\tilde{\tau}_{1,p})\mathbf{x}(t)dt \\
&= \sum_{p=1}^{P} MGw_{1,p}^* \tilde{s}_p(\tilde{\tau}_{1,p}) + \sum_{p=1}^{P} w_{1,p}^* u_p(\tilde{\tau}_{1,p}) \\
&= \mathrm{S}(n) + \mathrm{I}(n)
\end{aligned}
\tag{5.1}
$$

where M is the number of antenna elements, G is the processing gain, $w_{1,p} = \tilde{\alpha}_{1,p} e^{j\tilde{\phi}_{1,p}}$ represents the estimated channel parameters,

$\tilde{s}_p(t) = \sqrt{p_1}\alpha_{1,p}e^{j\phi_{1,p}}b_1(n)$, $u_p(t)$ is the summation of all undesired signals plus thermal noise at the p^{th} beamformer output, and $d_1(n)$ is the decision variable of the 2D-RAKE receiver output. It can be easily shown that $S(n)$ has the same polarity as $b(n)$ if the channel parameters $\tilde{\alpha}_{1,p}$, $\tilde{\phi}_{1,p}$, and $\tilde{\theta}_{1,p}$ are accurately estimated. The output *SINR* of 2D-RAKE receiver can be written as

$$SINR = \frac{E\{S(n)\}}{E\{I(n)\}} = \frac{MGE\left\{\left|\sum_{p=1}^{P} w_{1,p}^{*}\tilde{s}_p(t)\right|^2\right\}}{E\left\{\left|\sum_{p=1}^{P} w_{1,p}^{*}u_p(t)\right|^2\right\}} \tag{5.2}$$

In this beamforming algorithm we do not attempt to null the interferers. It is known that the maximum number of interferers that can be nulled is M-1 if M antenna elements are employed. In the W-CDMA environment, however, the number of interferers in general exceeds the number of array elements. Furthermore, it can be shown that our proposed beamforming vector, $\mathbf{a}_1^*(\tilde{\theta}_{1,p})$, is the optimum solution if the number of interferers becomes very large [26].

If we assume that the system has a perfect power control so that all users have the same power level and the MAI and noise are both temporally and spatially white, the *SINR* after the 2D-RAKE receiver can be approximated by [46]

$$SINR = \frac{(GM)SNR}{(K-1)SNR + 1} \tag{5.3}$$

where *SNR* is the reverse link signal-to-noise ratio for each antenna element, *G* is the processing gain of the matched correlator, *M* is the number of antenna elements, and *K* is the total number of active users. It is noted that the above expression is valid only if the channel parameters can be accurately obtained. If the wrong paths from the MAI were used for RAKE combining, the detection performance will be greatly degraded and eq. (5.3) will not apply any more. The eq. (5.3) implies that the capacity in terms of the number of users supported is

$$K = [1 + \frac{G \cdot M}{E_b / N_0} - \frac{1}{SNR}] \qquad (5.4)$$

where E_b/N_o is the *SINR* value required for adequate performance. From the last equation, it is clear that the increase in system capacity is in an order of M and G.

5.2 Simulation Results

First we evaluate the *SINR* performance after the 2D-RAKE receiver when various numbers of pilot bits and antenna elements are employed in the system. The parameters about the desired user are also shown in Table 4.2, except that the relative path amplitudes are 1 for all the desired signal paths. Assume that there are K active co-channel users and each user also has 3 multipaths. Further assume that the distributions of the parameters $\alpha_{k,l}$, $\phi_{k,l}$, and $\tau_{k,l}$ for the undesired users are Rayleigh, uniform over [0, 2π], and uniform over [0, τ_{max}] respectively, where τ_{max} is the maximum delay spread of the channel. Also assume that the DOA $\theta_{k,l}$ of the undesired users are uniformly distributed over [$-\pi/3$, $\pi/3$]. We use the channel estimation method described in the previous chapter to determine the channel parameters in Q-channel and these parameters are applied in the data channel (I-channel) for RAKE combining. Shown in Fig. 5.2(a) to 5.2(c) are plots of *SINR* versus number of interferers for various numbers of antenna elements obtained by three different methods respectively. They are: only one pilot bit and only one antenna element (without coherent and incoherent integration), one pilot bit and M

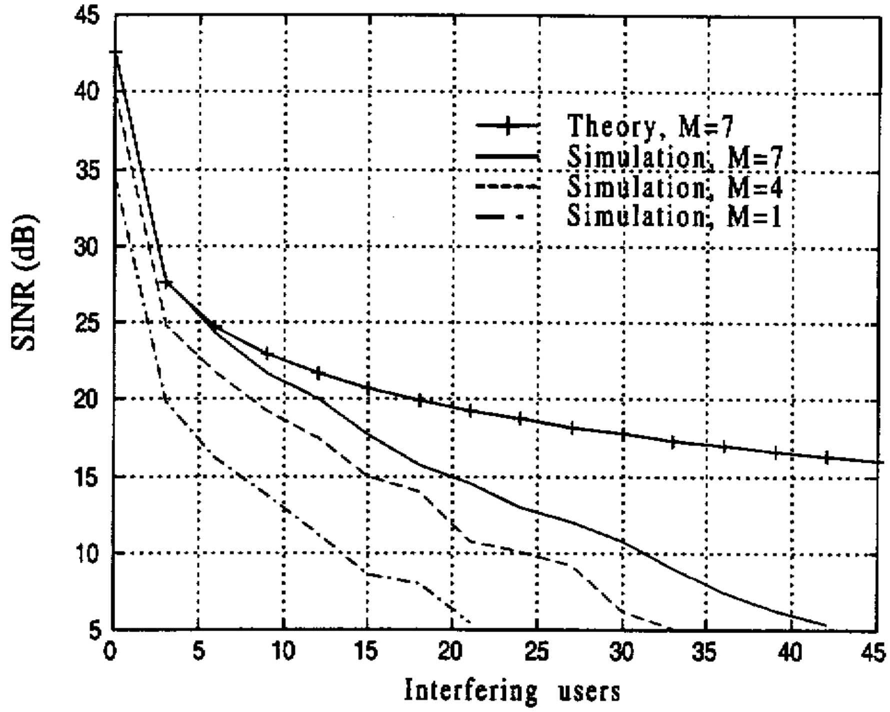
Theory, M=7
Simulation, M=7
Simulation, M=4
Simulation, M=1
SINR (dB)
Interfering users
45
40
35
30
25
20
15
10
5
0
5
10
15
20
25
30
35
40
45

(a)

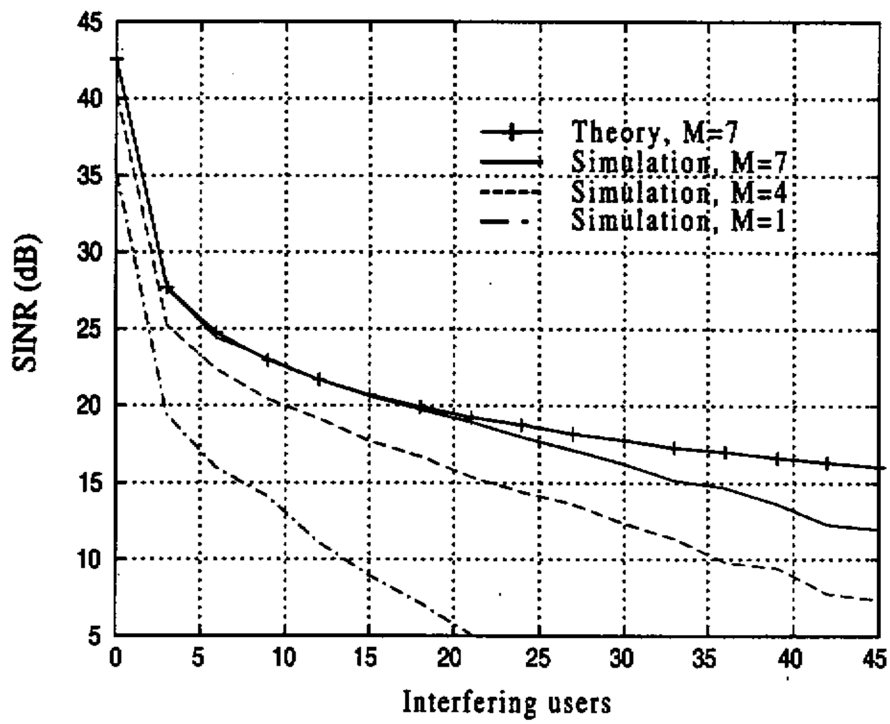
Theory, M=7
Simulation, M=7
Simulation, M=4
Simulation, M=1
SINR (dB)
Interfering users
45
40
35
30
25
20
15
10
5
0
5
10
15
20
25
30
35
40
45

(b)

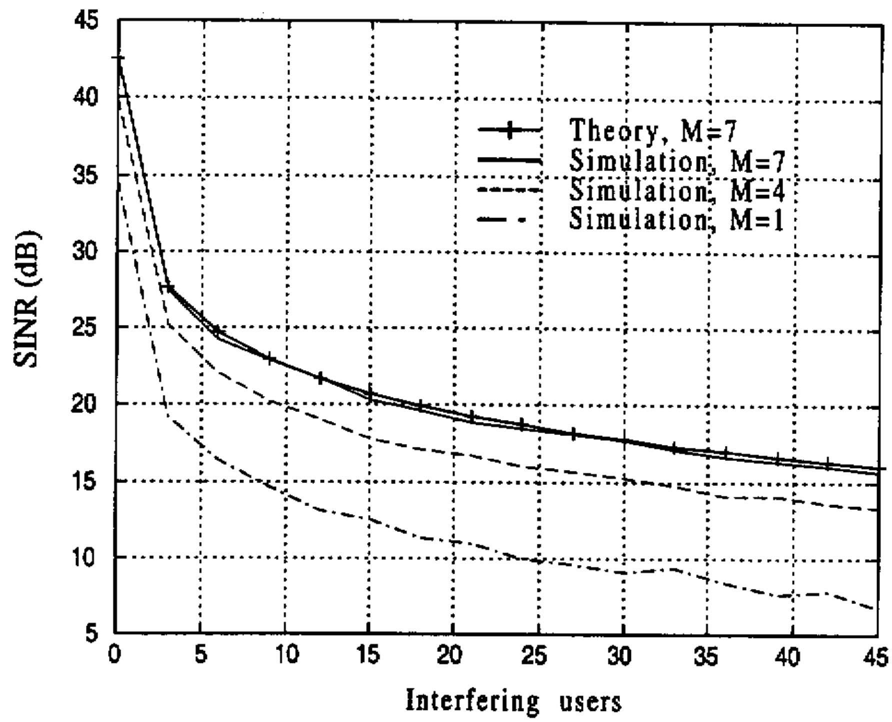

(c)

Fig. 5.2 Plots of SINR versus number of tnterferers for various number of antenna elements and various methods: (a) one pilot bit and one antenna element are used, (b) one pilot bit and M antenna elements are used, and (c) 6 pilot bits and M antenna elements are used.

antenna elements (with incoherent integration only), and 6 pilot bits and M antenna elements (with coherent and incoherent integration), being used to obtain the TOA of the desired user. The theoretical values of eq. (5.3) for M=7 are also plotted for comparison. It is noted that in the data channel, the data cannot be coherently or incoherently integrated. Therefore, if the channel parameters are correctly estimated, the three methods should have the same *SINR*. However, if the channel parameters are not correctly estimated, the *SINR* after RAKE combining will be greatly degraded. By comparing the results of Table 4.3, we can explain why the SINR curves in Fig. 5.2(a) and (b) start to deviate from the theoretical values after the number of interferers is increased to a certain amount. While in Fig. 5.2(c), the results obtained by our proposed methods approach the theoretical values. The benefit of employing antenna array is that the *SINR* can be improved by 10 $log(M)$ dB.

Next, we demonstrate the *SINR* performance of the 2D-RAKE receiver when different data rates are transmitted. In the simulation we have neglected the ISI effects, which means that the time delay spread of the desired paths is smaller than a symbol interval. If six pilot bits and 7 antenna elements are used to estimate the channel parameters and these parameters are applied in the 2D-RAKE receiver, the

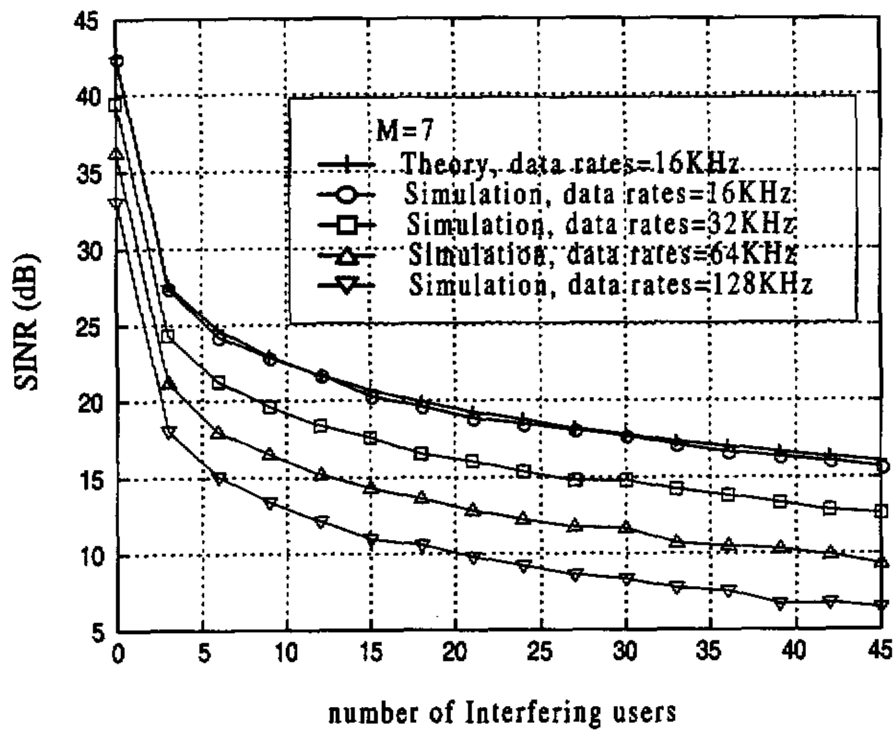

Fig. 5.3 SINR as a function of number of interferers and different data rates after RAKE combining

SINRs versus number of interferers for different data rates are shown in Fig. 5.3. Because the channel can be correctly estimated, the simulated *SINR* also approach the theoretical value of eq. (5.4). The *SINR* is reduced by a factor of 10 log (B/B_0), where B is the data rate transmitted and B_0 is 16KHz.

Finally, the results for the increase in system capacity are shown in Fig. 5.4. With eq. (5.4), we plot the predicted results for the number of users K as a function of the number of antenna M with different processing gain G (assuming a required E_b/N_o of

15 dB for adequate performance). It is noted that system capacity is much depend on the Processing gain and only a few active users can be simultaneously transmitted with high data rates.

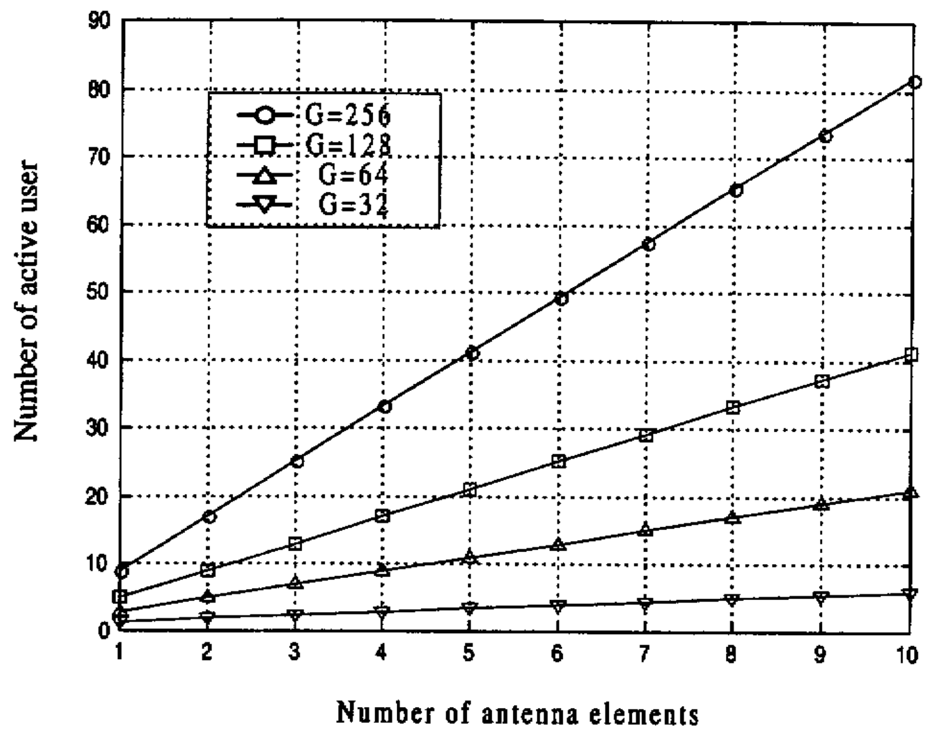

Fig. 5.4 Capacity of the W-CDMA system as a function of the number of antenna elements

5.3. Summary

In this chapter we have exploited the estimated channel parameters by our proposed algorithm to the data-branch for 2D-RAKE combining. The purpose of the 2D-RAKE receiver is to maximize the SINR at the basestation. This object can be achieved via three basic approaches: delay shifting, beamforming, and RAKE combining. Because the channel parameters can be accurately estimated, the SINR performance after RAKE receiver can approach the theoretical values. We also show that incorporating antenna arrays in a CDMA system improves the detection performance and the increased output SINR will consequently result in higher system capacity. Simulation results have verified the effectiveness of our proposed algorithms. By using the estimated DOAs at the basestation, we can determine the downlink weighting vectors for performing beamforming on the transmitted signals. The SINR performance of different algorithms for downlink transmission will be discussed in the next chapter.

Chapter 6 Comparison of Beamforming Techniques for W-CDMA Communication System

Beamforming is a technique to focus the antenna beam to the desired user so that the SINR can be increased. RAKE combining is a technique that fully utilizes the multipath energy so that fading effect can be reduced and the signal power can be enhanced. We have proved that both beamforming and RAKE combining can effectively increase channel capacity.

In the W-CDMA system, an antenna array at the basestation can be utilized to form beam patterns for the uplink and downlink. In the uplink, the received signal is first proceeded by a matched filter so that the chip positions (or time delays) of the dominant multipaths of the desired user can be determined. The antenna array is then used to determine the DOA of the multipath or to form beam pattern so that the desired signal can be constructively enhanced. In the downlink, the antenna array has to focus the beam to the desired user. However, due to the factors that in the uplink and downlink, for example, the carrier frequencies are different, and the fading effect can be independent, the beamforming effect can be different if the same weighting sets are used in both the uplink and downlink. Several beamforming methods have been proposed and compared [29,45,46]. Among these techniques, the complex conjugate (spatial signature [29]) method is the simplest one. It is based on the concept of retrodirectivity and it has the advantage that no additional computation loading is required in the uplink and downlink beamforming. However, the different carrier frequencies can degrade the downlink beamforming performance. To overcome this beamforming degradation, we can first determine the DOA of each dominant path of the desired user, and then use the array manifold to calculate the required weighting factor for downlink. This method will increase the computation load and memory for signal processing. Since the fading effect may be uncorrelated for the uplink and downlink, it is interesting to compare the transmission performance when different beamforming algorithms are employed.

In this chapter we will compare the SINR performance obtained by different beamforming methods. We will apply a suitable propagation model and numerically calculate the SINR statistics for both uplink and downlink when different beamforming methods are used.

6.1 Description of the Complex Conjugate Method and the DOA Method

As presented in chapter 5, the 2D-RAKE receiver is a bank of P adaptive beamformer, shown in Fig. 5.1. The *p-th* beamformer has an associated antenna weight vector, $\mathbf{a}^*(\tilde{\theta}_{1,p})$, which adapts to the *p-th* multipath component. The output of each beamformer is then treated as the signal present at the corresponding tap of the standard RAKE receiver. The RAKE receiver appropriately delays the beamformer outputs and coherently combines them. In this case, the parameters include TOAs, DOAs, path phases, and path amplitudes must be determined following the channel estimation algorithm described in chapter 4. In fact, these parameters may not need to be determined independently. This depends on which algorithms are used for the array processing. If the channel parameters including DOAs, path phases and path amplitudes cab be associated into the array weighting vectors $w_{m,p}(t)$, one can drive another structure of 2D-RAKE receiver, shown in Fig. 6.1. The structure is the called joint 2D array processing algorithm [28,29]. The parameter $w_{m,p}(t)$ (called spatial signature) is a complex number denoting the amplitude gain, phase shift, and angle of arrival of the *p-th* multipath component at the *m-th* antenna element. It has the advantage that no additional computation loading is required to separately estimate the DOAs, path phase, and path amplitude. It is interesting to note that there is no difference in structure between the 2D-RAKE receiver and the 2D-Array processor. Therefore, the aforementioned channel estimation algorithm can be still applied to estimate the spatial signature parameters.

The method is described as follows:

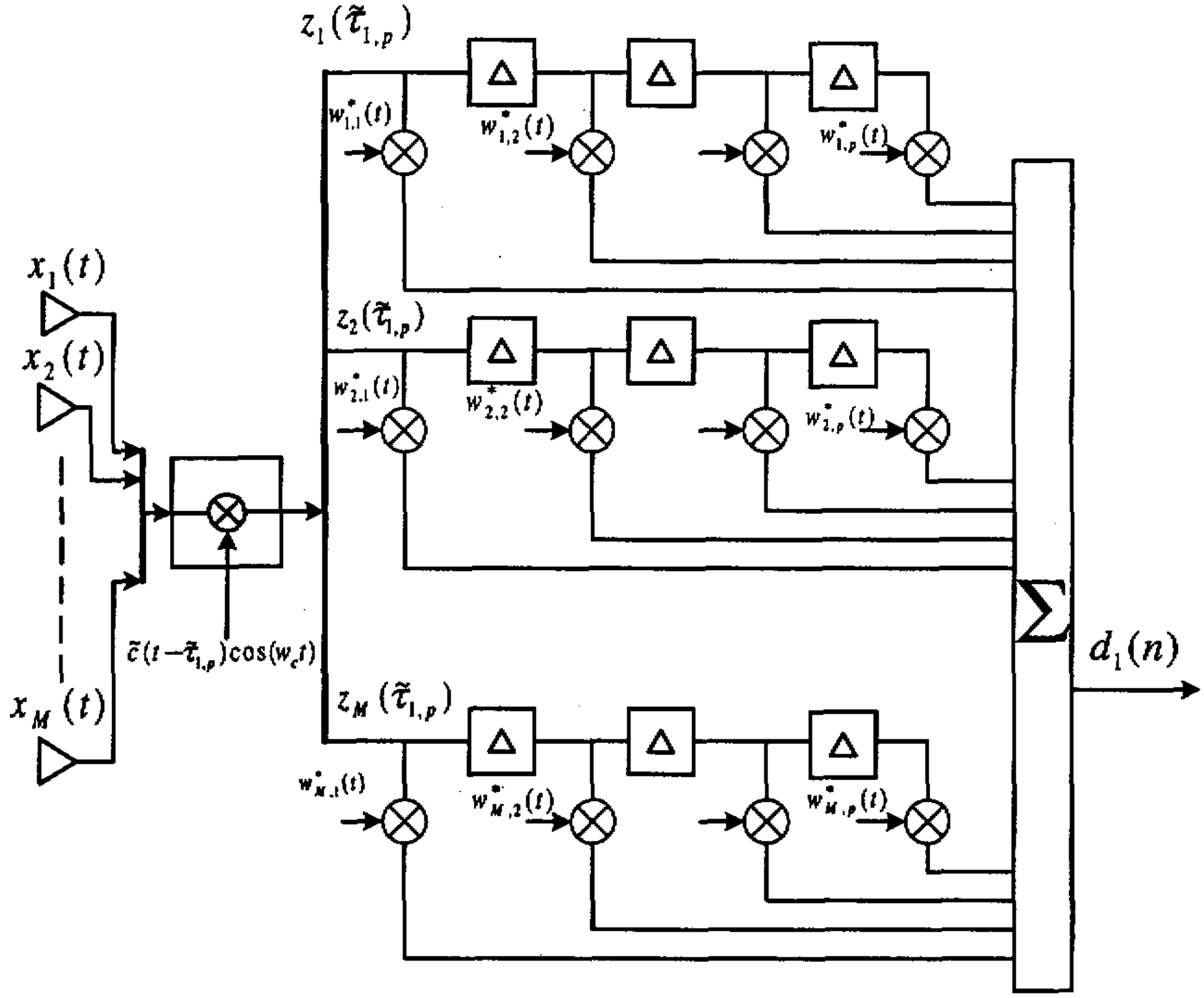

Fig. 6.1 2D Array Processor

1. In the Q-channel we have obtained the mean delay profile of each element, which is calculated by Eq. (4.22). Denote the value sampled at the estimated delay time $\tilde{\tau}_{1,p}$ by $\bar{z}_1^m(\tilde{\tau}_{1,p})$.
2. The correlator output of the *m-th* element in the I-channel is then multiplied by the complex conjugate of $\bar{z}_1^m(\tilde{\tau}_{1,p})$.

3. Coherently integrate all the M multiplication values. This is the output of the *p-th* beamformer.

4. The RAKE combiner then coherently combines the *P* beamformer outputs.

The beamforming can also be obtained by multiplying the correlator output of each element by an array factor formed by the DOA of the desired path. The DOA of the desired path can be obtained by applying the Fourier transform to the sample value $\overline{z}_1^m(\tilde{\tau}_{1,p})$ in the Q-channel. Denote the estimated DOA and amplitude of the p-*th* path as $\tilde{\theta}_{1,p}$ and $\hat{\alpha}_{1,p} = \tilde{\alpha}_{1,p} e^{-j\tilde{\phi}_{1,p}}$ respectively. Then the p-*th* correlator output is multiplied by $a_1^{m^*} = e^{j2\pi(m-1)d\sin\tilde{\theta}_{1,p}/\lambda}$, where *d* is the spacing between antenna elements. With this method, the antenna array will form a beam to the DOA of the desired signal. In the RAKE combiner, the p-th correlator output will multiply $\hat{\alpha}_{1,p}^*$, the complex conjugate of $\hat{\alpha}_{1,p}$, and then coherently integrated. It is noted that the DOA information can have several applications. For example, it can be used for the downlink beamforming. It can also be used to locate the mobile location [26, 52].

After multipath parameters of the desired signals have been estimated, these data can be fed into the data channel to evaluate the SINR of the 2D-RAKE receiver. Equation (5.2) and (5.3) can be used to evaluate expected SINR of the 2D-RAKE receiver.

6.2 Downlink Beamforming and signal processing

In the W-CDMA/FDD (frequency division duplex) system, there is more than 190 MHz difference between the uplink and downlink carrier frequencies. Measurement studies have indicated that multipath fading can be very sensitive to the carrier frequency. In downlink beamforming, several factors can be considered. For example, how will the performance be changed if the same element weightings as used in the uplink beamforming were used in the downlink? Should the downlink pattern be beamformed to a single dominant direction or to several multipath directions? If multiple beams were used, how to decide the energy ratio among different beams? In the following we will discuss several downlink beamforming algorithms. We will consider the problem from several points of views, such as the complexity of implementation, the effect of fading, and the multiple access interference etc. In the downlink, denote the weighting of the m-*th* element for the desired user as w^d_m. To evaluate the downlink SINR performance, we further made the following assumptions.

1. The reciprocity property holds for the uplink and downlink. Therefore, the uplink and downlink will encounter the same multipath. However, the amplitudes of each multipath component can be different due to different carrier frequencies and different radiation patterns of the uplink and downlink.
2. Only the intra-cell interference is considered.
3. The basestation transmits the same power for each coding channel.

The beamforming algorithms to be considered are the complex-conjugate method and the DOA method. The types of beams to be synthesized are the single-beam and multiple-beam types. The weightings of different combinations are described as follows:

1. The single-beam complex-conjugate method:

In the uplink, from the mean delay profile obtained by Eq.(4.22), choose the time bin with the largest peak value, denote it by $\tau_{\max}$. The matched filter output of the m-*th* element sampled at $\tau_{\max}$ is denoted by $\bar{z}_1^m(\tau_{\max})$. For the downlink, the weighting of each element is given by

$$w_m^d = \bar{z}_1^{m^*}(\tau_{\max}) \qquad (6.1)$$

2. The multiple-beam complex conjugate method:

From the uplink mean absolute delay profile of Eq. (4.11), choose the P peak positions with the first P largest values and denote these peak positions as $\tau_1, \ldots, \tau_p$.

Denote the matched filter output of the m-*th* element sampled at $\tau_1, \ldots, \tau_p$ as $\bar{z}_1^m(\tau_1), \ldots, \bar{z}_1^m(\tau_P)$. The weighting of the m-*th* element is then given by

$$w_m^d = \sum_{p=1}^{P} \bar{z}_1^{m^*}(\tau_p) \qquad (6.2)$$

3. The single-beam DOA method:

Denote the DOA of the dominant path as $\theta_{\max}$. The weighting of the m-*th* element is given by

$$w_m^d = e^{jk(m-1)d\sin(\theta_{\max})} \qquad (6.3)$$

where k is the wavenumber at the downlink carrier frequency.

4. The equal-gain multiple-beam DOA method:

Suppose that the estimated DOAs of the dominant paths of the desired user are $\tilde{\theta}_1, \ldots, \tilde{\theta}_P$. The weighting of the m-*th* element is given by

$$w_m^d = \sum_{p=1}^{P} e^{jk(m-1)d\sin(\tilde{\theta}_p)} \qquad (6.4)$$

5. The maximal-ratio multiple-beam DOA method:

Suppose that the estimated DOAs of the dominant paths and their corresponding magnitudes are $\tilde{\theta}_1, \ldots, \tilde{\theta}_P$ and $\tilde{m}_1, \ldots, \tilde{m}_P$ respectively. Then the weighting of the m-th element is given by

$$w_m^d = \sum_{p=1}^{P} \tilde{m}_p e^{jk(m-1)d\sin(\tilde{\theta}_p)} \qquad (6.5)$$

In order to have a fair comparison, we constrain that the total radiated power to be constant for different beamforming algorithms. Therefore, each element weight should be normalized by

$$\tilde{w}_m^d = w_m^d \Big/ \left(\sum_{m=1}^{M} | w_m^d |^2 \right)^{1/2} \qquad (6.6)$$

If the channel were stationary, it would be better to have a single beam because the antenna pattern will be focused to the direction with the maximum transmission. However, as the uplink and downlink fading are independent due to the different carrier frequencies, the use of a single-beam pattern will be more likely to suffer from deep fading than the multiple-beam pattern. The relation between the fourth method and the fifth method is equivalent to that of the equal-gain and maximum-ratio gain combining in the RAKE combiner.

From the interference point of view, it is reasonable to assume that the DOA distribution of the undesired users is uniform if the number of users is large (for example, more than 30). It is known that the beamwidth is proportional to the antenna size or number of elements. If a single beam is used, the number of interfering users within the mainlobe coverage will be smaller than that when a multiple-beam is used, because the multiple-beam pattern will have a wider angular coverage.

In the next section we will use a propagation model to numerically calculate the SINR statistics when different beamforming techniques are employed in the uplink and downlink.

6.3 Simulation Results

In this section we compare the uplink and downlink SINR performance obtained by different beamforming algorithms.

Assume that in the control channel a slot time (0.625ms) contains 6 pilot bits in the uplink and 4 pilot bits in the downlink and these pilot bits are used to estimate the channel parameters. Consider a uniformly spaced linear array with 7 antenna elements and $d = \lambda_u / 2$ spacing, where λ_u is the uplink wavelength. The major uplink and downlink radio parameters of the simulations are listed in Table 4.1.

Assume that the signal to noise ratio for each antenna element is 10 dB. The channel parameters about the desired user are shown in Table 4.2. Assume there are 40 active co-channel users and each user also has 3 multipaths. Assume that the distributions of the channel parameters $\alpha_{k,l}$, $\phi_{k,l}$, and $\tau_{k,l}$ for the undesired users are Rayleigh, uniform over [0, $\pi/2$] and uniform over [0, $\tau'_{\max}$] respectively, where $\tau'_{\max}$ is the maximum delay spread of the channel. Also assume that the DOA $\theta_{k,l}$ of the undesired users are uniformly distributed over [-$\pi/3$, $\pi/3$].

First we compare the patterns formed by the complex-conjugate method and the DOA method. At each estimated $\tilde{\tau}_{1,p}$, we obtain the $\bar{z}_1^m(\tilde{\tau}_{1,p})$ for each element. The pattern formed by the complex-conjugate method can be expressed by $\sum_{m=1}^{M} \bar{z}_1^{m*}(\tilde{\tau}_{1,p}) \cdot a_m(\theta)$, where $a_m(\theta) = e^{jk(m-1)d\sin(\theta)}$. This pattern is the FT (Fourier transform) of $\bar{\mathbf{z}}_1^*(\tilde{\tau}_{1,p})$ with respect to m. By the DOA method, we apply the FT to the sampled value $\bar{z}_1^m(\tilde{\tau}_{1,p})$ and obtain the DOA $\tilde{\theta}_{1,p}$. The beam pattern formed by the DOA method can then be expressed by $\vec{\mathbf{a}}^*(\tilde{\theta}_{1,p}) \cdot \vec{\mathbf{a}}(\theta)$. The resultant patterns obtained by the above two methods are shown in Fig. 6.2 (a), (b) and (c) respectively for p=1, 2, 3. In fact, the patterns formed by the complex-conjugate method and the DOA method should be identical if the SINR is significantly high. However, the pattern formed by the complex-conjugate method will be degraded if the MAI is increased. One can easily find that in Fig. 6.2 patterns obtained by both methods have almost the same mainlobe level, but the patterns obtained by the complex-conjugate method (dashed curves) have higher sidelobe levels.

Next we demonstrate the downlink patterns formed by the five beamforming techniques stated in the previous section. Use the same parameter sets of the above example, the five downlink-synthesized patterns are shown in Fig. 6.3 (a) and 6.3 (b).

It is seen that the mainlobe directions obtained by the complex-conjugate method have shifted a small value due to the difference between the uplink and downlink carrier frequencies. The pattern difference between the complex-conjugate method and the DOA method is more pronounced in the multiple-beam case than in the single-beam case.

Neglect the uplink and downlink fading effect. Assume that the channel parameters of the desired user and the parameter distributions of the undesired users are the same as in the previous example. We conducted 200 independent interference simulations for each fixed number of active users. We first calculate the uplink SINR after RAKE combiner using the two-uplink beamforming techniques for each parameter set and then calculate the mean SINR averaged over the 200 simulations. The resultant mean SINR versus number of interfering users are shown in Fig. 6.4. The theoretical values (obtained by Eq. (5.3)) are also shown in the figure for comparison. It is seen that both methods almost have the same performance and approach the theoretical values. This result can be explained by observing the synthesized antenna patterns of Fig. 6.2. Although the two patterns have different sidelobe levels, they have almost the same mainlobe level. The sidelobes have little contribution to the SINR when the SINR is high (for example, greater than 10 dB). Therefore the resultant SINRs for both methods are almost the same.

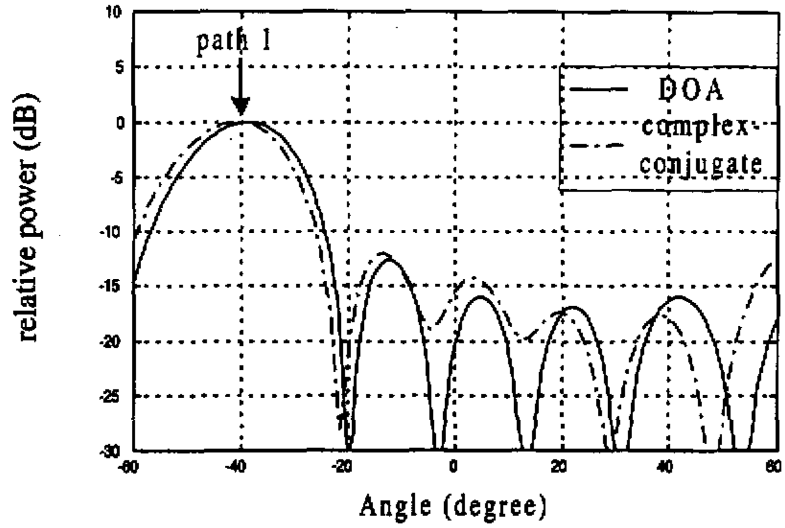

(a)

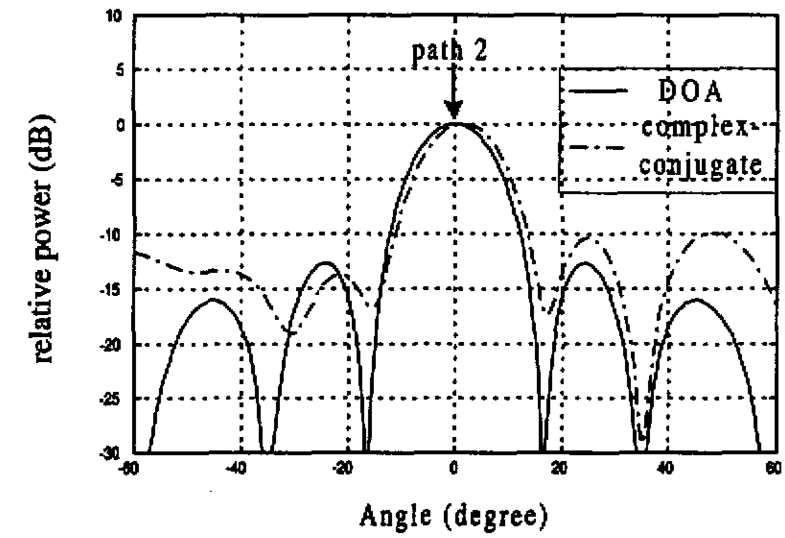

(b)

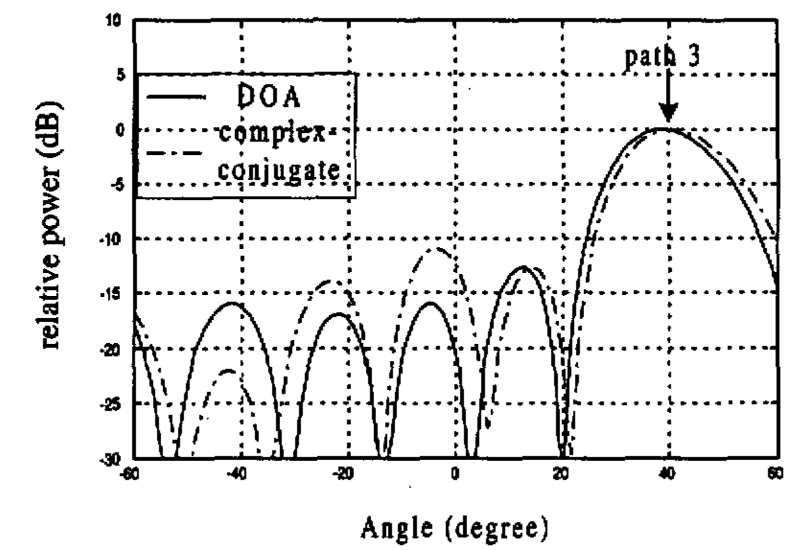

(c)

Fig. 6.2 Uplink antenna patterns synthesized by the DOA and complex-conjugate method for: (a) Path 1, (b) Path 2, (c) Path 3

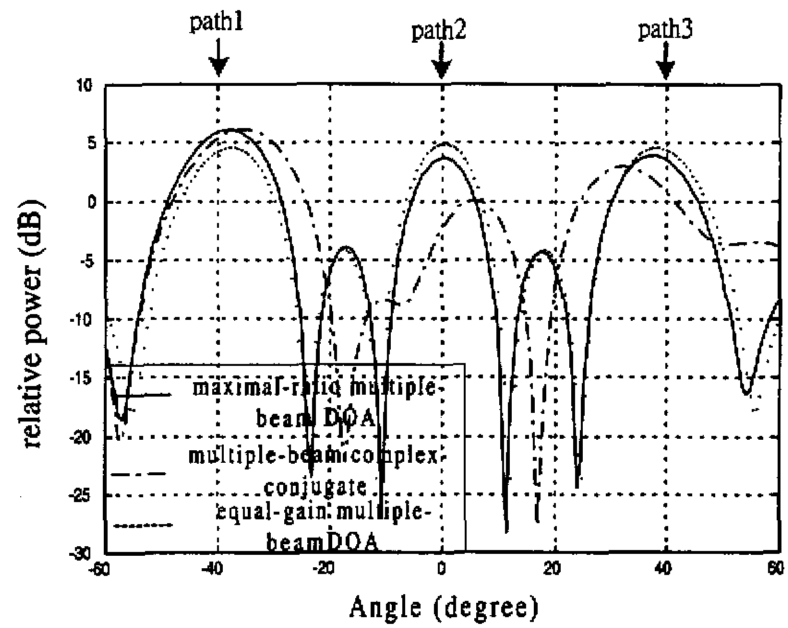

(b)

Fig. 6.3 Downlink patterns synthesized by different beamforming

conjugate method, (b) by maximal-ratio multiple-beam DOA, equal-gain multiple-beam DOA, and multiple-beam complex-conjugate method

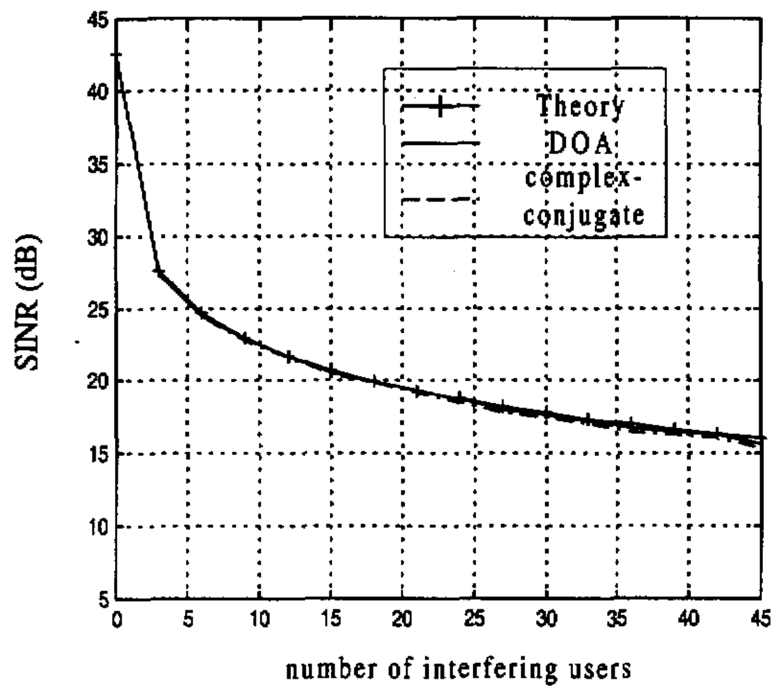

Fig. 6.4 Plots of the uplink mean SINR versus number of interferers

Next we compare the downlink SINR performance obtained by the five different beamforming techniques. We use the measured matched filter output and the

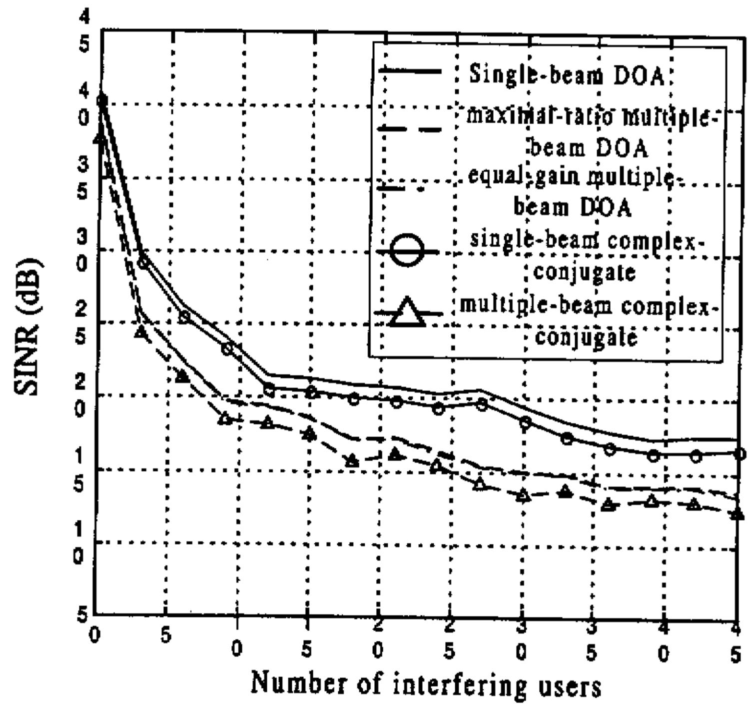

Fig. 6.5 Plots of the downlink mean SINR versus number of interferers when different downlink beamforming methods are used

derived DOA at the uplink and then apply the five downlink beamforming techniques to calculate the field, including the desired signal and interference, received at the mobile. Assume that a time slot contains 4 pilot bits in the downlink. For each parameter set we calculate the downlink SINR after RAKE combiner. The mean SINRs obtained by the five techniques are shown in Fig. 6.5. It is seen that the single-beam method has a much better performance than the multiple-beam method. In downlink, the code sequences among different users are orthogonal to each other if no multipaths exist. Moreover, the DOA method gives a better performance than the complex conjugate method. This result can also be explained by observing the synthesized patterns of Fig. 6.3. It is noted that the single-beam method has a higher gain in the desired path direction and smaller total angular coverage in the mainlobe. This will give a higher desired signal level and a smaller MAI in the mobile receiver.

Next we consider the fading effect of each multipath. The channel parameters of the desired user are shown in Table 6.1. The desired user has three clusters of multipaths. Each cluster contains two paths. The mean DOAs of these three clusters are -40^0, 0^0, and 40^0 respectively and each DOA of the multipath is uniformly distributed over $[-5^0, 5^0]$ about the respective mean DOA. Assume that the distance between the BS (base station) and the desired MS (mobile station) is 1.4Km and the relative time delays of multipath components are shown in Table 6.1. We also assume that each co-channel user has six paths and the DOAs of each path are uniformly distributed over $[-\pi/3, \pi/3]$. The instantaneous amplitude of each path has a Rayleigh fading. The uplink and downlink have independent Rayleigh fading for the FDD system considered in the simulation. The phase shifts of each path are uniformly distributed over $[0, 2\pi]$.

Table 6.1 Channel parameters of the desired user (with fading)

CLUSTER	1		2		3	
PATH#	1	2	3	4	5	6
$\theta_{1,1}$ $(\pm 5^0)$	0^0 $(\pm 5^0)$	0^0 $(\pm 5^0)$	-40^0 $(\pm 5^0)$	-40^0 $(\pm 5^0)$	40^0 $(\pm 5^0)$	40^0 $(\pm 5^0)$
$\tau_{1,1}$	0	$2T_c$	$4T_c$	$7T_c$	$8T_c$	$9T_c$
fading	Rayleigh	Rayleigh	Rayleigh	Rayleigh	Rayleigh	Rayleigh

For each of the three cases of 1, 20, 40 total active users, we randomly generate 1000 parameter sets for each case. For each parameter sets we calculate the fields received by each antenna element and find the required weightings for the downlink using the five beamforming techniques. For the downlink, we assume that the basestation transmits equal power for each user channel. Using the propagation model described in the previous paragraph, we calculate the downlink SINR after the mobile station's RAKE combiner. For the three different numbers of active users we count the cumulative distribution function (CDF) of the SINR for five different beamforming techniques. The SINR statistics are shown in Fig. 6.6(a) and 6.6(b) respectively.

Fig. 6.6(a) compares the performance obtained by the single-beam method and the multiple-beam method. It is seen that in the low SINR region the multiple-beam method has a better SINR performance because the probability that all paths having deep fading are much smaller. While in the high SINR region the single-beam method has a better SINR performance because at the mobile receiver it has a stronger desired signal and a smaller interference as explained in the previous example. Fig. 6.6(b) compares the SINR performance obtained by the complex-conjugate method, the DOA method with equal-gain and the DOA method with maximal-ratio, all using the multiple-beam beamforming technique. It is seen that the DOA method has a better performance than the complex conjugate method. The maximal-ratio method has a slightly better performance than the equal-gain method, but the difference is very small.

6.4 Summary

In this chapter we study and compare the uplink and downlink SINR performance when different beamforming techniques are applied in the antenna array of the basestation. In the uplink we compare the DOA method and the complex conjugate method and we found that these two methods have almost the same SINR performance. However, the complex conjugate method does not need any additional computation loading. In the downlink we compare the single-beam and multiple-beam beamforming techniques and we found that the multiple-beam method has a better SINR performance in the low SINR region because the single-beam method is more likely to suffer from deep fading. While in the moderate or high SINR region the single-beam method has a much better SINR performance because it has a higher antenna gain in the main path direction and a smaller angular coverage of the mainlobe, which will result in a stronger signal level and smaller MAI at the mobile receiver. The complex conjugate method will shift the downlink mainlobe a slightly due to the difference in carrier frequencies between the uplink and downlink. This will cause SINR degradation. However, the degradation is smaller than 1 dB. Therefore, the complex conjugate method is a valuable method if the DOA information is not needed for further applications. We also found that the DOA method with maximal-ratio gain has a slightly better SINR performance than that with the equal-gain beamforming. However, the difference is very small.

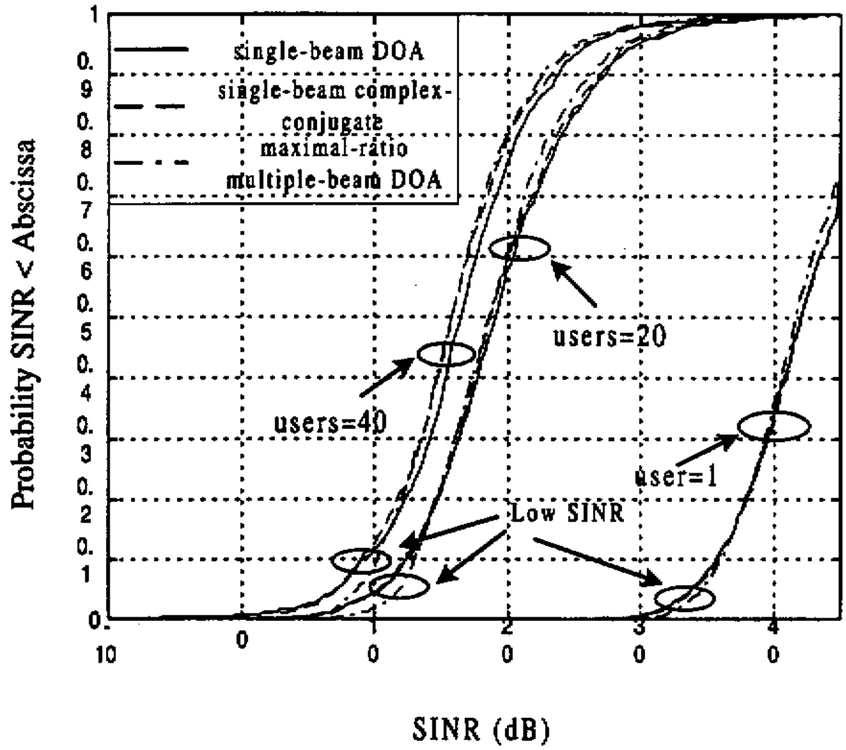

(a)

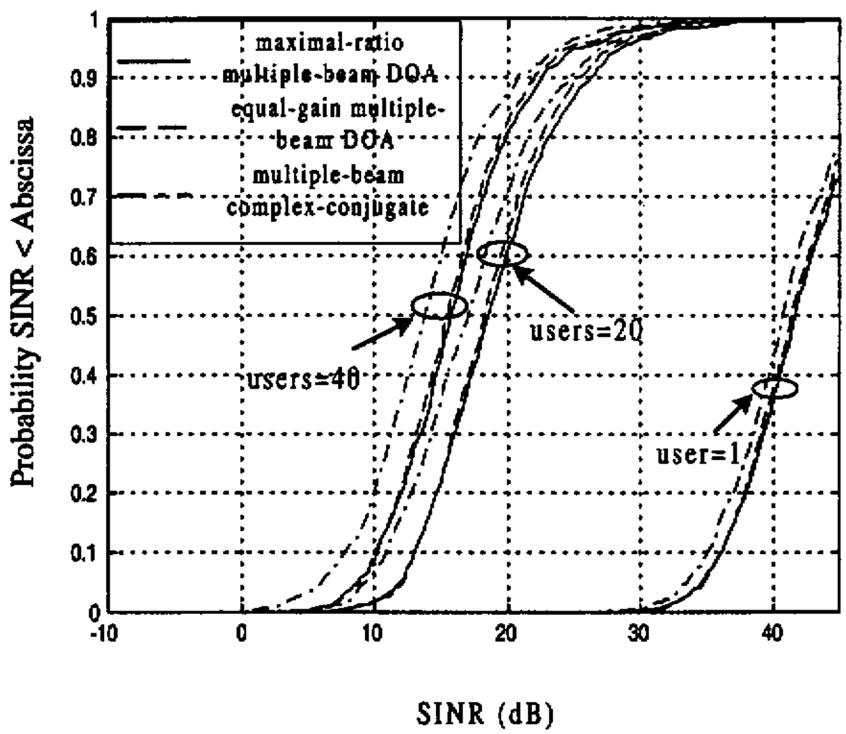

(b)

Fig. 6.6 Plots of the downlink SINR statistics obtained by different beamforming methods: (a) by single-beam DOA, Single-beam complex-conjugate and multiple-beam maximal-ratio combining method, (b) by multiple-beam maximal-ratio combining, multiple-beam equal-gain combining, and multiple-beam complex-conjugate method

Chapter 7 Comparison of Different Adaptive array Techniques for W-CDMA Communication System

It is anticipated that antenna array together with adaptive spatial-temporal processing techniques will be used in the future high capacity cellular communication systems, to combat co-channel interference, time dispersion and multipath fading. In previous chapters, we have proposed a channel estimation algorithm of 2D-RAKE receiver for the W-CDMA systems. We have also studied and compared the uplink and downlink SINR performance when the DOA method and the complex conjugate method are applied in the antenna array of the basestation. These two methods are designed to match the desired signal waveform to obtain the maximal desired signal power, but not to reduce the co-channel interference. In fact, the co-channel interference in previous studies can be considered as white Gaussian noise when the number of interfering signals is large. Under this condition, the maximal ratio combining approach produces the highest output SINR at the receiver. On the contrary, the adaptive array is designed to null stronger interfering signals, and therefore it can achieve higher output SINR when only a few simultaneous active users exist.

In cellular mobile systems, the adaptive array is usually designed to form beams to the uplink desired signals. However, the adaptive array beamforming in downlink will suffer more challenging than in the uplink. The main difficulty is due to the different frequency bands being used in uplink and downlink while the FDD strategy is employed. The difference in frequency may shift the null and mainbeam directions, which may degrade SINR at the mobile receiver.

The remain of this chapter will compare the uplink and downlink SINR performance when the adaptive array method and the DOA method are applied in the antenna array of the basestation. In addition, we will derive an analytic solution of the SINR after 2D-RAKE receiver for the optimal combination approach. The derivation follows the concept of adaptive array and the equation (5.3).

7.1 Adaptive Algorithm and Weight Equation

The adaptive weighting vector can be estimated by a number of different techniques. If a periodic block training sequence is exploited in the system, the techniques (such as the Least Mean Square (LMS) method [47,48], or the Direct Matrix Inversion (DMI) method [5,49]) can be applied to calculate the adaptive weighting vector. In these approaches, the basestation uses the known training sequence as reference signals to estimate the adaptive weights. Since these reference signals are correlated with the desired signal and uncorrelated with any other interfering signals, it can be used by the adaptive array to distinguish the desired from the interfering signals. Similarly, the pilot signal in the W-CDMA system proposed by ETSI can also be used as the reference for estimating the adaptive weights. Thus, the DMI technique can be employed in the W-CDMA communication system.

There is another type of adaptive algorithm which does not need training sequence but uses the special code properties of CDMA systems called code filtering [4,50] to estimate channel response. This approach uses both the pre-processing and post-processing array covariance matrices to estimate the array response vector and the interference plus noise covariance matrix. With appropriate estimates of the array response vector and covariance matrix, the adaptive weight can be calculated. In fact, the pilot sequence can be easily applied to the code filtering to reduce the computational loading and decrease the system complexity.

The remain of this section will describe how to exploit the channel estimation algorithm described in chapter 4 into the DMI or code filtering algorithms to estimate the adaptive weight.

7.1.1 DMI Algorithm

With equation (4.3) and perfect instantaneous power control assumption, the equivalent complex baseband signal vector x(t) at the basestation can be expressed by

$$\mathbf{x}(t) = \sum_{k=1}^{K} \sum_{l=1}^{L_k} \hat{\mathbf{a}}_k(\theta_{k,l}) \sum_{n=-\infty}^{n=\infty} b_k(n) c_k(t - nT_b - \tau_{k,l}) + n(t) \tag{7.1}$$

where K is the number of simultaneous active users (one desired and K-1 interfering users), L_k is the number of propagation paths of the *k-th* user. The parameters $\alpha_{k,l}, \phi_{k,l}, \tau_{k,l}, \theta_{k,l}$ and $\mathbf{a}_k(\theta_{k,l})$ defined previously are all now associated into $\hat{\mathbf{a}}_k(\theta_{k,l})$, which represents the complex propagation vector of the *k-th* user, $b_k(n)$ is the *n-th* bit value and $c_k(t)$ is the spreading waveform assigned to the *k-th* user and T_b is the bit period.

With DMI approach, the adaptive weights of the *k-th* user are given by [5,49]

$$\mathbf{a}_{opt}^{k} = R_{xx}^{-1} \hat{\mathbf{a}}_k \tag{7.2}$$

where the superscript –1 denotes the inverse of the matrix and R_{xx} is the covariance matrix given by

$$R_{xx} = E\{XX^H\} = \frac{1}{\overline{K}} \sum_{j=1}^{\overline{K}} \mathbf{x}(j) \cdot \mathbf{x}^H(j) \tag{7.3}$$

where $\overline{K}$ is the number of samples used and the superscript H denotes Hermitian transposition that is transposition combined with complex conjugate. In practice, the $\hat{\mathbf{a}}_k$ is unknown to the basestation, but this can be estimated if each mobile transmits a pilot signal with data, or by using periodic training sequences combined with decision feedback schemes. With equation (4.21) and (4.22) and assuming that the 1st user is the desired user, the channel response vector of each dominant multipath, $\tau_{1,l}$, of desired user can be estimated and used to calculate the optimal weight $\mathbf{a}^{1}_{opt}$ by equation (7.2), i.e.

$$\mathbf{a}^{1}_{opt}(\tau_{1,l}) = R_{xx}^{-1}\overline{\mathbf{Z}}_{1}(\tau_{1,l}) \qquad (7.4)$$

where $\overline{\mathbf{Z}}_{1}(\tau_{1,l})$ is the mean delay profile vector of the *l-th* dominant multipath of the desired user.

7.1.2 Code Filtering Algorithm

The basic concept of adaptive antenna beamforming is to steer nulls to interfering signals so that SINR can be much improved. Thus, the desired signal subspace and the interference plus noise subspaces should be decomposed [50]. With equation (4.15) the matched filter output (or post-processing) of the desired user can be written as

$$\begin{aligned}\mathbf{Z}_{1}(\tau) &= \int_{(n-1)T_b+\tau}^{nT_b+\tau} \mathbf{X}(t)\tilde{\mathbf{c}}_{1}(t-\tau)dt \\ &= T_b b_1(n)\hat{\mathbf{a}}_1(\theta_{1,1}) + T_b b_1(n)\sum_{l=2}^{L_1} \hat{\mathbf{a}}_1(\theta_{1,l})\delta(t-\tau_{1,l}) \\ &+ \mathbf{S}_1(\tau) + \mathbf{m}_1(\tau) + \eta_1(\tau), \qquad 0 \le \tau \le T_b \qquad (7.5)\end{aligned}$$

where $\mathbf{S}_1$ represents self-interference due to other multipath components and has non-zero correlation sidelobes due to non-perfect orthogonality of codes, $\mathbf{m}_1$

represents MAI due to other user's signals, and η_1 is due to thermal noise. Considering the 1st path of the desired user and following as [4,50], the pre-processing and post-processing array covariances are given

$$R_{xx} = E\{XX^H\} = \hat{\mathbf{a}}_1(\theta_{1,1})\hat{\mathbf{a}}_1^H(\theta_{1,1}) + Q \qquad (7.6)$$

$$R_{zz} = E\{Z_1 Z_1^H\} = T_b^2 \hat{\mathbf{a}}_1(\theta_{1,1})\hat{\mathbf{a}}_1^H(\theta_{1,1}) + T_b Q \qquad (7.7)$$

where **Q** represents the array covariance due to all antenna signals other than the 1st path signal of the desired user. The interference plus noise covariance can be calculated by

$$Q = \frac{T_b}{T_b - 1}(R_{xx} - \frac{1}{T_b^2} R_{zz}) \qquad (7.8)$$

or

$$Q = [R_{zz} - T_b^2 \hat{\mathbf{a}}_1(\theta_{1,1})\hat{\mathbf{a}}_1^H(\theta_{1,1})] / T_b \qquad (7.9)$$

The principal eigenvector of (R_{xx}, R_{zz}) is used as an estimate of the multipath array vector $\mathbf{a}_1(\theta_{1,l})$. Then, the adaptive array vector is calculated by

$$\mathbf{a}_{opt} = \frac{Q^{-1}\mathbf{a}_1}{\mathbf{a}_1^H Q^{-1} \mathbf{a}_1} \qquad (7.10)$$

Unfortunately, the eigenvector cannot provide an estimate of the absolute phase $\phi_{1,1}$ of the channel when calculating the autocorrelation matrix. Therefore, non-coherent data detection may be required. Instead, the channel response vector and time delay of each dominant multipath component can be estimated with equation (4.21) and (4.22) and the $Q_{1,l}$ of each *l-th* tracked multipath can be calculated by

$$Q_{1,l} = R_{xx} - \frac{1}{T_b^2}[\overline{\mathbf{Z}}_1(\tau_{1,l})\overline{\mathbf{Z}}_1^H(\tau_{1,l})] \qquad (7.11).$$

or

$$Q_{1,l} = R_{zz} - [\overline{Z}_1(\tau_{1,l})\overline{Z}_1^H(\tau_{1,l})] \qquad (7.12)$$

Then, the adaptive array vector is calculated as

$$\mathbf{a}_{opt}^1(\tau_{1,l}) = \frac{Q_{1,l}^{-1}\overline{\mathbf{Z}}_1(\tau_{1,l})}{\overline{\mathbf{Z}}_1^H(\tau_{1,l})Q_{1,l}^{-1}\overline{\mathbf{Z}}_1(\tau_{1,l})} \qquad (7.13)$$

After the adaptive weights have been estimated, they are used to adapt to the multipath signal component with corresponding delay, and then summed together of each delaying paths to give the 2D-RAKE received output.

If the co-channel interference can be considered as white Gaussian noise, the *SINR* after the 2D-RAKE receiver can be approximated by equation (5.3). In some cases, the co-channel interference can not be modeled as white Gaussian noise. For examples, only a few simultaneous active users, the uniform distribution of interfering signals can not be assumed, a few users loss the power control strategy, or some data are transmitting with high data rates and produce stronger interfering signals etc. These stronger interfering signals may seriously degrade the *SINR* performance and the purpose of adaptive array is designed to null out them to improve the *SINR* performance. It is well known that the maximum number of interfering signals that can be nulled is M-1 if M antenna elements are employed. Therefore, if the optimal combination approach is exploited, the equation (5.3) has to be modified and can be expressed in terms of a simple function by

$$SINR = \frac{(GM)SNR}{(K-1-(\frac{M-1}{L}))SNR+1}, \quad L(K-1) \geq M-1 \qquad (7.14)$$

where *SNR* is the reverse link signal-to-noise ratio for each antenna element, G is the processing gain, M is the number of antenna elements, *K* is the total number of active users, and L is the number of multipath for each user *k*. It is noted that the above expression implies some important information. First, if only a few active users exist and most parts of interfering signals have been nulled out by the adaptive array, the SINR performance can be improved significantly. Second, if the number of interfering signals become large, the SINR performance with equation (7.14) will approach the results of equation (5.3). It means that the co-channel interference approach the uniform distribution and can be considered as white Gaussian noise.

In the next section we will use the same propagation model as used in chapter 4 and 5 to numerically calculate the mean SINR when different adaptive algorithms are employed in the uplink and downlink.

7.2 Simulation results

In this section we first compare the uplink and downlink beam patterns formed by different adaptive weight algorithms and then compare the uplink and downlink SINR performance obtained by different beamforming algorithm described in chapter 6.

Considering a uniformly spaced linear array with M antenna elements and $d=\lambda_u/2$ spacing, where λ_u is the uplink wavelength. The major uplink and downlink radio parameters of the simulations are listed in Table 4.1. Assume that the signal to noise ratio for each antenna element is 10 dB. The channel parameters about the desired user are shown in Table 4.2. There are three paths and the DOAs are -40^0, 0^0, and

40^0 respectively; the relative time delays are 0, $4T_c$, and $8T_c$ respectively; where T_c is the chip duration. Ideally, the 2D-RAKE receiver of the desired user has a bank of 3 adaptive beamformers. The *l-th* beamformer has an associated antenna weight vector, $\mathbf{a}_{opt}^{1}(\tau_{1,l})$, which adapts to the *l-th* multipath component and nulls out the other two multipath components. Fig. 7.1 (a) to (c) and Fig. 7.2 (a) to (c) show the uplink patterns beamformed to the *l-th* incident angle or path using different adaptive algorithms with M=4 or M=7 antenna elements, respectively. For the *l-th* beam pattern, it is obviously that the optimal weight (DMI or code filtering algorithm) has deep nulls at the other two path directions but the DOA algorithm does not. This property will improve the SINR performance. It is also noted that the gain at the *l-th* incident angle with optimal weight algorithms degrades a little due to insufficient separations between multipaths. If the DOAs of interfering signal are very close to the desired DOA, the gain at the desired direction will be seriously degraded compared to that of the DOA algorithm. Fig. 7.3 (a) and (b) show the beam patterns when an additional interfering signal is incident at angle 50^0 with antenna element number M equals to 4 and 7 respectively. It is noted that the additional interfering signal has been nulled out, but the gain at the direction of the desired signal has been seriously degraded and the sidelobes also become larger. The reduction in the mainlobe direction and the increase of sidelobe may greatly degrade the downlink performance if the same weights are used in the downlink.

While the number of interfering signals becomes very large, the beam patterns formed by adaptive weights no longer can significantly attenuate interfering signals. Especially when the interfering signals are uniformly distributed in the coverage range. Thus, the array will act as if it were in the environment of thermal noise. Fig. 7.4 shows the beam patterns with M=7, where 24 co-channel interfering users and each user having 3 multipaths have been assumed. Obviously, the nulling capability is no longer very effective. It is noted that the gain of mainlobe is decreased due to the

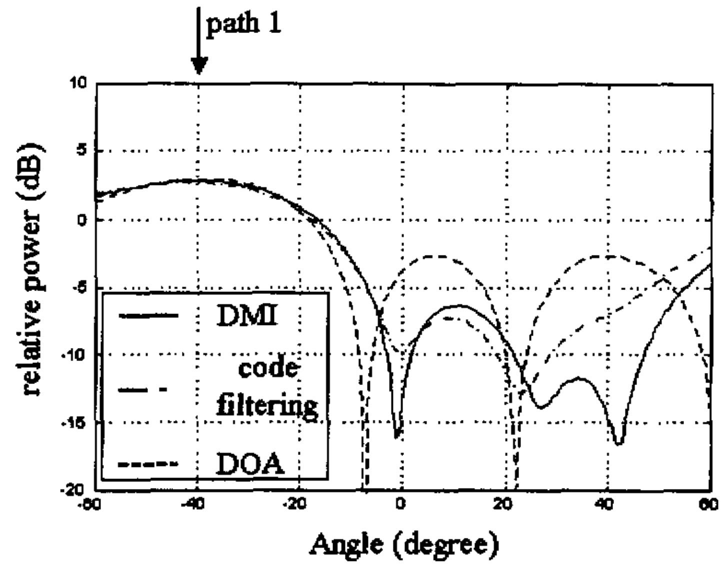

(a)

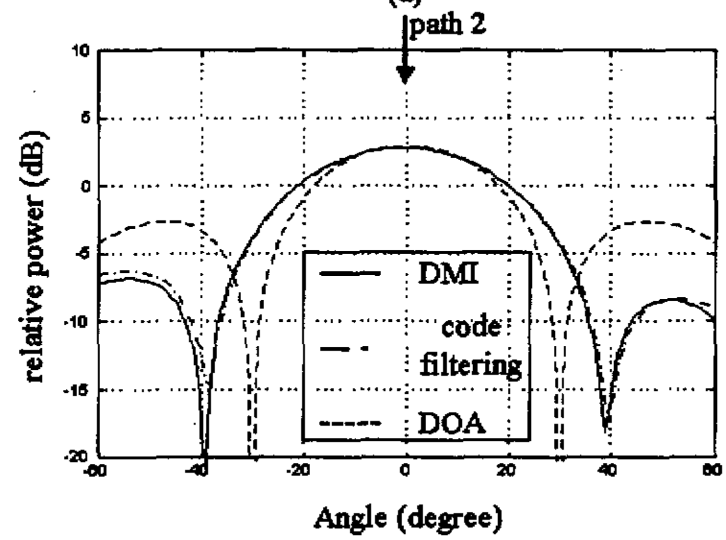

(b)

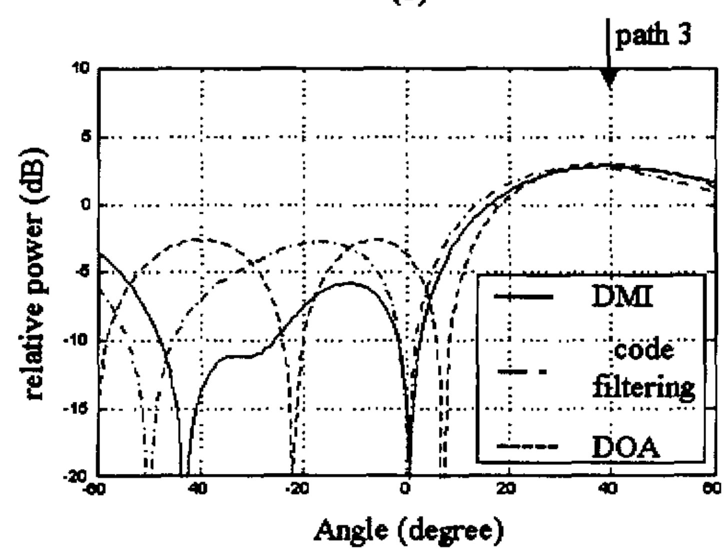

(c)

Fig. 7.1 Uplink antenna patterns synthesized by DMI, code filtering, and DOA methods with M=4 for : (a) path 1, (b) path 2, (c) path 3

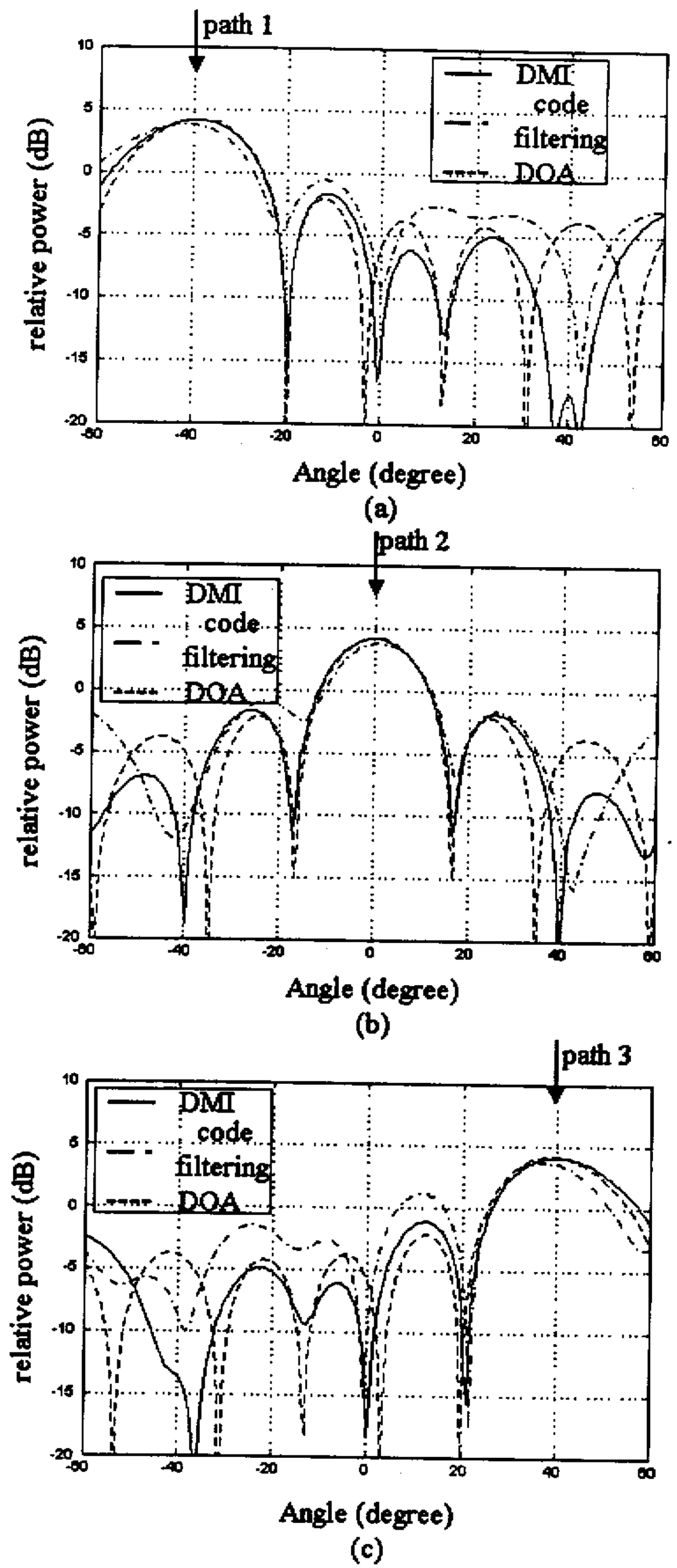

Fig. 7.2DOA Uplink antenna patterns synthesized by DMI, code filtering, and DOA methods with M=7 for : (a) path 1, (b) path 2, (c) path 3

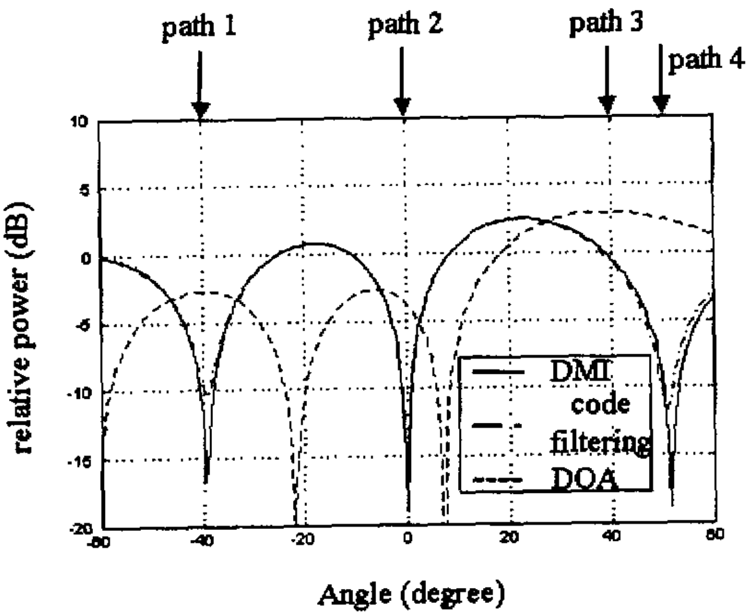

(a)

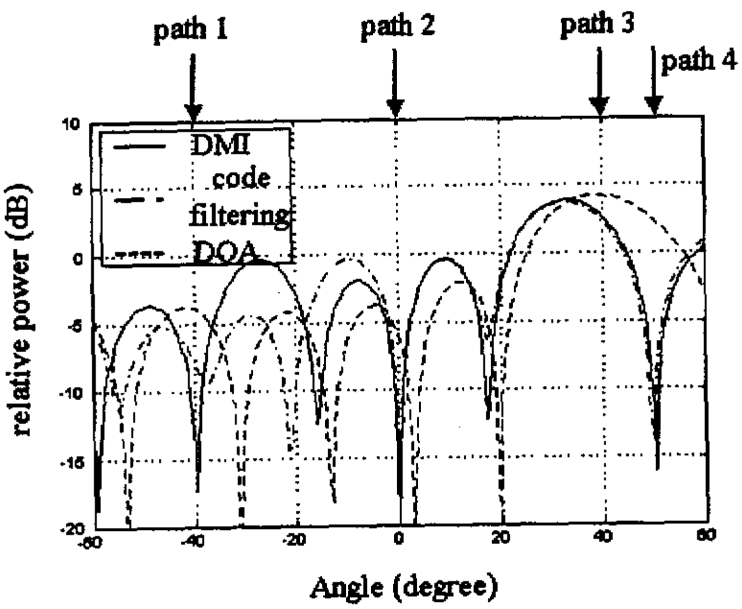

(b)

Fig. 7.3 Uplink antenna patterns synthesized by DMI, code filtering, and DOA methods with additional interfering signal from at 50^0 for: (a) M=4,(b) M=7

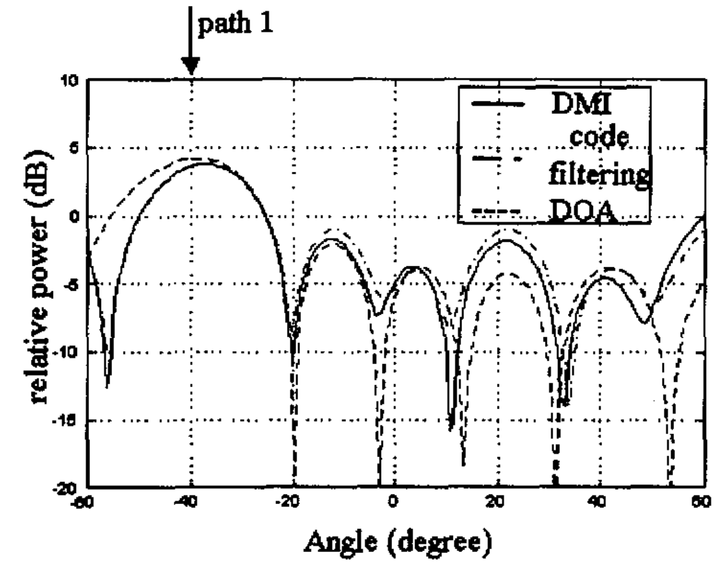

(a)

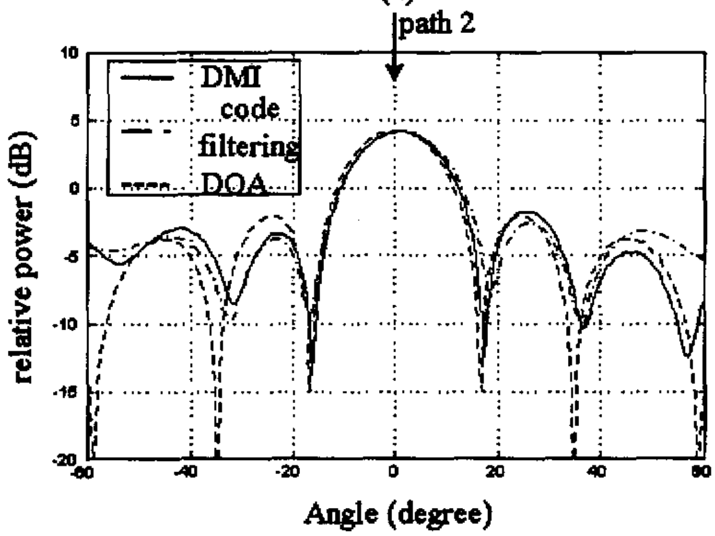

(b)

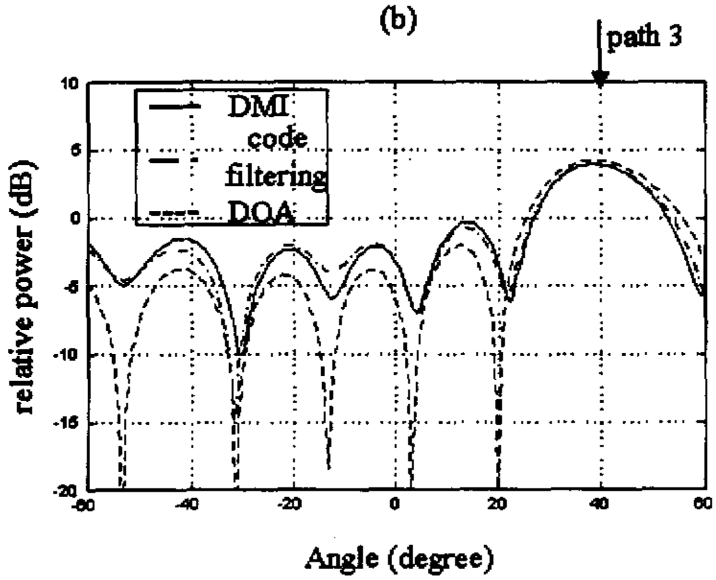

(c)

Fig. 7.4 Uplink antenna patterns synthesized by DMI, code filtering, and DOA methods having 24 co-channel interfering users with M=7 for : (a) path 1, (b) path 2, (c) path 3 increase of sidelobe. However, the array can still null partial of stronger interfering signals, and thus the SINR performance of the optimal combining is better than that of the maximal ratio combining.

Next we demonstrate the downlink patterns with single-beam and multiple-beam formed by code filtering and DOA techniques. The downlink beamforming algorithms are described in chapter 6. Assume that there are four active co-channel users (one desired user and three interfering users) and each user having three multipaths as assumed before. The uplink and downlink patterns with M=7 are shown in Fig. 7.5. Clearly, it is seen that the mainlobe direction obtained by code filtering method has been shifted from the desired direction due to the difference between the uplink and downlink carrier frequencies. The nulling positions of stronger interfering signals shown in Fig. 7.5(a) have also been changed.

It is also noted that the difference between the code filtering and the DOA method is more obvious in the multiple-beam case. The sidelobe becomes larger, mainlobes have been shifted, and the gains of mainlobes are decreased in the code filtering method. For the code filtering method whether in the single-beam or multiple-beam cases, the mainlobe shifted from the desired direction will decrease the signal power received at the mobile. The reduction of the interference nulling ability will produce more interference to other unwanted directions. Furthermore, the higher sidelobe will give more interference to other channels. These disadvantage factors in code filtering and DMI methods will cause significant degradation in SINR performance at the mobile end.

Next we compare the uplink and downlink mean SINR after RAKE combining using different adaptive weight algorithms. Assume that the channel parameters of the desired user and the parameter distributions of the undesired users are the same as in the previous chapters and neglect the uplink and downlink fading effect. We conducted 100 independent interference simulations for each fixed number of active users and average them to obtain the mean SINR. The received signal powers and

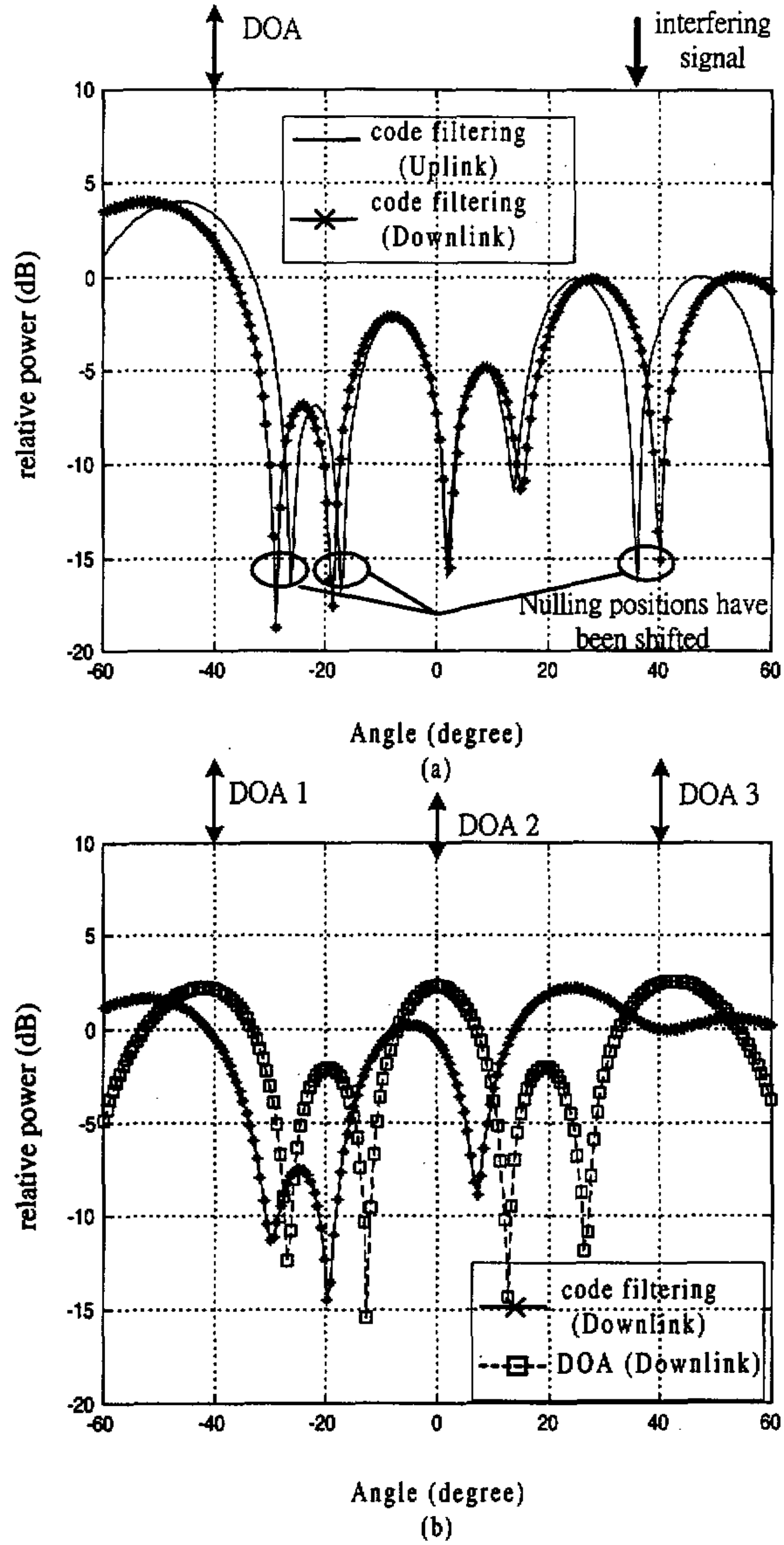

Fig. 7.5 (a)Comparison of Uplink and Downlink antenna patterns formed by single-beam code filtering method with M=7, (b) Downlink patterns synthesized by multiple-beam DOA and multiple-beam code-filtering method with M=7

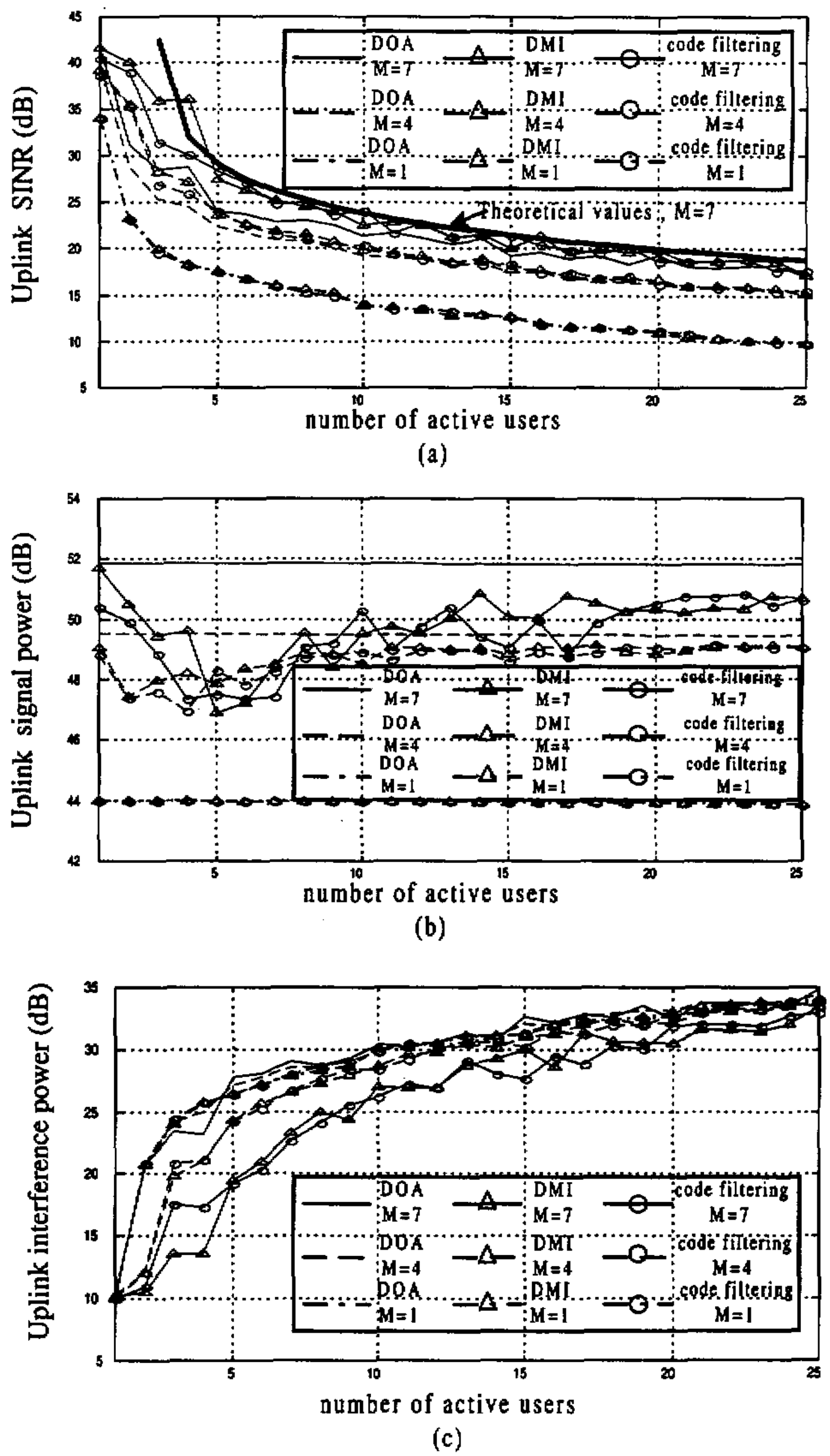

Fig. 7.6 plots of the uplink received SINR, signal power, and interference power versus number of co-channel active users when different adaptive-array algorithms are used

interference powers are also compared.

The results of the uplink mean SINR, the mean signal power and the mean interference power versus the number of interfering users are shown in Fig. 7.6 (a) to (c), respectively. The theoretical values of eq. (7.14) for M=7 are also plotted in Fig. 7.6(a) for comparison. In Fig. 7.6(a), it is noted that both DMI and code filtering methods almost have the same performance which is much better than the DOA method when the number of users is small. This is because the DMI and code filtering methods can null out partial of strong interfering signals. This result can also be explained by observing the received mean signal and interference powers of Fig. 7.6(b) and Fig. 7.6(c). Although the mean signal power (Fig. 7.6 (b)) of the optimal combining method decrease due to the reduction of the mainlobe, the mean interference powers (Fig. 7.6 (c)) have been significantly reduced due to the interference nulling effect. In Fig. 7.6(a), it is also noted that the results obtained by computer simulation approach the theoretical values.

However, as the number of interfering users increases to a certain amount, the SINR improvement becomes less obvious. It is also seen that the mean signal powers and interference powers obtained by the optimal combining method and the DOA method approach to the same performance as the number of co-channel users increases to a certain number. This result can be explained by observing the synthesized antenna patterns of Fig. 7.4. The optimal combining techniques can improve SINR performance, however, additional computation loading is needed to invert the covariance matrix and calculate the optimal weight.

For the downlink, we assume that the basestation transmits equal power for each user. The downlink mean SINR performances obtained by different methods are shown in Fig. 7.7. It is seen that the DOA method has a much better performance than those of the DMI and code filtering methods. This result can also be explained by observing the synthesized antenna patterns of Fig. 7.5. It is noted that the single-beam method has a higher SINR than the multiple-beam method when the all number of users have the same property. This is because the orthogonality of the OVSF codes during all stages of the transmission can be kept orthogonal. If the number of multipaths is increased, the OVSF code will no longer be orthogonal to

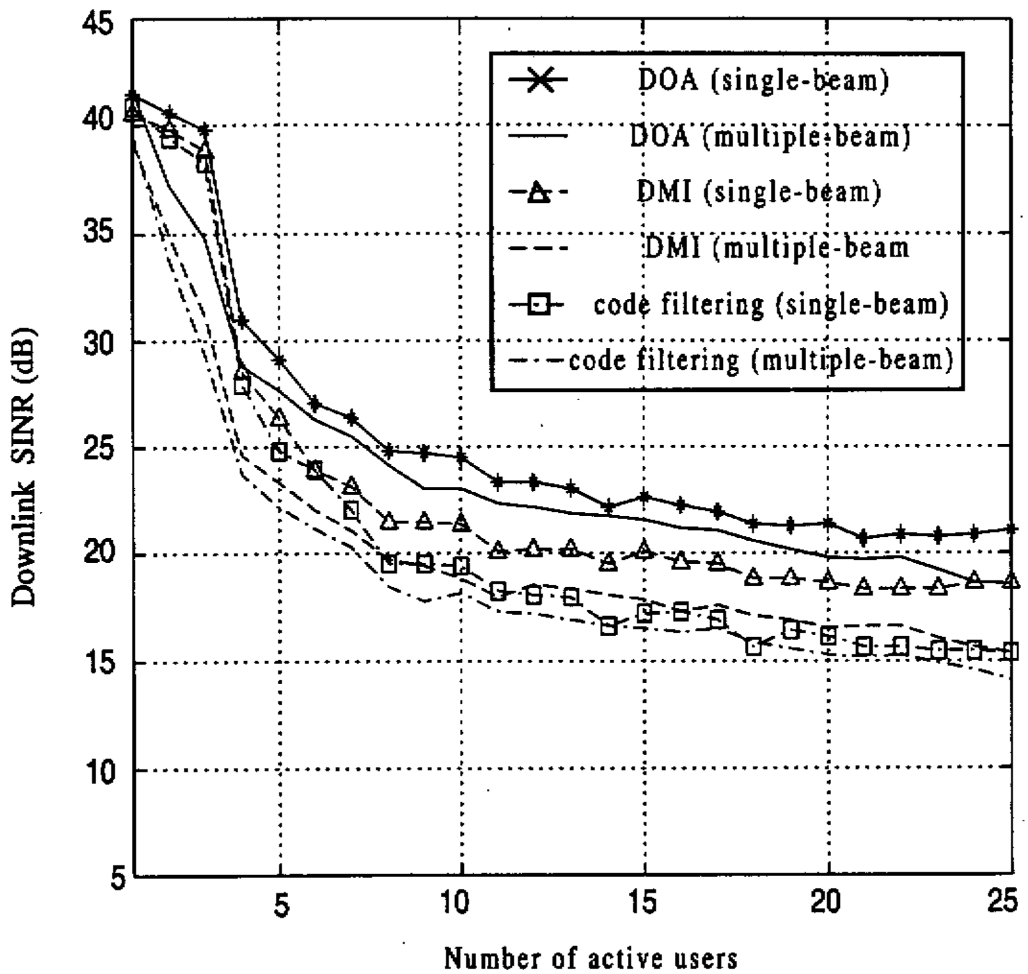

Fig. 7.7 plots of Downlink SINR versus number of active users obtained by different adaptive algorithms and by different beamforming techniques with M=7

other codes.

7.3 Summary

In this chapter we have applied different adaptive weight techniques and exploit the channel estimation algorithm proposed in chapter 4 to study and compare the uplink and downlink SINR performance. In addition, we derived an analytical form of the SINR after 2D-RAKE receiver for optimal combination approach. We found that simulation results are very close to the theoretical values. We also found that the optimal combining (DMI and code filtering techniques) have much better SINR performance than the DOA method in the uplink when few users are present in the channel. But the SINR improvement is not clear as the number of interfering users increases. On the contrary, we found that the DOA method have much better SINR performance than the optimal combining technique in the downlink. All these results can be explained by observing the synthesized antenna patterns. If we compromise the SINR performance of uplink and downlink and take into account the complexity of the overall system, the DOA method would seem more suitable and reasonable for the W-CDMA systems. If we wish to obtain the best SINR performance in both uplink and downlink transmissions, both DMI method and DOA method can be simultaneously exploited in the basestation. It means that the optimal combining approach is exploited in uplink to produce the highest output SINR at the basestation receiver and the DOA method is applied in downlink to give better SINR performance at the mobile receiver.

Chapter 8 Beamforming Performance Comparison Using Channel Measurement Data

In the previous chapters, we used propagation models and numerical methods to evaluate transmission performance with different adaptive algorithms. In those simulations we have assumed that uplink and downlink have the same delay and angle of arrival for each multipath component even there is a frequency difference between them. In this chapter we will use the newly purchased vector channel sounder to measure the real channel characteristics and from the measurement data to simulate the W-CDMA transceiver and evaluate the transmission performance.

The chapter is organized as follows: first the principle and functions of the vector channel sounder will be briefly summarized. Next the measurement setup, the simulation method, and the signal processing method will be detailedly described. The transmission performance using different adaptive techniques will be compared and discussed.

8.1 Principle and Functions of the Vector Channel Sounder System

Our newly purchased "Vector Channel Sounder System (VCSS)" was made by the MEDAV Company. It can measure the instantaneous channel parameters, including the time of arrival (TOA), direction of arrival (DOA), complex amplitude of multipath components, and frequency response of the channels. The block diagram of the VCSS is shown in Fig. 8.1. The transmitter and receiver are coherently driven by highly stable Rubidium references. The transmitting antenna is an Omni-directional antenna, and the receiving antenna is an 8-element linear uniform array. The antenna element is vertically polarized and has an azimuthal beamwidth of 120^0. Bandwidth of the receiver can be up to 120 MHz and the time resolution of the channel impulse response can be up to 15nsec. There are two center frequencies: 1.95GHz and 2.44GHz.

The channel impulse response measurement is based on broadband periodic multi-frequency excitation signals and correlation processing. Due to the high bandwidth of 120 MHz and the reasonable array dimensions a large number of different multipaths can be resolved in the joint delay-angular domain. High repetition rates in data acquisition allow statistical analysis of the instantaneous channel characteristics. With the ESPRIT algorithm, super-high azimuthal resolution can be obtained. The technical data of our VCSS is shown in Table 8.1.

With the offline digital signal processing, several parameters, including impulse response, delay spectrum, delay-azimuth spectrum, Doppler-azimuth spectrum, delay-Doppler spectrum, over a snapshot or a collection of snapshots can be obtained and graphically displayed. The other statistical parameters, such as the root mean square delay spread, the coherent bandwidth, the root mean square Doppler spread, and the coherent time can also be derived.

In the following we will use the VCSS to measure the real channel characteristics.

8.2 Measurement Setup and Measurement Results

At the beginning of the measurement, the two Rubidium references of the transmitter and receiver should be calibrated so that they have the same frequency and can be considered as coherently driven. The receiving array was placed at Room 502 (on the 5^{th} floor of the Electrical Engineering Building) and faced on the campus through a window. The mobile (transmitter) moves along the campus and the traveling routes are depicted in Fig. 8.2. We divide the whole routes into 8 paths. Path 1, path 2 and path8 have a direct path, although the direct paths suffer tree-penetration loss. Along path 3, path 4, path 5 and path 6, the direct paths are blocked by buildings and the shortest paths are from rooftop edge diffraction. Along path 7, the mobile is in the shadow region and the signal cannot be detected. Plots of delay-snapshot along each path are shown in Fig. 8.3, where the abscissa represents the TOA in microsecond, the ordinate represents the snapshot number, and the color represents the magnitude. From the delay-spectrum plots we can trace multipaths when the mobile is moving.

For each snapshot (i.e., each mobile location), using the delay profiles received by each antenna and applying the ESPRIT algorithm, we can obtain the corresponding complex amplitudes and DOAs of multipath components for each time delay bin. In other words we can obtain the parameters set $\{\alpha_{il}, \theta_{il}, \tau_{il}\}$ of each snapshot *i*, where α_{il} and θ_{il} are the complex amplitude and the DOA of the l^{th} path with time delay τ_{il} respectively. The azimuth spectra of each path are shown in Fig. 8.4.

The above figures are obtained from signals with a bandwidth of 120MHz. Therefore, the time resolution can be as high as 15nsec. In the W-CDMA system, however, both the uplink and downlink signals could only have a bandwidth of 5MHz and there is a 190MHz difference in carrier frequencies between them. In the simulations of previous chapters, we have assumed that the magnitude, the TOA and the DOA of multipath components are invariant in the uplink and downlink although the carrier frequencies are different. In the following we will use the measured channel impulse responses (CIR) obtained from the respective lowest 5MHz band and the highest 5MHz band to evaluate the transmission performance.

The simulation procedure is as follows: for a single snapshot k, the uplink CIR (obtained from the lowest 5MHz band) measured by the m^{th} antenna element is denoted by $h_k(t,\tau,m)$. The complex amplitude and time delay of the l^{th} path are denoted by α_{ml}^{k} and τ_{ml}^{k} respectively. The digital signal received by the m^{th} element contributed by the mobile at this snapshot *k* can then be expressed by

$$E_m^k(t) = \sum_{l}^{L_k} \alpha_{ml}^{k} c_k(t - \tau_{ml}^{k}) \qquad (8.1)$$

where $C_k(t)$ is the modulated signal of the k^{th} user, *K* is the number of the simultaneous users. These *K* users' locations are randomly chosen from snapshots of the 8 paths. The total field received by the m^{th} element is then

$$E_m(t) = \sum_{k=1}^{K} \sum_{l}^{L_k} \alpha_{ml}^{k} c_k (t - \tau_{ml}^{k}) + n_m(t) \qquad (8.2)$$

where $n_m(t)$ is the noise of the m^{th} element.

Assume that the system is with perfect power control, therefore $\sum_{l=1}^{L_k} |\alpha_{ml}^{k}|^2$ is constant for all k. For each k, let $E_k(t)$ be the desired signal and $\sum_{j \neq k}^{K} E_j(t)$ be the interference. We then follow the same procedure as stated in the previous chapters and use different adaptive techniques to calculate the *SINR* at the output of the RAKE combiner. The normalized CIRs received by each antenna element at a given snapshot are treated as the desired signals. Given a number of users K, we generate 100 different sets of snapshots, which are randomly selected from the 8 paths, as the locations of the undesired users. For a Given number of users K, we calculate the respective *SINR* of each set of snapshots and then calculate the average *SINR* over the 100 sets. For each path every three snapshots we choose one snapshot as the desired user's location and randomly generate 100 sets of undesired users' locations and then calculate the average *SINR* for that location. The resultant average *SINR* at different desired locations obtained by the DOA method and the DMI method for K=1, 11, 21, 31 for different paths are shown in Fig. 8.5 (a) to (h). In Fig. 8.5 (f) and (g), some points are missing because the received fields are below the sensitivity level due to shadowing effect. Observing from the plots, we can find that the results almost have the same trends as those of the previous chapters. The *SINR* difference obtained by DOA method and the DMI method is small. There is no obvious evidence that those channels with LOS (path 1, 2, and 8) have better *SINR* performances than those of channels without LOS (path 3, 4, 5, 6, and 7) because perfect power control has been assumed in the simulations.

Next we use the measured downlink CIR (obtained from the highest 5MHz band) to evaluate the downlink transmission performance. If there is a direct path between the mobile and the basestation, the downlink CIR almost has the same shape as the uplink CIR. Shown in Fig. 8.6 are examples of the uplink and downlink CIRs of a certain snapshot with LOS. However, when the direct path is blocked and the angular spread of multipath components is large, we found that the uplink and downlink CIRs are very different in shape. Also they have different DOA distributions. Shown in Fig. 8.7 are examples of the uplink and downlink CIR and DOA at a certain snapshot without line of sight. If the weightings derived from the uplink were used for downlink beamforming, the downlink transmission performance may be much worse than what we expected.

In the following we describe the procedure how we use the measured uplink and downlink CIRs to evaluate the downlink transmission performance.

Let the downlink CIR measured by the m^{th} antenna element at snapshot k be denoted by $h_k'(t,\tau,m)$. The complex amplitude and time delay of the l^{th} path are denoted by $\alpha_{ml}'^{k}$ and $\tau_{ml}'^{k}$ respectively. It is noted that information of the downlink DOA is implicitly included in the phase of the complex amplitude $\alpha_{ml}'^{k}$. Assume the downlink weighting sets for each mobile user has been determined based on the uplink-measured field and the weighting set for the k^{th} user is denoted by $\{w_m'^{k}\}$. Also assume that each downlink channel has the same transmission powers. Then the received signal contributed by the k^{th} user is

$$E_k'(t) = \sum_{m=1}^{M} \sum_{l=1}^{L_k} \alpha_{ml}'^{k} c_k'(t-\tau_{ml}'^{k}) w_m'^{k} \qquad (8.3)$$

The interference received by the k^{th} user is

$$E_i'(t) = \sum_{j\neq k}^{K} \sum_{m=1}^{M} \sum_{l=1}^{L_k} \alpha_{ml}'^{k} c_j'(t-\tau_{ml}'^{k}) w_m'^{j} \qquad (8.4)$$

It is noted that all interference signals and the desired signal will travel through the same multipaths as those of the desired user because all channels use the same transmitting and receiving antennas. To evaluate the downlink *SINR*, we can consider it from different points of views. The first point of view is the code orthogonality. It is known that different user's downlink code sequences are orthogonal to each other. Therefore, $c'_k(t-\tau'^k_{ml})$ is orthogonal to all $c'_j(t-\tau'^k_{ml})$ for $j \neq k$. If the mobile is at a location having a strong LOS or dominant path, then the MAI will not be a problem even if a large number of interferers are present in the cell (here we neglect the intercell interference). If the mobile is at a location without a dominant path and having multipaths with time delay difference greater than a chip interval, the non-orthogonality between the code sequences of different users will be a serious problem. The second aspect is from the fading and beamforming points of view. In the W-CDMA/FDD system, the uplink and downlink have a 190MHz difference in carrier frequency, which may cause independent fading for each multipath components. The most significant path chosen from the uplink may suffer deep fading in the downlink. If the mainbeam is focused to that direction, then the beamforming will be a waste. If the delay bins chosen by the downlink are different from those chosen by the uplink, the mainbeam directions formed by the uplink may not be at the desired directions. In that case the signal power received at the mobile will not be at the optimum level and the *SINR* performance will be degraded.

In the downlink, for each given desired user's location and given numbers of users *K*, we use the same snapshot sets generated by the uplink to calculate the downlink mean *SINR*. We have employ the downlink code sequences, the complex CIRs obtained from the downlink band and the weighting sets derived from the uplink in the calculation. The resultant average *SINR* at different mobile locations for different paths are shown in Fig. 8.8 (a) to (h). It is seen that the downlink *SINR* performance is very different from that of the uplink and the performance is very location dependent. In general, the DOA method has better performance than that obtained by the DMI method. We have found that at some locations the *SINR*s are very high and almost independent of the number of users. The reason is that there is a strong direct path at these locations and the MAI is very small due to the orthogonal property among different user's spreading sequences. We also found that the *SINR* highly depends on the CIR and DOA distribution of the desired user. The higher the delay spread, the greater the MAI due to the nonorthogonality among the shifted code sequences and therefore the smaller the *SINR*. The greater the angular spread of the multipaths, the smaller the *SINR*. As seen from Fig. 8.7, we can find that the downlink DOA distribution is different from that of the uplink. The directions formed by the uplink may be different from those of the dominant paths of the downlink. The reduction in the gain pattern will cause *SINR* degradation.

The reason that DOA method has better performance than that of the DMI method can be explained as follows: the main concept of an adaptive array is to null the interference and maximize the *SINR*. In the uplink, the causes of interference can be from the large cross-correlation of the code sequences and /or the strong power level of the undesired signals. The multipath parameters, including the TOA and DOA, are different for different users. The antenna beams of the uplink are formed to null the interference. On the contrary, in the downlink, all channels, including the desired and the undesired, travel to the mobile through the same multipaths. All channels have the same TOA and DOAs. The code sequences of the uplink and downlink also have different cross-correlation property. In other words, the uplink channels and downlink channels are not reciprocal if both code sequences and multipaths traveled are considered. Therefore, we can not expect that the DMI method will have optimum downlink *SINR* performance even if the uplink and downlink use the same carrier frequency.

Table 8.1 Technical Data of Vector Channel Sounder System

Item Description	Specification
RF center frequency	1.95 and 2.44GHz
Measurement Bandwidth	Up to 120MHz
TX power	1~10 Watt +-0.5dB
Sensitivity	<= -87dBm
Dynamic range for automatic	51 dB
Observation time	Typ. 6.4 μs at bandwidth 120MHz
Time resolution	Typ. 15 ns at bandwidth 120MHz
TX antenna	omnidirection
Gain	< 3dBi
Polarization	vertical
RX array antenna	8 elements
Element Spacing	$\lambda/2$
Aperture	1200
polarization	vertical
Switching time of antenna multiplexer	< 1μs
Frequency reference	Internal Rubidium clock, 10MHz sine
Repetition time (typ.):	
Standard Doppler	> 1.024 msec
FAST Doppler	> 100μs

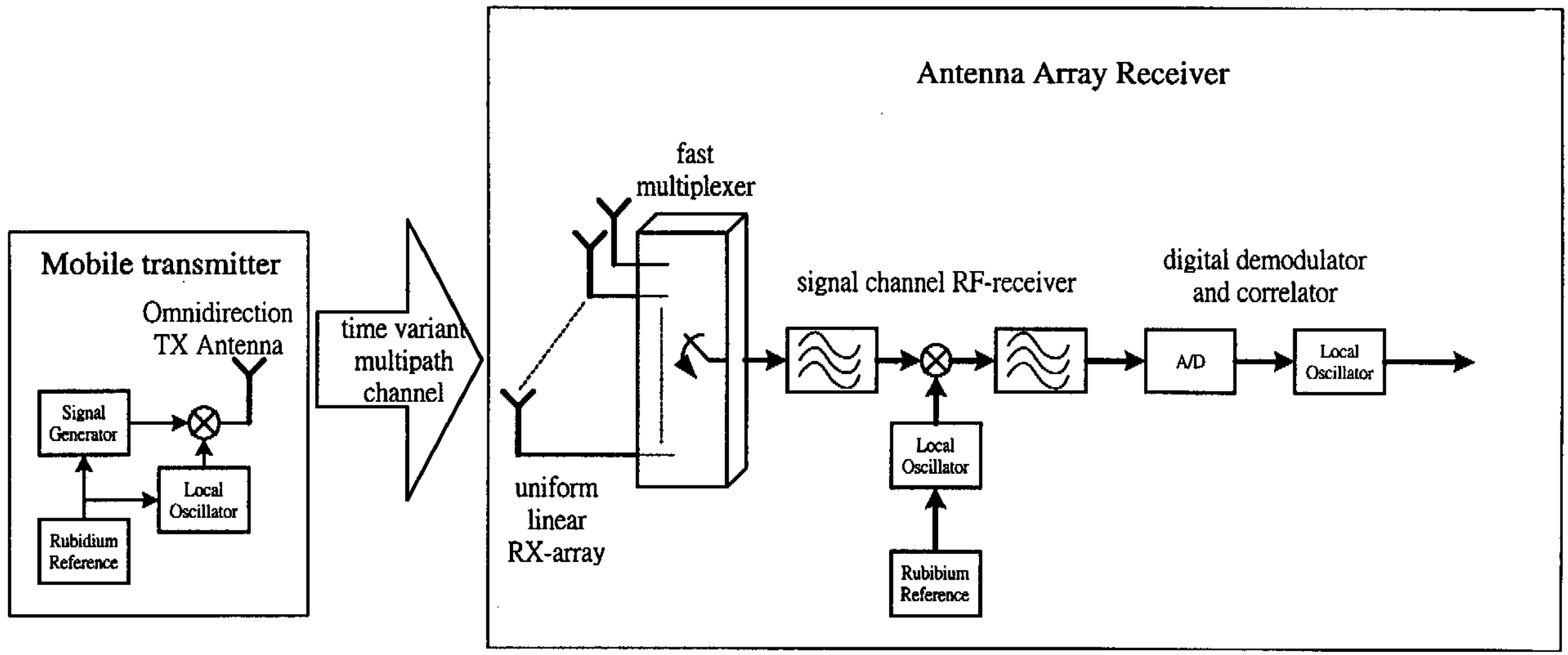

Fig. 8.1 Block diagram of the Vector Channel Sounder System

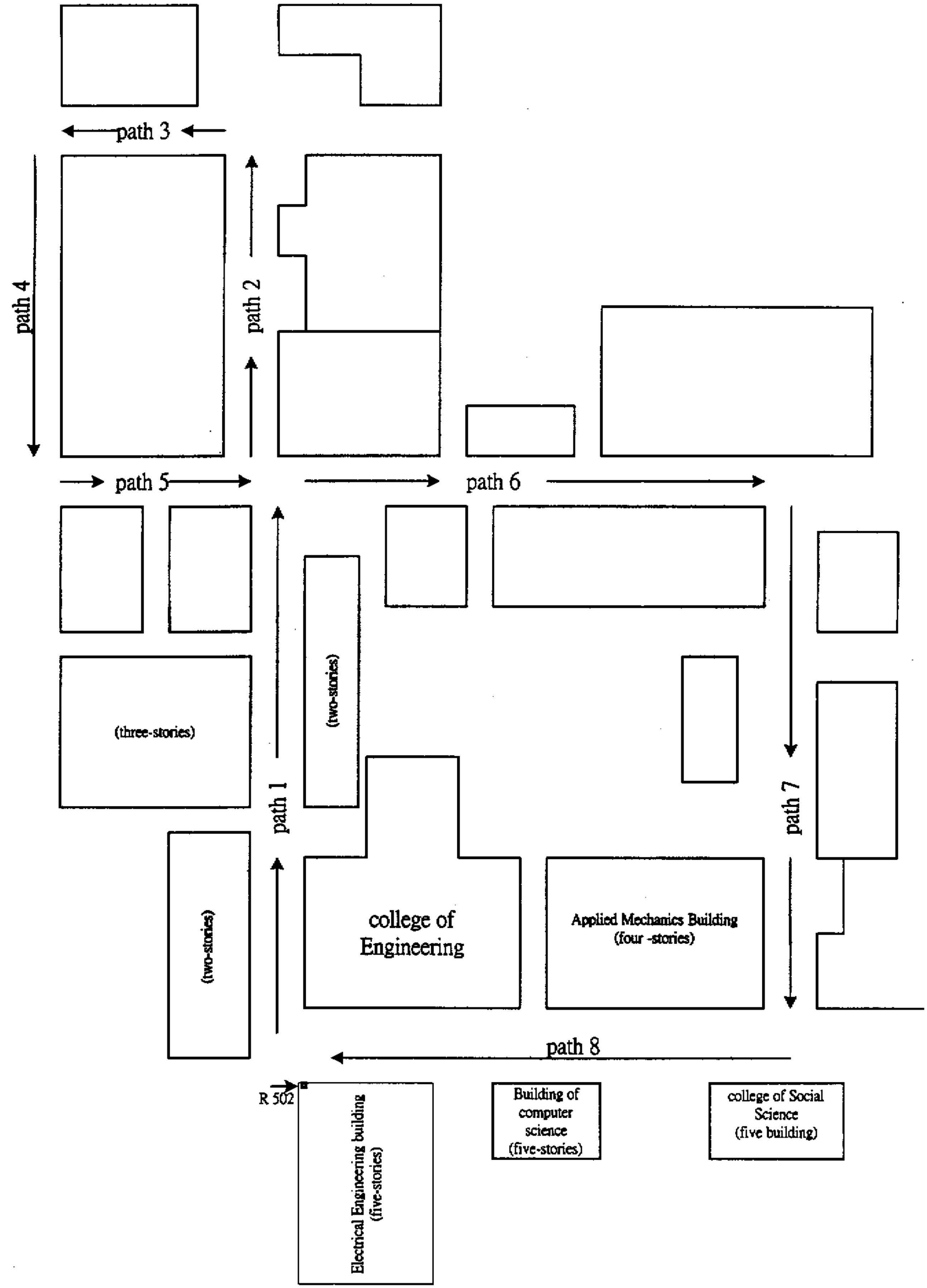

Fig. 8.2 Sketch of the environment for measurement

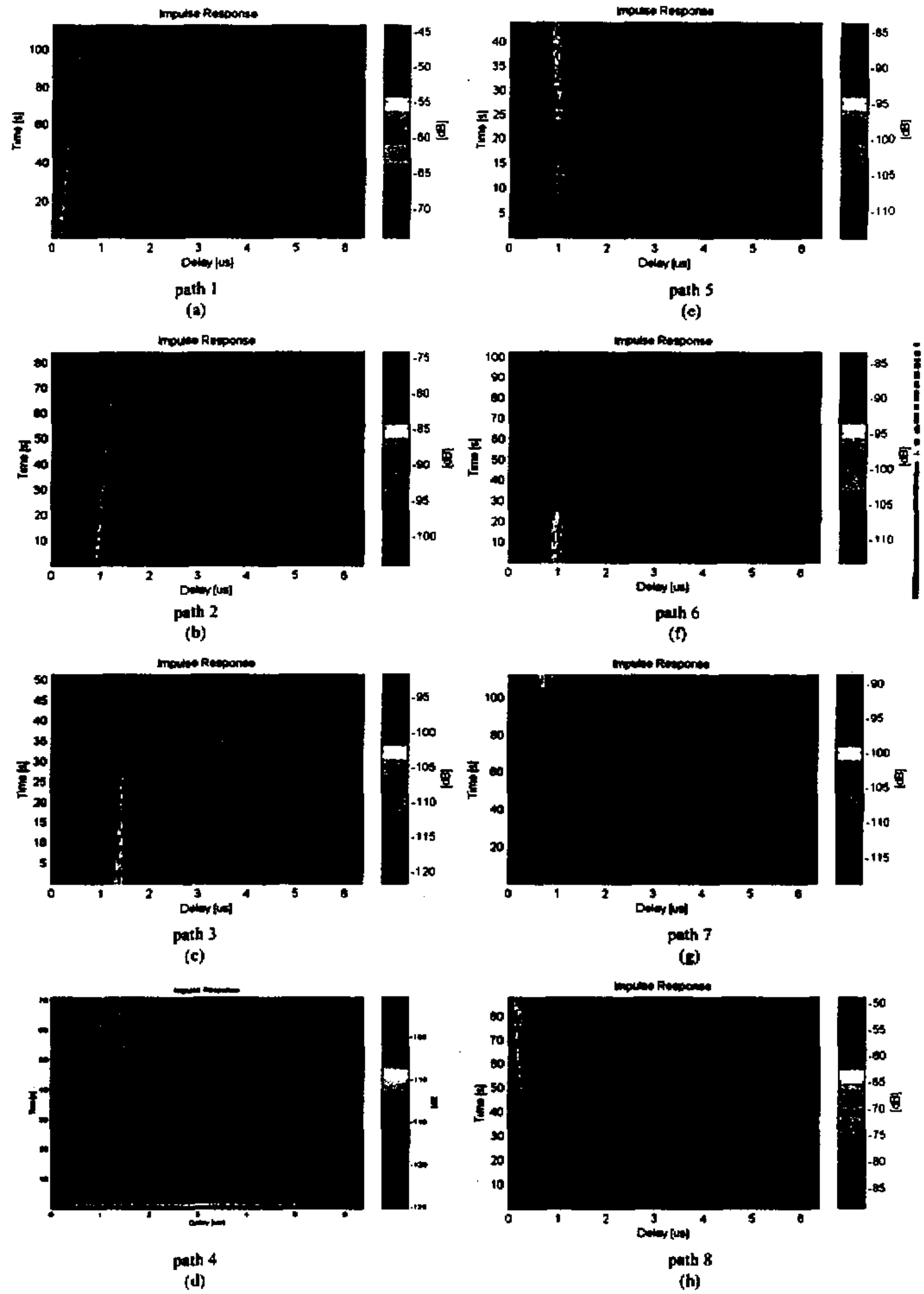

Fig. 8.3 plots of delay-snapshot along different paths with a bandwidth of 120MHz

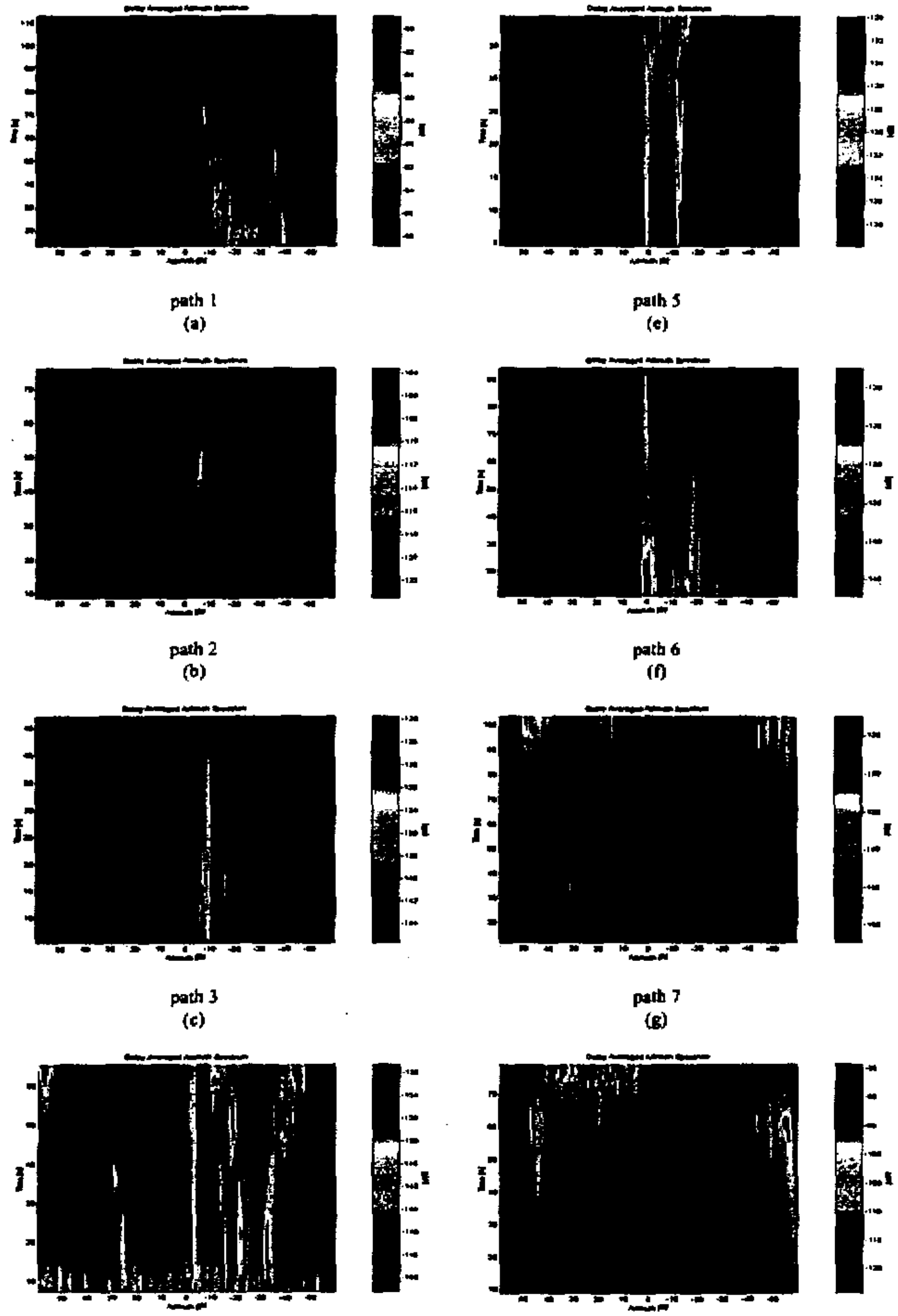

path 1
(a)

path 5
(e)

path 2
(b)

path 6
(f)

path 3
(c)

path 7
(g)

path 4
(d)

path 8
(h)

Fig. 8.4 plots of delay averaged azimuth spectrum for different paths with a bandwidth of 120MHz

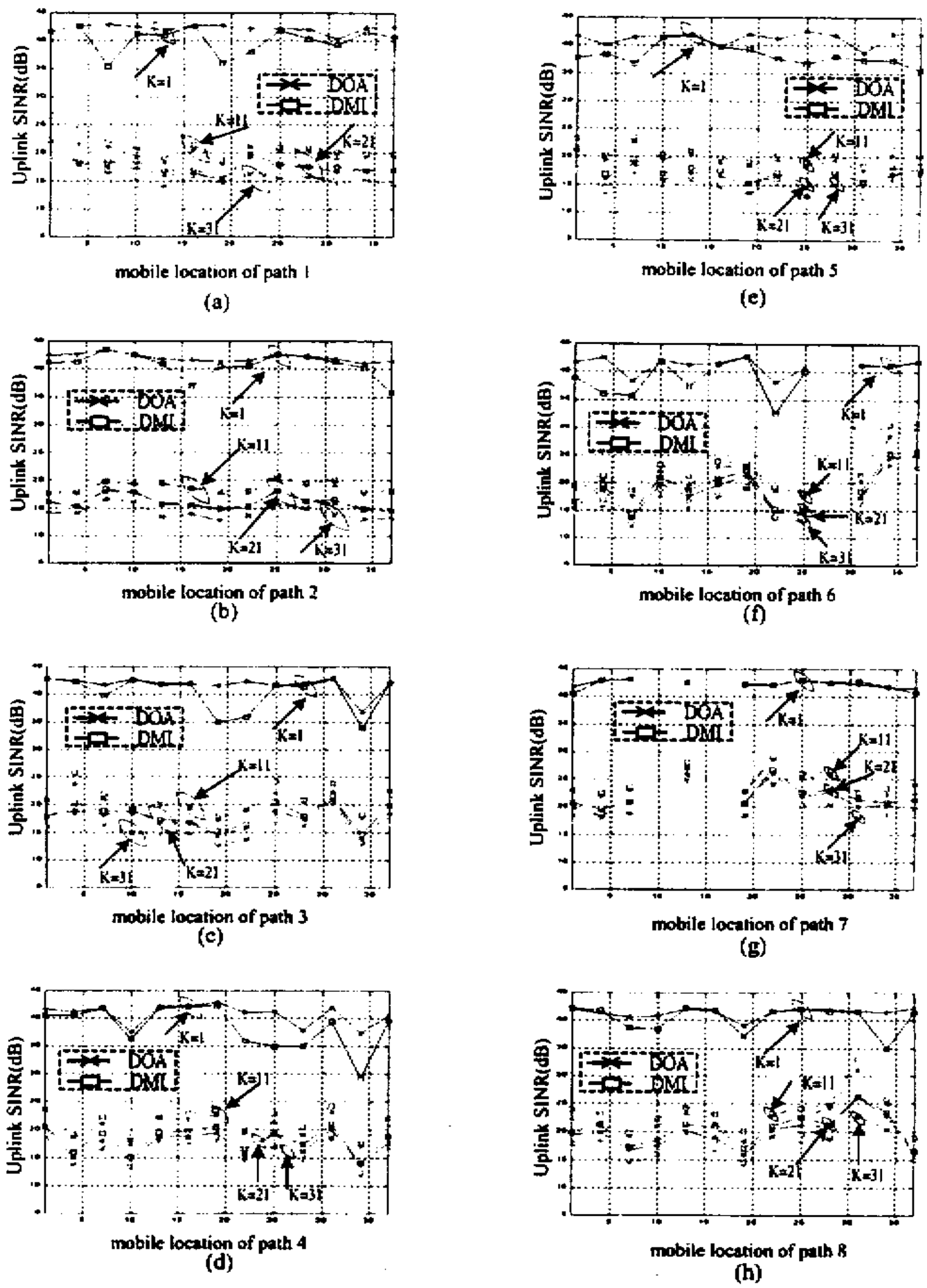

Fig. 8.5 plots of Uplink SINR versus mobile locations for given number of K (K=1, 11, 21, 31)users and obtained by different adaptive algorithms with M=7:(a),(b) and (h) with LOS cases, (c)~(g) with NLOS cases

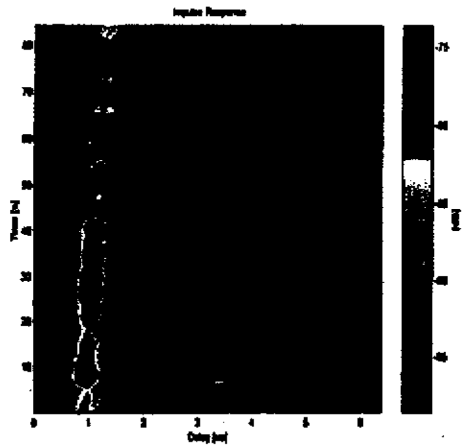

(a) Uplink CIR

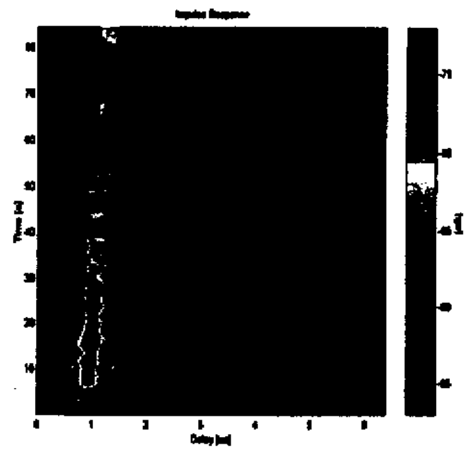

(c) Downlink DOA

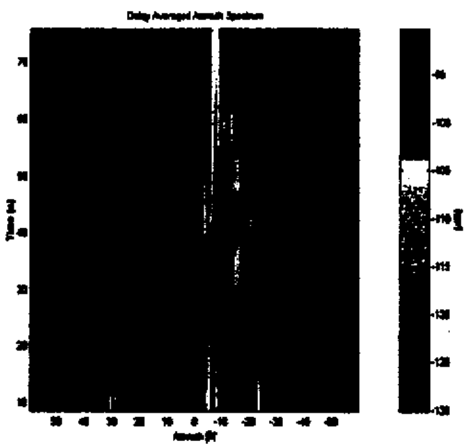

(b) Uplink CIR

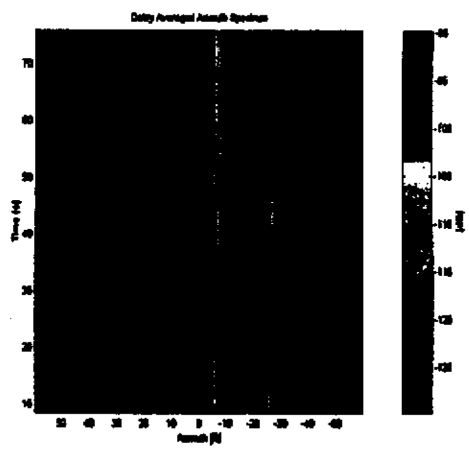

(d) Downlink DOA

Fig. 8.6 plots of Uplink and Downlink delay snapshot and delay azimuth spectrum obtained from the lowest and highest 5MHz band with path 2

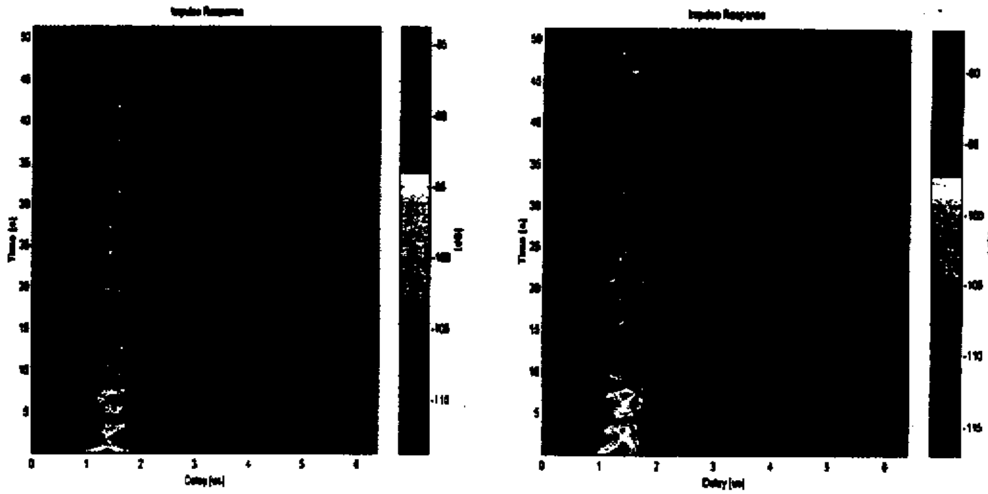

(a) Uplink CIR

(c) Downlink DOA

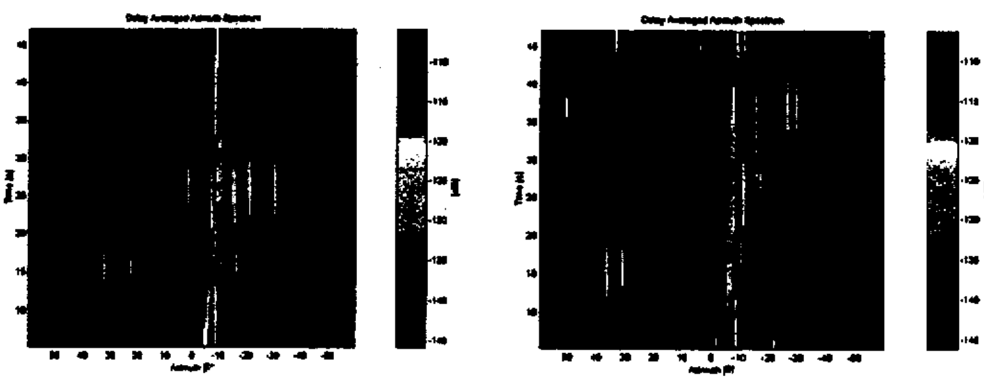

(b) Uplink CIR

(d) Downlink DOA

Fig. 8.7 plots of Uplink and Downlink delay snapshot and delay azimuth spectrum obtained from the lowest and highest 5MHz band with path 3

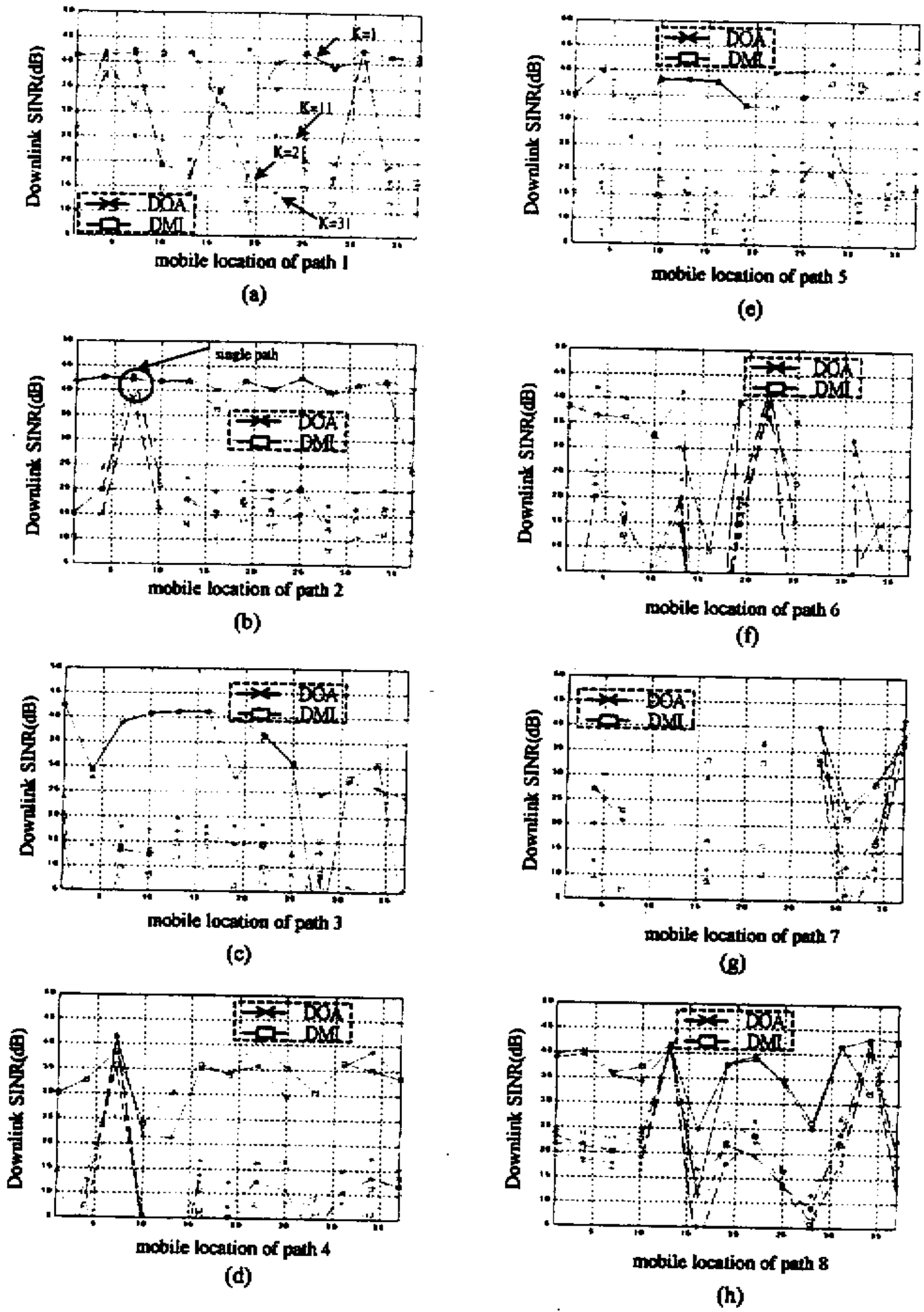

Fig. 8.8 plots of Downlink *SINR* versus mobile locations for given number of K (K=1, 11, 21, 31)users and obtained by different adaptive algorithms with M=7:(a),(b) and (h) with LOS cases, (c)~(g) with NLOS cases

Path 1

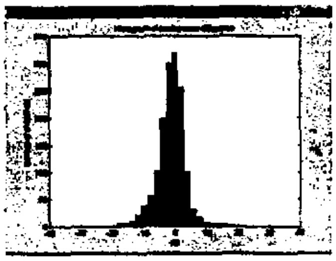

Path 2

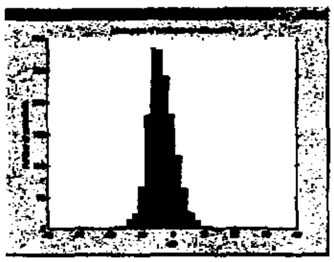

Path 3

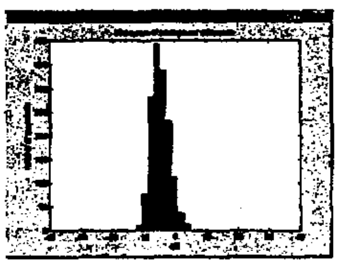

Path 4

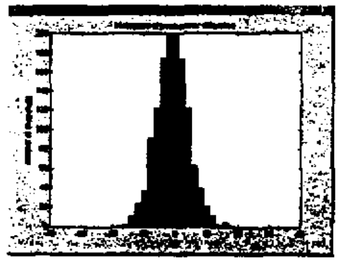

Path 5

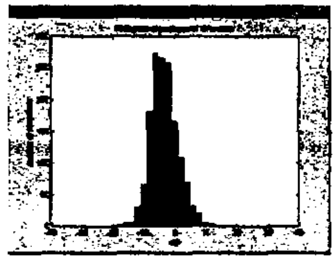

Path 6

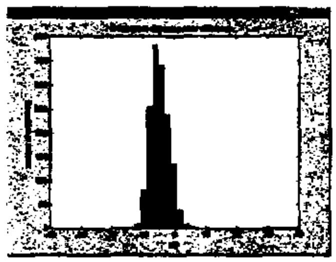

Path 7

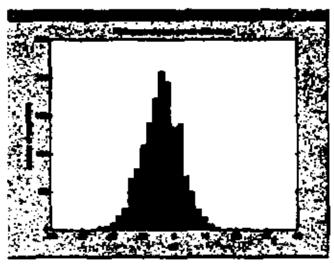

Path 8

	Path1	Path2	Path3	Path4	Path5	Path6	Path7	Path8
Mean(dB)	0.8751	-0.2908	-2.5017	-3.8441	-0.0688	-2.2985	-3.6794	-3.0942
STD(dB)	6.0527	4.5786	4.2446	3.0174	5.2034	4.4659	3.0438	6.4289

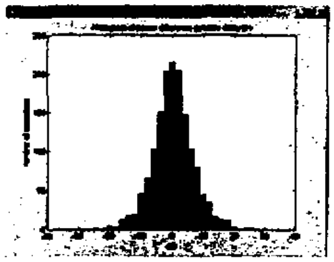

Path 1

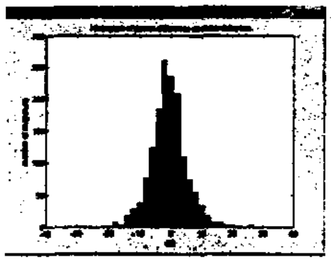

Path 2

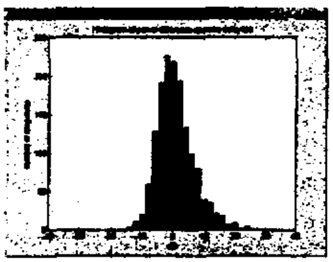

Path 3

Path 4

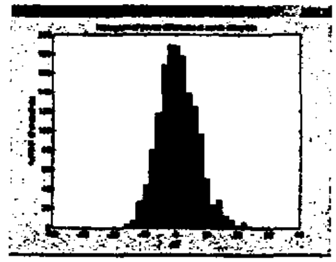

Path 5

Path 6

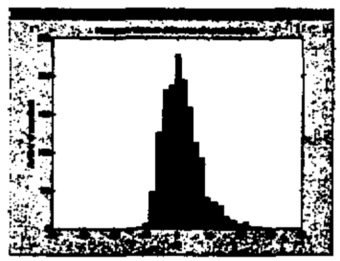

Path 7

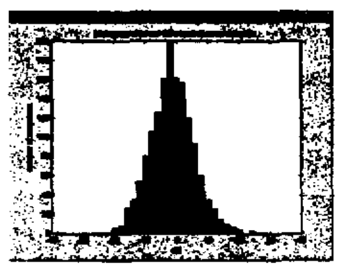

Path 8

	Path1	Path2	Path3	Path4	Path5	Path6	Path7	Path8
Mean(dB)	1.3382	0.3214	1.8034	1.4352	1.6019	1.8552	2.5937	-0.4012
STD(dB)	6.4385	5.9269	6.1045	5.8221	6.3752	6.3786	6.2422	7.2663

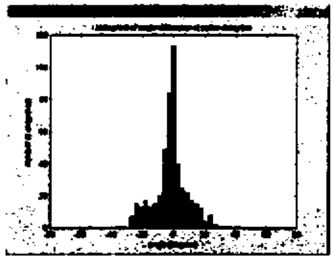

Path 1

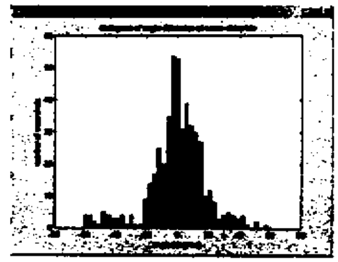

Path 5

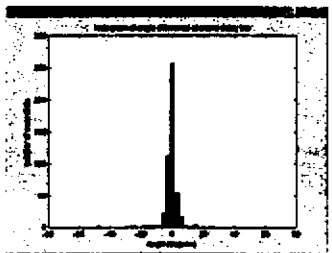

Path 2

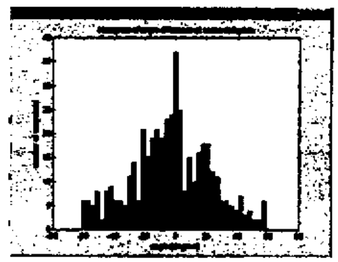

Path 6

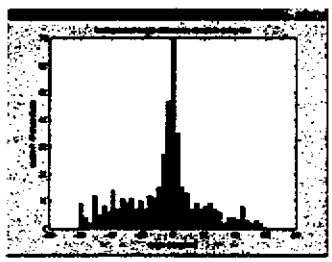

Path 3

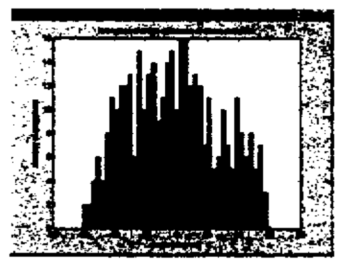

Path 7

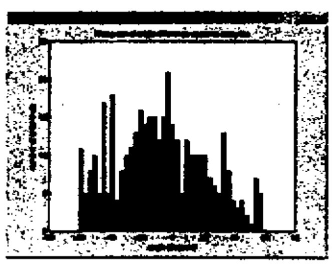

Path 4

Path 8

	Path1	Path2	Path3	Path4	Path5	Path6	Path7	Path8
Mean(degree)	-0.2508	0.7331	-8.0630	-11.6903	0.4682	-2.9426	-4.4791	3.7258
STD(degree)	11.7651	8.9811	32.8020	46.6177	23.1408	34.8423	49.7230	52.4215

Chapter 9 Discussion and Conclusion

In this thesis we have briefly reviewed the time-varying radio fading channel characteristics. We have also overviewed the specification of the physical layer of the W-CDMA communication system. Based on the understanding of the channel characteristics, the correlation properties of the code sequence, the data structure of the physical channel, and the architecture of the basestation transceiver, we have proposed channel parameters estimation algorithms and beamforming algorithms for the 3G W-CDMA basestation transceiver employing antenna array.

To accurately estimate the channel parameters, including the TOA, DOA, and complex amplitude, of the dominant paths of the desired user in the presence of MAI, we propose a method to increase the *SINR* of the resultant delay profile, which is obtained by coherently integrating the matched filter output over different pilot bits and incoherently integrating all matched filter outputs of antenna array elements. With these two stages of integration, the desired signals are greatly enhanced. The TOA, the DOA, and the corresponding complex amplitude of the desired multipath components are then accurately obtained. We have exploited the estimated channel parameters to the data-branch for 2D-RAKE combining. We found that the *SINR* performance after RAKE receiver can approach the theoretical values.

We have compared the uplink and downlink *SINR* performance obtained by different beamforming methods. In the uplink, we found that the DOA method and the complex conjugate method almost have the same *SINR* performance. However, the complex conjugate method doesn't need any computational loading. The DMI method can have much better performance than the DOA method when few users are present in the channel. When the number of users is much greater than the number of antenna element we found that these two methods almost have the same performance. Nevertheless, the DMI method requires much higher computation loading. We have derived an analytical form of the *SINR* after 2D-RAKE receiver for the DMI method and the simulation results are very close to the analytic value.

In the downlink, we found that the complex conjugate method is worse than the DOA method, due to the slight shift of the mainlobe direction. However, the degradation is smaller than 1 dB. We have compared the single-beam and multiple-beam beamforming techniques considering the independent fading of the uplink and downlink. We found that the multiple-beam method has a better *SINR* performance in the low *SINR* region because the single-beam method is more likely to suffer from deep fading. While in the moderate or high *SINR* region, the single-beam method has a much better *SINR* performance because it has a higher antenna gain in the main path direction, a smaller angular coverage of the mainlobe and the orthogonality between different code sequences when the multipath delay difference is smaller than a chip interval.

We have employed the channel data measured by a newly purchased vector channel sounder to simulate the W-CDMA system and compare the uplink and downlink *SINR* performance using different beamforming techniques. In the uplink we found that the *SINR* performance obtained by measurement data has the same trend as that obtained by the simulation data. However, the channel properties and correlation properties of the code sequences are different in the uplink and downlink. We cannot expect that the beamforming technique, which has good performance in the uplink, can also be applied to the downlink. From the real channel measurement data we have observed several interesting phenomena and we understand more about the channel properties and the W-CDMA system. Based on the new understanding we give suggestions for future further studies.

Suggestion for Future Studies

Several further studies are suggested as follows:

1. Use more measurement data to statistically analyze the uplink and downlink

channel properties.

2.Consider the possibility of power control by adjusting the power and beamforming pattern rather than only adjusting the power.

Bibliography

[1]. The ETSI UMTS Terrestrial Radio Access (UTRA) ITU-R RTT Candidate Submission, European Telecommunications Standards Institute (ETSI), July 1998.

[2]. I. Seskar and N. B. Mandayam, "Software defined Radio architectures for Interference Cancellation in DS-CDMA Syatems," IEEE Personal Commun., August 1999, pp. 26~34.

[3]. K. S. Gilhousen, I. M. Jacobs, R. Padovani, A. J. Viterbi, L. A. Weaver, and C. E. Wheatley, "On the Capacity of a Cellular CDMA System," IEEE trans. Veh. Technol., Vol. 40, N0. 2, May 1991, pp. 303~312.

[4]. A. F. Naguib, A. Paulraj, and T. Kailath, "Capacity Improvement with Base-Station Antenna Array in Cellular CDMA," IEEE Trans. Veh. Technol. Vol. 43, No. 3, August 1994, pp. 691~698.

[5]. J. H. Winters, J. Salz, and R. D. Gitlin, "The Impact of Antenna Diversity on the Capacity of Wireless Communication Systems," IEEE Trans. Commun. Vol. 42, No. 2/3/4, Febuary/March/April 1994, pp.1740~1750.

[6]. A. K. Djedid and M. Fujita, "Adaptive Array Sensor processing Applications for Mobile telephone communications," IEEE Trans. Veh. Technol. Vol. 45, No. 3, August 1996, pp. 405~416.

[7]J. Salz and J. H. winters, "Effect of fading Correlation on Adaptive Arrays in Digital Wireless Communications," in Proc. IEEE Int. Conf. Commun., Genvea, Switzerland, Vol. 3 , May 1993, pp. 1768~1774.

[8]. W. C. Y. Lee, "Effects on Correlation Between Two Mobile Radio Base-Station Antennas," IEEE Trans. Commun., Vol. 21, No. 11, November 1973, pp. 1214~1224.

[9]. R. Price and P. E. Green, "A Communication technique for Multipath Channels," Proceeding IRE, Vol. 46, March 1958, pp. 555~570.

[10]. G. L. Turin, "Introduction to Spread-Spectrum Antimultipath Techniques and Their application to Urban Digital Radio," Proceeding IEEE, Vol. 68, No. 3, March 1980, pp. 328~353.

[11]. T. Inoue and Y. Karasawa, "Two-Dimensional RAKE reception Scheme for DS/CDMA Systems in Beam Space Digital beam Forming Antenna Configuration," IEICE Trans. Commun. Vol. ES1-B, No. 7, July 1998, pp.1374~1383.

[12]. F. Min, Z. Jian, W. Jing, and Y. Yan, "Performance of Coherent DS-CDMA with 2D-RAKE Receiver," Electronics Letters, Vol. 34, No. 14, May 1998, pp. 955~957.

[13]. J. Ylitalo and M. Jarvela, "On RAKE Allocation for CDMA Receiver Employing Antenna Array," PIMRC'97., Vol. 1, 1997, pp. 73~78.

[14]. T. Inoue and Y. Karasawa, "Channel Capacity Improvement by Means of 2D-RAKE for DS/CDMA Systems," IEEE VTC 98., Vol. 2, 1998, pp. 786~790.

[15]. 3rd Generation Partnership Project (3GPP), "Spreading and Modulation (FDD)," Tech. Rep. TS 25.213 V2.0.0 (1999-4).

[16]. W. C. Y. Lee, "Overview of Cellular CDMA," IEEE Trans. Veh. Techno. Vol. 40, No. 2, May 1991.

[17]. K. Pahlavan and A. H. Levesque, Wireless Information Networks, New York : Wiley, 1995.

[18]. W. C. Jakes, Microwave Mobile Communications. New York : Wiley, 1974.

[19]. W. R. Braun and U. Dersch, "A Physical Mobile Radio Channel model," IEEE Trans. Veh. Technol. Vol. 40, No. 2, May 1991, pp. 472~482.

[20]. G. Turin, "A Statistical Model of Urban Multipath propagation," IEEE trans. Veh. Technol. Vol. 21, No. 1, February 1980, pp. 1~9.

[21]. G. Ralgigh, S. N. Diggavi, A. F. Naguib, and A. Paulraj, "Characterization of Fast Fading Vector Channels for multi-Antenna Communication Systems," in Proc. 27th Asilomar Conference on Signal, systems and Computers, Vol. II, (Pacific Grove, CA), November 1994.

[22]. P. Zetterberg and B. Ottersten, "The Spectrum Efficiency of a Basestation Antenna Array System for Spatially selective Transmission," IEEE Trans. Veh. Technol. Vol. 44, No. 3, August 1995, pp. 651~660.

[23]. G. G. Raleigh and A. Paulraj, "Time Varying Vector Channel estimation for Adaptive Spatial Equalization," Proc. IEEE Globecom. 1995, pp. 218~224.

[24]. T. S. Rappaport, Wireless Communication Principle and Practice, New Jersey : Prentice Hall, 1996.

[25]. R. F. Harrinton, Time-Harmonic Electromagnetic Fields, McGraw-Hill, 1993.

[26]. J. C. Liberti, Jr. and T. S. Rappaport, Smart Antenna for Wireless Communications IS-95 and Third Generation CDMA Applications, New Jersey : Prentice Hall, 1999.

[27]. J. H. Winter, "Optimum Combining in Digital Mobile Radio with Cochannel Interference," IEEE J. Select Areas in Commun., Vol. SAC-2, July 1984, pp. 528~539.

[28]. R. A. Monzingo and T. W. Miller, Introduction to Adaptive arrays, New York : john Wiley & Sons, 1980.

[29]. S. S. Jeng, G. T. Okamoto, G. Xu, H. P. Lin, and W. J. Vogel, "Experimental Evaluation of Smart Antenna System Performance for Wireless Communications," IEEE trans. Antennas Propagat., Vol. 46, No. 6, June 1998, pp. 749~757.

[30]. A. Paularj,. R. Roy, and T. Kailath, "Estimation of Signal Parameters Vis Rotational Invariance techniques-ESPRIT," Proc. of 19th Asilomar Conf. On

Circuits and Systems, 1985, pp. 83~89.

[31]. L. C. Godara, "Application of Antenna Arrays to Mobile Communications, part Ⅱ: beamforming and direction-of-arrival considerations," Proc. IEEE, Vol. 85, No. 8, August 1997, pp. 1195~1245.

[32]. S. C. Yang, CDMA RF System Engineering, MA : Artech House, 1998.

[33]. F. Adachi, M. Sawahashi, and H. Suda, "Wideband DS-CDMA for next –generation Mobiles communications Systems," IEEE Communications magazine, Vol. 36, No. 9, September 1998, pp. 56-69.

[34]. S. Ogawa, A. Higashi, H. Horitani, and K. Hatta, "W-CDMA System Experiments," IEEE VTC 2000-Spring Tokyo, Vol. 1, pp. 143~147.

[35]. A. P. Nash, G. Freeland, and T. Bigg, "Practical W-CDMA Receiver and Transmitter System Design and simulation," 3G Mobile Communication Technologies, 2000. First International Conference on (Conf. Publ. No. 471), pp. 117~121.

[36]. G. Tsoulos, M. Beach, and J. McGeehan, "Wireless Personal Communications for the 21st Century: European Technological Advances in Adaptive Antennas," IEEE Commun. Magazine, Vol. 35, No. 9, September 1997, pp. 102~109.

[37]. T. sawahashi and F. Adachi, "Pilot Symbol-Assisted Decision-Directed Coherent Adaptive Array Diversity for DS-CDMA Mobile Radio," Proc. Wireless 97, July 1997, pp. 444~451.

[38]. Don J. Torrieri, "Performance of Direct-Sequence System with Long Pseudonoise Sequence," IEEE J. Select. Areas Commun., Vol. 10, No. 4, May 1992, pp. 770-781.

[39]. G. L. Turin, "The Effects of Multipath and Fading on the Performance of Direct-Sequence CDMA System," IEEE Trans. Veh. Technol., Vol. VT-33, No. 3, August 1984, pp. 213-219.

[40]. A. F. Naguib and A. Paulraj, "Performance of Cellular CDMA with M-ary Orthogonal Modulation and Cell Site Antenna Arrays," in Proc. ICC'95, June 1995, pp. 697-702.

[41]. B. H. Khalaj, A. Paulraj, and T. Kailath, "Antenna Arrays for CDMA Systems with Multipath," Milcom., pp. 624-628, 1993.

[42]. M. Chan and J. C-I Chuang, "The Effects of Delay Spread on Multicode Interference Cancellation," in IEEE 47th VTC'97, Vol. Ⅲ, pp. 2153-2157, 1997.

[43]. J. G. Proakis, Digital Communications, New York: McGraw-Hill Inc., Third ed., 1995.

[44]. J. E. Hudson, Adaptive Array Principles. Stevenage, UK: Peter Peregrinus Ltd., 1989.

[45]. H. Asakura and T. Matsumoto, " Cooperative Signal Reception and Downlink Beam Forming in Cellular Mobile Communications," IEEE Trans. Veh. Technol., Vol. 48, No. 2, March 1999, pp. 333-341.

[46]. J. Ylitalo and M. Katz, "An Adaptive Antenna Method for Improving Downlink performance of CDMA Base Station," Proc. ISSSTA'98,1998, pp. 599-603.

[47]. B. Widrow, J. McCool, and M. Ball, "The Complex LMS Algorithm," Proc. Letters, IEEE, April 1975, pp. 719~720.

[48]. J. R. T. Compton, "An Adaptive Array in a Spread-Spectrum Communication System," Proc. IEEE, Vol. 66, No. 3, pp. 289~298, 1978.

[49]. J. H. Winters, "Signal Acquisition and Tracking with Adaptive Arrays in the Digital Mobile Radio System IS-54 with Flat Fading," IEEE trans. Veh. Technol. Vol. 42, No. 4, November 1993, pp. 377~384.

[50]. A. F. Naguib and A. Paulraj, "Performance of CDMA Cellular Networks with Base-Sataion Antenna Arrays" in Proc. International Zurich Seminar on Digital Communications, (Zurich, Switzerland), March 1994, pp. 87~100.

[51]. X. Wang and H. V. Poor, "A New Adaptive Array Algorithm for Interference Suppression in Wireless Communication," VTC 98 IEEE, Vol. 3, pp.1655~1659, 1998.

[52]. H. J. Li, J. Lee, and T. Y. Liu, "Subscriber Geolocation with W-CDMA," Submitted for Publication.